Genomic regions associated with leaf rust and end-use quality traits in hexaploid wheat

by

Marshall Clinesmith

B.S., Kansas State University, 2013
M.S., Kansas State University, 2016

AN ABSTRACT OF A DISSERTATION

submitted in partial fulfillment of the requirements for the degree

DOCTOR OF PHILOSOPHY

Department of Agronomy
College of Agriculture

KANSAS STATE UNIVERSITY
Manhattan, Kansas

2026

Abstract

The goal of wheat breeding programs is to develop elite germplasm with attributes desired by producers, millers, bakers, and consumers. Successful wheat cultivars and hybrids are high yielding and possess acceptable end-use quality and effective levels of disease resistance. Advancements in molecular breeding technology have allowed identification of genetic architecture controlling these traits. The following work describes genetic mapping of quantitative trait loci (QTL) associated with end-use quality, leaf rust resistance, and expression of leaf tip necrosis (LTN).

In the first study we investigated the haplotypes introgressed from both *Ae. tauschii* ssp. *strangulata* and *Ae. tauschii* ssp. *tauschii* and their association with end-use quality traits in common bread wheat (*Triticum aestivum* L.). We developed 351 introgression lines from six hexaploid winter wheat parents and 21 *Ae. tauschii* accessions and collected phenotypic data on all introgression lines from field trials grown in Kansas between 2018 and 2020. Haplotype-trait associations were detected for lactic acid-sodium dodecyl sulfate solvent retention capacity (LA-SDS SRC) on chromosomes 3DS and 6DS, for protein quality score on chromosomes 1DS, 1DL, and 6DL, and for grain protein concentration on chromosome 6DL. Two introgressed haplotypes were unique to *Ae. tauschii* and were associated with increases in LA-SDS SRC. These detected haplotypes contain potentially novel alleles for improving end-use quality in common wheat.

The second study used a biparental population to identify QTL associated with adult plant resistance (APR) to leaf rust. A doubled haploid (DH) population consisting of 159 lines was developed from a cross between cultivars ’Everest’ and ’WB-Cedar’. The DH population and parents were scored for leaf rust reaction at the seedling stage and adult plant stage using artificial inoculation in the greenhouse, and at Castroville, TX under natural inoculum. Nine QTL were detected on chromosomes 1BL, 2AS, 2AL, 2BS, 3BL, 4DL, 5AL, 7BL, and 7DS. WB-Cedar was confirmed to carry the APR race non-specific gene *Lr34* while the slow rusting APR gene *Lr68* was shown to be present in Everest. Everest also contributed *QLr.ksu-2AL*, a potential all-stage resistance (ASR) locus, observed at both seedling and adult plant stages.

In a third study, a greenhouse experiment was performed to phenotype LTN traits on the Everest by WB-Cedar DH population. Five QTL associated with LTN were detected on chromosomes 1D, 2A, 4D, 5A, and 7D. The QTL on 2A was previously associated with an all-

stage resistance (ASR) gene for leaf rust. *Ltn1/Lr34* (7D) contributed the greatest effect on LTN expression, whereas no evidence for any association was detected in the region containing Ltn4/Lr68 (7B). The results of these studies impart important insights into the genetic basis of end-use quality and leaf rust resistance in elite cultivars adapted to the Great Plains. The associated loci described provide a base for further exploration and development of diagnostic markers to facilitate breeding for improved germplasm.

Genomic regions associated with leaf rust and end-use quality traits in hexaploid wheat

by

Marshall Clinesmith

B.S., Kansas State University, 2013
M.S., Kansas State University, 2016

A DISSERTATION

submitted in partial fulfillment of the requirements for the degree

DOCTOR OF PHILOSOPHY

Department of Agronomy
College of Agriculture

KANSAS STATE UNIVERSITY
Manhattan, Kansas

2026

Approved by:

Major Professor

Allan K Fritz

Copyright

Abstract

The goal of wheat breeding programs is to develop elite germplasm with attributes desired by producers, millers, bakers, and consumers. Successful wheat cultivars and hybrids are high yielding and possess acceptable end-use quality and effective levels of disease resistance. Advancements in molecular breeding technology has allowed identification of genetic architecture controlling these traits. The following work describes genetic mapping of quantitative trait loci (QTL) associated with end-use quality, leaf rust resistance, and expression of leaf tip necrosis (LTN).

In the first study we investigated the haplotypes introgressed from both *Ae. tauschii* ssp. *Strangulate* and *Ae. tauschii* ssp. *tauschii* and their association with end-use quality traits in common bread wheat (*Triticum aestivum* L.). We developed 351 introgression lines from six hexaploid winter wheat parents and 21 *Ae. tauschii* accessions and collected phenotypic data on all introgression lines from field trials grown in Kansas between 2018 and 2020. Haplotype-trait associations were detected for Lactic acid-sodium dodecyl sulfate solvent retention capacity (LA-SDS SRC) on chromosomes 3DS and 6DS, for protein quality score on chromosomes 1DS, 1DL, and 6DL, and for grain protein concentration on chromosome 6DL. Two introgressed haplotypes were unique to *Ae. tauschii* and were associated with increases in LA-SDS SRC. These detected haplotypes contain potentially novel alleles for improving end-use quality in common wheat.

The second study used a biparental population to identify QTL associated with adult plant resistance (APR) to leaf rust. A doubled haploid (DH) population consisting of 159 lines was developed from a cross between cultivars ’Everest’ and ’WB-Cedar’. The DH population and parents were scored for leaf rust reaction at the seedling stage and adult plant stage using artificial inoculation in the greenhouse, and at Castroville, TX under natural inoculum. Nine QTL were detected on chromosomes 1BL, 2AS, 2AL, 2BS, 3BL, 4DL, 5AL, 7BL, and 7DS. WB-Cedar was confirmed to carry the APR race non-specific gene *Lr34* while the slow rusting APR gene *Lr68* was shown to be present in Everest. Everest also contributed *QLr.ksu-2AL*, a potential all-stage resistance (ASR) locus, observed at both seedling and adult plant stages.

In a third study, a greenhouse experiment was performed to phenotype LTN traits on the Everest by WB-Cedar DH population. Five QTL associated with LTN were detected on chromosomes

1D, 2A, 4D, 5A, and 7D. The QTL on 2A was previously associated with an all-stage resistance (ASR) gene for leaf rust. *Ltn1/Lr34* (7D) contributed the greatest effect on LTN expression, whereas no evidence for any association was detected in the region containing Ltn4/Lr68 (7B). The results of these studies impart important insights into the genetic basis of end-use quality and leaf rust resistance in elite cultivars adapted to the Great Plains. The associated loci described provide a base for further exploration and development of diagnostic markers to facilitate breeding for improved germplasm.

Table of Contents

List of Figures

List of Tables

Chapter 1 - Contribution of Haplotypes Introgressed from *Aegilops tauschii* to End-Use Quality Traits in Common Bread Wheat

Marshall Clinesmith[1*], Moses Nyine[2], Eduard Ahkunov[2], Nora M. Bello[3], Mary Guttieri[4], Allan Fritz[1], Jessica Noller[2]

[1] Department of Agronomy, Kansas State University, Manhattan, KS 66506
[2] Department of Plant Pathology, Kansas State University, Manhattan, KS 66506
[3] Department of Animal Sciences, The Ohio State University, Columbus, OH, 43204
[4] USDA, Agricultural Research Service, Center for Grain and Animal Health Research, Hard Winter Wheat Genetics Research Unit

Abstract

Wild relatives of wheat are a potential source of genetic diversity for improving traits of primary focus in breeding programs. The D-genome of wheat originated from its wild relative, *Aegilops tauschii*, and has limited diversity relative to the A and B genomes. Therefore, the D-genome is a primary candidate for introgressing beneficial alleles from accessions of *Ae. tauschii*. Our objective in this study was to evaluate haplotypes introgressed from *Ae. tauschii* for genome-wide associations with grain protein concentration and bread-making quality in hard red winter wheat. We developed 351 introgression lines from six hexaploid winter wheat parents and 21 *Ae. tauschii* accessions and collected phenotypic data on all introgression lines from field trials grown in Kansas between 2018 and 2020. We used whole-genome sequencing of parental lines followed by sequence-based genotyping of the introgression population resulting in 5.2 million imputed D-genome SNPs. A haplotype-based-genome-wide association mapping approach was performed using 15,967 haplotype blocks (HB) inferred using the 5.2 million D-genome SNPs. Haplotype-trait associations were detected for lactic acid-sodium dodecyl sulfate solvent

retention capacity (LA-SDS SRC) on chromosomes 3DS and 6DS, for protein quality score on chromosomes 1DS, 1DL, and 6DL, and for grain protein concentration on chromosome 6DL. Most haplotypes associated with improvements in end-use quality traits were present in both parental species. Two introgressed haplotypes were unique to *Ae. tauschii* and were associated with increases in LA-SDS SRC. Detection of introgressed haplotypes from wild relatives associated with trait improvements suggests wild sources may harbor valuable genetic diversity for improving end-use quality in wheat.

Introduction

Wheat, *Triticum aestivum* (2n = 6x = 42, AABBDD), is a broadly adapted crop planted in many diverse regions globally and provides around 20 percent of the proteins and calories consumed worldwide (Pena, 2007; Shiferaw et al., 2013). In the U.S., wheat currently ranks third in total production, behind corn and soybeans (USDA NASS, 2020). The number of acres planted in the U.S. peaked in 1981 at 88.3 million. Since then, a steady decline has been observed with only 45.2 million acres of wheat planted in 2019 (USDA NASS, 2020). Limited profitability in wheat production due in part to increased competition in wheat production internationally and domestic competition with increases in corn and soybean acres is one of the main factors driving the reduction in U.S. wheat acres (Pena, 2007; Aguilar et al., 2015; Wang, 2020). In addition, continued global development and industrialization has changed consumer preferences, and increased demand for specific quality grades of wheat needed to produce a diverse array of finished wheat products (Pena, 2007). Millers and bakers desire specific values for end-use quality traits in grain or flour to produce these products. High grain test weight (GTW) and flour yield are traits preferred in the milling industry. Grain hardness is also an important trait with harder grain wheat being used primarily for bread products. Desired traits for

bakers in hard wheat include gluten strength, grain protein concentration (GPC), mixing time and mixing tolerance, loaf volume, and water absorption (Zhang et al., 2020).

Wheat is an allohexaploid species generated from a hybridization event between cultivated forms of *Triticum turgidum* (2n = 4x = 28, AABB) and *Ae. tauschii* ssp. *strangulata* (2n = 2x = 14, DD) (Haudry et al., 2007; Luo et al., 2007; Wang et al., 2013). Since this hybridization event, the processes of wheat domestication, hybridization, and subsequent human-driven selection to develop locally adapted varieties have reduced genetic diversity through loss or fixation of alleles (Haudry et al., 2007). Specifically, studies have shown reduced genetic diversity in the D-genome of wheat compared to the A and B genomes (Wang et al., 2014; Jordan et al., 2015; Balfourier et al., 2019; Mourad et al., 2020). These inter-genomic differences in the levels of genetic diversity are associated with the reduced rate of gene flow from *Ae. tauschii* into the D-genome compared to the rate of gene flow from tetraploid wild ancestors into the A and B genomes (He et al., 2019). Thus, efforts directed towards introgressing novel allelic diversity from *Ae. tauschii* into wheat provide unique opportunities to make quick advances in improving important traits in hexaploid wheat. Specifically, breeding strategies aimed at identifying novel alleles associated with increasing quality traits, such as GPC and gluten strength, can improve the end-use quality in commercial wheat varieties, thereby enabling new marketing opportunities for producers.

The end-use quality characteristics of wheat are controlled by a complex interaction of management, environment, and genetics (Jernigan et al., 2018; Souza et al., 2012; Zörb et al., 2018) making it difficult to consistently produce grain with desired specifications. In wheat, quality traits refer to the physical and chemical properties of kernels, flour, and dough relevant to the downstream manufacturing pipeline. These properties include size, shape, hardness, and

342 density of the kernels; as well as GPC and protein quality (PQ) in the grain and flour (J.G.
343 Nuttall et al., 2017). GPC is a major indicator of both the end-use quality and nutritional aspect
344 of food produced from grain (Zhao et al., 2010), with its primary components being glutenin,
345 gliadin, albumin and globulin (Shewry & Halford, 2002; Xue et al., 2019). Specifically,
346 glutenins have been shown to have the largest impact on GPC and gluten strength while gliadins
347 control the viscosity and extensibility of the dough (Torbica et al., 2007).
348 Previous studies have identified genomic regions associated with end-use quality traits.
349 For instance, *GPC1* includes three homoeologous genes (*GPC-A1, GPC-B1,* and *GPC-D1)*
350 located on the short arms of chromosomes 6A, 6B, and 6D and associated with GPC (Avivi,
351 1978; Joppa et al., 1997; Uauy et al., 2006; Avni et al., 2013). *GPC-B1* located on chromosome
352 6B was discovered in wild emmer (*Triticum turgidum* ssp. *dicoccoides* (Körn) (Avivi, 1978) and
353 has been transferred into a limited number of modern hexaploid varieties with no
354 commercialized HRW varieties currently known to carry the gene (Mesfin et al., 1999; Khan et
355 al., 2000). Glutenins are divided into groups based on the molecular weight of their protein. High
356 molecular weight glutenins (HMW-GS) are controlled by loci *Glu-A1, Glu-B1,* and *Glu-D1*
357 located on the long arms of chromosomes 1A, 1B, and 1D (Payne et al., 1980), while low
358 molecular weight glutenins (LMW-GS) are controlled by *Glu-A3*, *Glu-B3,* and *Glu-D3* on the
359 short arms of chromosomes 1A, 1B, and 1D (Singh & Shepherd, 1988). In addition, six loci
360 encoding gliadins have been detected. Specifically, *Gli-A1, Gli-B1,* and *Gli-D1* loci are located
361 on the short arms of chromosomes 1A, 1B, and 1D and linked to the LMW-GS loci (Boyd &
362 Lee, 1967; Payne et al., 1984), while *Gli-A2, Gli-B2,* and *Gli-D2* are located on the short arms of
363 chromosomes 6A, 6B, and 6D (Shewry et al., 2003; Qi et al., 2006). Besides these major loci
364 controlling GPC and gluten content, several studies reported QTL associated with these traits on

all 21 chromosomes of wheat (Kulwal et al., 2005; Zhang et al., 2008; Bogard et al., 2012; Kumar et al., 2018).

Another important variable used by producers to assess the quality of grain is GTW. It can serve as a proxy indicating total flour yield, which is of interest to millers when purchasing grain (Gwirtz et al., 2006). QTL for GTW have also been reported on all 21 chromosomes (Narasimhamoorthy et al., 2006; Sun et al., 2009; Carter et al., 2011; Simons et al., 2012; Cabral et al., 2018; Chen et al., 2020).

Furthermore, rheological properties describe the viscosity and elasticity of dough, which are important in the baking industry (Song & Zheng, 2007). Common tests used to measure rheological properties of dough in hard wheat include the farinograph and mixograph, which measure water absorption, dough development time, and stability of the dough to overmixing (Chung et al., 2001). While these tests have become standard for measuring wheat end-use quality and functionality, they are costly and time consuming making them impractical for use in evaluating large numbers of breeding lines. The sodium dodecyl sulfate sedimentation (SDS-SED) test provides a quicker method of predicting end-use quality of wheat through the determination of gluten quality and quantity from a small amount of sample (Axford et al., 1979; Blackman and Gill, 1980). This makes SDS feasible for running quality tests on many samples generated by breeding programs (Moonen et al., 1982). QTL for SDS-SED have been detected on chromosomes 1A, 1B, 1D, 3A, 4A, 4B, and 7A of wheat (Goel et al., 2019; Ruan et al., 2020). Solvent retention capacity (SRC) is another test used to approximate dough-level end-use quality and measures the functional polymeric components of the flour including gluten, damaged starch, and pentosans by measuring the absorption of a set of solvents by flour (Slade & Levine, 1994). These parameters of flour functionality also cumulatively contribute to the

388 factors measured using rheological tests such as the farinograph and mixograph suggesting that
389 SRC can provide an accurate measure of functionality and end-use quality (Kweon et al., 2011).
390 The high heritability of SRC makes it a useful tool for evaluating samples across different
391 environments (Guttieri et al., 2001; Guttieri & Souza, 2003). Previous studies have discovered
392 QTL associated with SRC on chromosomes 1B, 2B, 2D, 4A, 4D, 7B, and 7D of wheat (Smith et
393 al., 2011; Jernigan et al., 2018). Both SDS-SED and SRC have some limitations as SDS-SED is
394 not strongly correlated with loaf volume and lactic acid SRC is not strongly correlated with
395 dough rheology. Therefore, Seabourn et al., 2012 developed a hybrid LA-SDS SRC protocol that
396 includes components from both tests to provide a rapid test for predicting end-use quality that is
397 applicable in large scale breeding programs (Wilson et al., 2020).
398 Due to the polygenic basis of wheat end-use quality (Turner et al., 2004; Naraghi et al.,
399 2019) quantitative trait loci (QTL) mapping has shown to be a useful tool for breeders and
400 geneticists to search for genomic regions associated with quality-related traits. Specifically,
401 genome-wide association study (GWAS) has become a prominent method for QTL detection in
402 the panels of unrelated lines, as commonly found in wheat breeding programs. GWAS has been
403 applied successfully in numerous commercial crop species including corn, soybean, sorghum,
404 rice, and wheat (Morris et al., 2012, Guttieri et al., 2015, Kaler et al., 2017, Xiao et al., 2017,
405 Cruppe et al., 2020, Yuan et al., 2020). One of the most used models for traditional GWAS is
406 based on a linear mixed model (MLM) (Yu et al., 2005, Zhang et al., 2005). The MLM includes
407 both fixed and random effects, where the population structure is fitted as a fixed effect and the
408 kinship is fit as a variance-covariance structure of individual genetic effects, which are
409 considered random (Zhang et al., 2010). The inclusion of population structure and kinship into
410 the model was shown to be effective at reducing the rate of type I error (Yu et al., 2005).

The detection of marker-trait associations in mapping studies was substantially accelerated by reduction in the cost of next-generation sequencing that allows for sequence-based genotyping of large populations. In this study, our objective was to evaluate haplotypes introgressed from *Ae. tauschii* on grain protein concentration and bread-making quality in hard red winter wheat. For this purpose, we developed lines of hexaploid wheat containing introgressed haplotypes from a genetically diverse set of *Ae. tauschii* accessions. The whole-genome sequencing of parental lines was combined with reduced sequencing of the entire set of introgression lines to impute 5.2 million SNPs and identify haplotypes introgressed from *Ae. tauschii* (Nyine et al., 2021). Phenotypes associated with a panel of end-use quality traits were collected on multi-environment field trials. A haplotype-based GWAS analysis was then used to identify chromosomal regions within the D-genome significantly associated with end-use quality traits.

Materials and Methods

Plant Material

Plant material for this study consisted of 351 $BC_1F_{3:5}$ *Ae. tauschii* introgressed hexaploid wheat lines (IL). These lines were developed by initially crossing 21 *Ae. tauschii* accessions with six hexaploid wheat varieties (Table A-1). Embryos of the F_1 hybrids were rescued and treated with colchicine to produce synthetic octoploids (Dale *et al.* 2017). Octoploid lines were then crossed once to the recurrent hexaploid wheat parent (backcross) or to a different hexaploid wheat parent (topcross). The BC_1F_1 plants generated from crosses between the *T. aestivum* and *Ae. tauschii* parents were selfed and advanced by single seed descent to the BC_1F_3 generation. Seed from individual BC_1F_3 plants was bulked and grown in single rows in the field at the Kansas State University Ashland Research Farm near Manhattan, KS in the 2016-17 growing season. This

yielded a full panel of 2,861 lines developed, representing 31 families. From this panel, a subset of lines were selected for general adaptive and agronomic traits including maturity, plant height, seed amount, and threshability, resulting in 351 IL representing 26 families used in the current study.

Field Trials

Plots of the 351 ILs, the six recurrent parents, were evaluated in four environments during the growing seasons of 2018(E1) and 2019 (E2 and E3) at the Northwest Research-Extension Center in Colby, Kansas and during 2020 (E4) at the Ashland Bottoms Research Farm in Manhattan, Kansas (Table A-2). Within each environment, lines were randomized to plots and arranged using a modified augmented design (type 2) (Lin and Poushinsky, 1985). Plots were planted using a 6-row wheat drill. Plot dimensions were 2.5 meters long by 0.5 meters wide and consisted of three rows with 18-cm row spacing. Starter fertilizer was applied with the seed at planting using granular 18-46-0 diammonium phosphate (DAP) at a rate of 168.1 kg/ha. Additional nitrogen was applied as a topdress in the spring using liquid 28-0-0 urea ammonium nitrate (UAN) at a rate of 100.9 kg N/ha. A lateral irrigation system was used at the Colby station to ensure uniform germination and emergence as well as to provide additional water throughout the growing season if natural rainfall was inadequate.

Data Collection and Definition of Quality Traits

Individual plots were mechanically harvested using a Zurn 150 universal plot combine (Zürn Harvesting, Ravenstein, Germany). Total harvested grain was collected from each plot and used for further analysis. GPC (%), GTW (kg/hl), and grain moisture (GM, %) from one plot sample were measured on whole grain using a Perten IM 9500 NIR grain analyzer using the default calibration for hard red winter wheat (HRW) (Perten Instruments, Huddinge, Sweden). Grain

protein yield (GPY, kg/ha) was calculated by multiplying grain yield in kg/ha by GPC. Six grams of seed from each plot were ground into whole meal using a UDY Cyclone Sample Mill with a 1.0 mm screen (Udy Corporation, Fort Collins, CO). LA-SDS SRC was measured on one sample from each plot following Seabourn et al., (2012) using grain moisture values. A protein quality score (PQS) for each sample was calculated by dividing LA-SDS SRC by GPC.

Genotyping

The procedure by which the genotype data were generated and processed is described in detail by Nyine et al. (2021). In brief, Whole-genome shotgun sequencing of 6 *T. aestivum* and 21 *Ae. tauschii* parental accessions was performed and the sequence reads were processed to generate high density SNP markers across the D-genome based on Chinese Spring v1.0 as the reference. The introgression lines were genotyped according to Nyine et al. (2020) using a low coverage skim-sequencing based approach. Using the high-density SNPs from parental lines as a reference panel, missing and ungenotyped SNPs in the GBS data were imputed using Beagle v.5.0 (Browning and Browning 2013) followed by filtering to remove SNPs with genotype probability below 0.7, which eliminates low confidence imputed SNPs, and minor allele frequency less than 0.05. This resulted in approximately 5.2 million SNPs which were used to calculate haplotype blocks as described below.

Model Specification and Data Analysis

Each phenotypic trait of interest was fitted with a general linear mixed model of the following specification:

$$y_{ij} = n + b_i + g_j + e_{ij}$$

where, y_{ij} is the observed response of the jth genotype within the ith environment, η is the intercept, b_i (i=1,…,4) is the ith environment, g_j (j=1,…,351) is the jth genotype, and e_{ij} is the

leftover residual unique to the jth genotype within the ith environment with $e_{ij} \sim N(0, \sigma_e^2)$. Genotype and environment were considered as random effects in the linear predictor of the statistical model with $g_j \sim N(0, \sigma_g^2)$ and $b_i \sim N(0, \sigma_b^2)$, and b_i, g_j, and e_{ij} are assumed to be independent of each other. Restricted maximum likelihood was used to estimate variance components. Studentized residuals were used to evaluate model assumptions. The GLIMMIX procedure in SAS (Version 9.4, SAS Institute, Cary, NC) was used to fit the model. For each phenotypic trait, broad-sense heritability (H^2) was computed using variance components estimates, as follows:

$$H^2 = \hat{\sigma}_g^2 \,/\, (\hat{\sigma}_g^2 + \frac{\hat{\sigma}_e^2}{r})$$

where σ_g^2, and σ_e^2 are the variance of the genotypes and residuals, respectively, and *r* is the number of environments (He et al. 2016). Pearson's correlations were calculated between each end-use quality trait across the four environments as well as between adjusted means of each trait using basic R functions (R Core Team, 2017).

Comparisons between the introgression lines relative to the parents were performed for each trait within environments via *t*-tests using a Dunnett adjustment to control experiment-wise Type I error at 5%.

Haplotype Blocks

To reduce the dimensionality of the genotype data and capture variation in the introgressed segments from *Ae. tauschii*, Nyine et al. (2021) converted the SNP data into HBs. The R package HaploBlocker v1.5.2 was used to infer HBs from the 5.2 million SNPs. Default parameters for HaploBlocker were used except node_min which was reduced to 2 (default is 5). This parameter controls the number of haplotypes calculated per node, where a node represents an allelic sequence. The value for this parameter was lowered to account for the low number of haplotype

variants within these families (Pook et al., 2019). HBs were split into genomic windows and the haplotype variants in each genomic window were scored to generate a numeric matrix of haplotypes that were used in the downstream analyses.

Population Structure

Principal component analysis (PCA) was performed using the R package GAPIT v3 (Wang & Zhang, 2018). The kinship matrix was generated from GAPIT using the VanRaden method (VanRaden, 2008). Haplotype block data was used to generate 2 dimensional PCA plots of the first two principal components showing genetic structure using the ggplot2 package (Wickham, 2016) in R (R Core Team, 2017). Plots were generated with and without the inclusion of the *T. aestivum* and *Ae. tauschii* parents.

Haplotype-Based GWAS

Genome-wide association mapping was performed for the five end-use quality traits for each individual environment using raw data and adjusted means calculated across environments. The analysis was conducted using the MLM statistical method (Yu et al., 2005) implemented in the R package GAPIT v3 (Wang & Zhang, 2018) using the following model specification:

$$y = S_i + Q + K + e$$

whereby y indicates end-use quality traits, Si represents the effect of the ith haplotype block, i = 1, 2, …, n, Q represents principal components included as explanatory covariate variables used to account for population structure, K is the individual genetic effects and are assumed random with variance structure (Zhang, 2022). The optimal number of PCs to include in the model was determined using the *model.selection* function. This function performs Bayesian information criteria (BIC)-based model selection comparing models including different numbers of PCs for

each trait-environment evaluated. The number of PCs with the smallest Bayesian information criteria (BIC) value was selected and used in the model to control population structure. The kinship matrix automatically calculated in GAPIT was used to adjust kinship between ILs. Corrections for multiple testing of HB-trait associations was performed using the false discovery rate (FDR) method (Benjamini & Hochberg, 1995) with an FDR corrected p-value < 0.05. The percentage of phenotypic variance explained by each HB was estimated as the difference between the likelihood ratio-based R^2 of the model with the HB and the likelihood ratio-based R^2 of the model without the HB, both of which were obtained from the GAPIT output file. Regions showing associations detected using the BLUPs were considered stable and were used for further investigation. Loci with significant HBs obtained from the GWAS analysis were further evaluated to determine the variation and effect of introgressions from *Ae. tauschii*. ILs were grouped based on the source of their haplotype regarding the parental species. A *t*-test was conducted to determine differences between the haplotypes.

Identification of Candidate Genes

The physical positions of flanking SNPs for each significant HB were used to identify potential candidate genes (CG) located in these regions. The sequence of each flanking SNP was aligned against the Chinese Spring reference genome, IWGSC RefSeq v1.0, in the Ensemble Plants window browser (http://plants.ensembl.org/index.html). The region in between these flanking SNPs was searched for potential candidate genes. The gene annotation and predicted function, if present, were extracted for each candidate using the gene ontology database available at Ensemble Plants.

Results

Phenotypes

Heritability across environments was low for GPY ($\hat{H}^2 = 0.25$), moderate for GTW ($\hat{H}^2 = 0.55$), and high for SRC ($\hat{H}^2 = 0.82$), GPC ($\hat{H}^2 = 0.87$), and PQS ($\hat{H}^2 = 0.88$). Figure 1-2(a-e) shows Pearson correlations of model estimates for each end-use quality trait between environments. Analysis of comparisons between environments within individual traits showed significant positive correlations at ($P<0.001$) between all environments for all traits. Pearson correlations were also calculated between BLUPs generated for each phenotypic trait (Figure 1-2f). BLUPs for LA-SDS SRC was significantly positively correlated ($P < 0.001$) with PQS, GPC, and GTW. GPY and GTW correlation were also significantly positive ($P<0.001$). GPC was significantly negatively correlated ($P < 0.05$) with PQS and GPY. For each trait, the estimated means of ILs and parents are reported in Table 1-1, while distributions of ILs are shown in Figure 1-1. The ILs showed significantly higher values relative to the parents for SRC in E1 and PRO in E1, E2, and E3. Meanwhile, significantly higher values were observed for the parents relative to the ILs for PQS in E2 and E3 and GPY in E2, E3, and E4.

Genotyping Data and Haplotype Inference

The detailed description of genome sequencing, SNP calling, and haplotype inference used in this study are provided in Moses et al. (2021). Briefly, a total of 5,207,921 high quality SNPs were generated for the introgression population. The SNPs spanned a total physical distance of 3,611.91 Mb. Marker density per chromosome ranged from .00049 Mb on chromosome 4D to .00281 Mb on chromosome 3D (Table 1-2). The number of SNPs present on each chromosome ranged from 189,535 on chromosome 3D to 1,033,061 on chromosome 4D.

The 5.2 million SNPs were placed into a total of 15,967 HBs across the seven D-genome chromosomes (Table 1-2). The greatest number of HBs was found on chromosome 7D with 3,177. Chromosome 3D had the fewest number of HBs with 687. A total of 403 SNPs were not placed into any HB. All chromosomes except 3D contained maximum HB sizes ranging from 2.03 Mb on chromosome 4D to 5.43 Mb on chromosome 1D. The largest HB on chromosome 3D was 16.16 Mb. The average spacing between HBs was 0.47 Mb across all chromosomes and ranged from 3.52 Mb on chromosome 6D to 17.13 Mb on chromosome 3D.

Population Structure

Figure 1-3a shows a PCA scatterplot of the first two principal components calculated for haplotype data including the ILs and the parents. PC1 explained 10.13 percent of the variability and PC2 explained 10.12% of the variability. The different colored points represent the ILs, *T. aestivum* parents, *Ae. tauschii* ssp. *strangulata* parents, and *Ae. tauschii* ssp. *tauschii* parents. The *T. aestivum* (purple) and *Ae. tauschii* ssp. *strangulata* parents (red) clustered to the far right of the figure while the *Ae. tauschii* ssp. *tauschii* parents (green) clustered to the far left. This pattern is consistent with previous studies suggesting *Ae. tauschii* ssp. *strangulata* as the original source of the D-genome in hexaploid wheat (Dvorak et al., 1998; Wang et al., 2013). The ILs (blue) are distributed between the parental clusters. The ILs show a pattern of clustering back towards the *T. aestivum* parents which is expected due to the backcross scheme used in population development. Figure 1-3b is the PCA scatterplot including only the ILs. In this figure, PC1 explained 14.21% of the variability while PC2 explained 10.51%. The different colored points represent the 26 different families. This figure does not show evidence of clustering based on family and the variability explained by PC1 appears to be due to differences in amount of genetic material introgressed from the *Ae. tauschii* accessions.

GWAS Analysis

Table 1-4 shows results for GWAS analyses on each of the end-use quality traits of interest. We identified four HBs associated with SRC on chromosomes 3D and 6D (Table 1-4; Figure A-1; Table A-4). HAP_6D_B2393 was associated with LA-SDS SRC and explained 5.72% to 6.64% of the phenotypic variance. HAP_6D_B2354 was linked with an increase in both SRC and PQS. HAP_6D_B2354 was associated with SRC in E2, E4, and the BLUP. The HAP_6D_B2354 haplotype conferring an increase in solvent retention capacity was found only in the *T. aestivum* parents and it explained 6.03% to 7.18% of the phenotypic variance for this trait. HAP_3D_B47 contained a haplotype unique to *Ae. tauschii* that was not found in any of the *T. aestivum* parents. This haplotype was associated with a greater LA-SDS SRC than the haplotype contributed by *T. aestivum* (Figure 1-4) and explained 5.09% to 6.62% of the variance for SRC. The positive haplotype was present in 19 of the 21 accessions including all ssp. *tauschii* accessions and one ssp. *strangulata* accession (Table 1-3). HAP_6D_B2384 also contained a haplotype unique to *Ae. tauschii* that was associated with an increase in LA-SDS SRC (Figure 1-4). This HB explained 5.58% to 5.75% of the variance for LA-SDS SRC. The positive haplotype was present in 18 of the 21 accessions including 16 ssp. *tauschii* accessions and two ssp. *strangulata* accession (Table 1-3).

Nine HBs were detected on chromosomes 1D and 6D (Table 1-4; Figure A-2; Table A-4) associated with PQS. Eight of these HBs associated with an increase in PQS were present in both a *T. aestivum* parent and *Ae. tauschii* accession with at least one accession representing each species. HBs HAP_1D_B188 and HAP_1D_B189 were located next to each other in the genome and likely are part of the larger haplotype spanning this genomic region. Both haplotypes were associated with PQS in E2 and E3 where they explained from 6.17% to 8.37% of the phenotypic

615 variance. These two HBs were also associated with GTW in E1 explaining 6.66% of the
616 variance. These results suggests that the genomic interval spanning HAP_1D_B188 and
617 HAP_1D_B189 contributes to both PQS and GTW. Five HBs including HAP_1D_B2116,
618 HAP_1D_B2117, HAP_1D_B2118, HAP_1D_B2121, and HAP_1D_B2122 were all located
619 within a 1.3 Mb interval on the long arm of chromosome 1D suggesting that they represent parts
620 of the larger haplotype block associated with variation in PQS. The HAP_1D_B2116 and
621 HAP_1D_B2117 haplotypes from this genomic region explained the largest proportion of
622 variance for PQS ranging from 6.05% to 12.18% and 6.43% to 11.89%, respectively. These two
623 regions also showed significant association with GPC in E4. HAP_6D_B2354 associated with
624 PQS contained a haplotype unique to *T. aestivum* conferring an increase in PQS relative to the
625 *Ae. tauschii* haplotype. This haplotype explained 6.66% to 8.62% of the variance for PQS and
626 was also associated with an increase in LA-SDS SRC.
627 Three HBs, HAP_1D_B2116, HAP_1D_B2117, and HAP_6D_B2399, showed
628 associations with GPC on chromosomes 1D and 6D (Table 1-4; Figure A-3; Table A-4).
629 Haplotypes unique to either the *T. aestivum* parents or the *Ae. tauschii* accessions were not
630 associated with differences in GPC. The HAP_1D_B2116 and HAP_1D_B2117 HBs were only
631 associated with GPC in E4; however, they were included since they co-localized with HBs for
632 PQS in multiple environments. HAP_6D_2399 was detected in E1, E2, and the BLUP on the
633 long arm of chromosome 6DS. This region explained 5.62% to 6.74% of the phenotypic
634 variation for GPC.
635 No stable associations between haplotypes and GTW were detected (Figure A-4). The
636 HAP_1D_B188_H2 and HAP_1D_B189_H2 HBs were only detected in E1 for GTW. These

637 blocks were also associated with PQS in multiple environments (Table 1-4; Table A-4). The
638 positive haplotypes for these two blocks were not unique to either parental source.

639 **Candidate Genes**

640 To facilitate future functional studies aimed at detection of candidate genes (CGs)
641 underlying variation in the end-use quality traits in wheat, we performed functional annotation of
642 genes in the regions overlapping with HBs showing significant association with the analyzed
643 traits. The results are presented in Table A-4. Candidate genes for *T. aestivum* within the
644 intervals or near them were identified and are listed along with *Ae. tauschii* orthologs and gene
645 ontologies if present. Five HBs contained CGs within their genomic interval. The remaining HBs
646 did not harbor annotated CGs located within the interval and were located between 545 bp and
647 2.9 kb away from the nearest CG. The identified CGs were mostly involved in oxidation
648 reduction processes, DNA-binding transcription factor activity, protein binding, and protein
649 phosphorylation. However, some HBs were ~2-3 Mb away from CGs encoding high molecular
650 weight glutenins.

651 **Discussion**

652 Wheat end-use quality is an important breeding target as millers and bakers in the
653 downstream industries rely on specific quality characteristics of the grain, flour, and dough to
654 make their products. Extensive research has been done investigating the genomic regions
655 associated with end-use quality traits (Shewry & Halford, 2002; Xue et al., 2019). Previous
656 studies have identified multiple alleles of glutenin and gliadin encoding genes with specific
657 alleles conferring more desirable bread-making quality depending on the market class (Payne et
658 al., 1980; Zheng et al., 2009; Henkrar et al., 2017; Utebayev et al., 2019). Selection pressure and
659 drift throughout the domestication process, polyploidization, and primary focus on increasing

yield levels through conventional plant breeding likely resulted in unintentional loss of allelic diversity associated with high end-use quality (Haudry et al., 2007; Akhunov et al., 2010; Venske et al., 2019). Therefore, breeders and geneticists are interested in searching through collections of wild relatives and related species to discover novel alleles with potential to improve end-use quality traits within breeding programs.

We used dense sequence-based genotyping data including nearly 5.2 million SNPs developed for a set of hexaploid wheat lines containing introgressions from *Ae. tauschii* accessions (Nyine et al., 2021) to conduct a haplotype-based GWAS for a set of end-use quality traits. This study identified 13 regions associated with SRC, PQS, GPC, and GTW in multiple environments on chromosomes 1D, 3D, and 6D. The higher number of associations found for SRC and PQS relative to other traits could be due to the robust nature of SRC to large environmental variability that can affect wheat yield consistently observed in Kansas (Guttieri et al., 2001; Guttieri & Souza, 2003). Two potential novel haplotypes on chromosomes 3D and 6D introgressed from *Ae. tauschii* were associated with PQS and SRC.

The region on chromosome 1D consisting of HBs HAP_1D_B2116 to HAP_1D_B2122 spanned a genomic interval of 1.3 Mb and was associated with PQS and GPC. Twenty-three CGs were identified within this main region ranging from TraesCS1D02G321500 to TraesCS1D02G323600 with functions including DNA-binding transcription factor, ion transport, transferase activity, serine-type peptidase activity, ADP binding, protein binding, and oxidation-reduction process. Proximal to HAP_1D_B2116 at 2.7 Mb is located a major HMW glutenin gene *GLU-D1* (International Wheat Genome Sequencing Consortium et al., 2018). This is a likely candidate for the association as variation in PQS is linked to glutenin composition of the flour. Several major alleles have been discovered at this locus, *Glu-D1a, b, c, d, e, and f*

683 (Nakamura, 1999). The *Glu-D1d* allele encodes the *1Dx5* and *1Dy10* subunits, which are
684 associated with higher dough strength resulting in increased bread making quality and are
685 typically desired in hard wheat breeding programs. The *Glu-D1a* allele encodes the *1Dx2* and
686 *1Dy12* subunits, which are preferred in soft wheat programs (Liu et al., 2014). No haplotypes
687 unique to either species were detected in this region suggesting that the alleles detected in this
688 study are present in both *T. aestivum* and *Ae. tauschii* which is consistent with previous reports
689 (Dong et al., 2013).
690 Three HBs, HAP_1D_120, HAP_1D_188, and HAP_1D_189 on the short arm of
691 chromosome 1D showed stable association with PQS, with the latter two also linked with
692 variation in GTW in a single environment. The LMW glutenin gene *Glu-D3* is located
693 approximately 85 kb to 100 kb from the distal end of the chromosome 1DS (International Wheat
694 Genome Sequencing Consortium et al., 2018). Numerous studies have detected QTL in this
695 region on 1DS (Liu et al., 2017; Goel et al., 2019; Zhou et al., 2021). The regions identified in
696 our study were located 42.2 and 55.3 Mb proximal to *Glu-D3*, suggesting that this region might
697 contain a separate locus affecting end-use quality. HAP_1D_120 contained one CG within the
698 interval, TraesCS1D02G062400 with unknown function. Another CG, TraesCS1D02G062300,
699 was located 29.6 kb distal and was associated with protein phosphorylation. HAP_1D_188
700 contained three CGs within the interval, TraesCS1D02G073900, TraesCS1D02G074300, and
701 TraesCS1D02G074400, which functioned as mitochondrial pyruvate transmembrane transport,
702 oxidation-reduction process, and transmembrane transport, respectively. A previous study by
703 Yang et al., 2020 detected a region associated with dough water absorption and SDS
704 sedimentation volume located 34.9 Mb from the distal end of 1DS. This region harbored a

candidate gene, TraesCS1D02G086700 located at 71.3 Mb, that encodes an aminotransferase whose homologue in rice is associated with variation in quality traits.

One HB associated with SRC was detected on the short arm of chromosome 3D. The haplotype contributed by *Ae. tauschii* was linked to an increase in LA-SDS SRC. The HB region spanned a relatively large physical distance of 355.6 kb. Chromosome 3D showed much less diversity overall compared to the other chromosomes with fewer SNPs, HBs, and larger HB sizes. Possible explanations for this occurrence could be limited diversity at this chromosome in the selected accession used in this study. The study by Nyine et al. (2019) did not show a significant reduction in diversity for chromosome 3D; however, a significantly lower number of SNPs were used in that study. The large size of the HB region resulted in 7 CGs located within the interval. Their functions involved myosin binding, response to abscisic acid, protein phosphorylation, enzyme inhibitor activity, and oxidation reduction. Previous studies have shown association between protein phosphorylation and oxidation-reduction processes with end-use quality traits in wheat (Li et al., 2020; Muqaddasi et al., 2020; Wang et al., 2020; Gao et al., 2021).

The gliadin gene *Gli-D2* associated with gluten composition and the grain protein gene *GPC-D1* are located on the short arm of chromosome 6D; however, no significant associations were detected in these regions in the current study. Four stable HBs, HAP_6D_2354 (SRC and PQS), HAP_6D_2384 (SRC), HAP_6D_2393 (SRC), and HAP_6D_2399 (GPC), were detected on the long arm of chromosome 6D. Haplotype block HAP_6D_2354 associated with improved SRC and PQS was unique to *T. aestivum* and was not present in any *Ae. tauschii* accessions. Four CGs, TraesCS6D02G365200, TraesCS6D02G365300, TraesCS6D02G365400, and TraesCS6D02G365600 were detected between 545 bp to 13.9 kb from this genomic interval.

728 TraesCS6D02G365200 was located 545 bp proximal to the HB and is associated with protein
729 binding. The other three genes were located distal to the region with one having an unknown
730 function and the other two involved in oxidation-reduction processes. The haplotype for
731 HAP_6D_2384 associated with an increase in LA-SDS SRC was unique to *Ae. tauschii* and was
732 not present in any of the *T. aestivum* parents. The CG TraesCS6D02G386300 fell within this HB
733 region and is involved in the oxidation reduction process. The consistency of CGs associated
734 with oxidation-reduction process suggests its importance in determining end-use quality in
735 wheat. This conclusion agrees with a recent study by Gao et al. (2021), which provides evidence
736 for the impact of oxidation-reduction genes on quality parameters and demonstrates that a gene
737 involved in the regulation of seed storage proteins and starch accumulation was also associated
738 with upregulation of oxidation-reduction processes. Another study showed an association
739 between oxidation reduction processes and seed-specific genes in rice (Yang et al., 2011). One
740 CG, TraesCS6D02G390100, detected 24.7 kb distal from HAP_6D_2393 was associated with
741 ATP binding and phosphatidylinositol phosphate kinase activity. Two CGs for HAP_6D_2399,
742 TraesCS6D02G393400 and TraesCS6D02G393300, were located10 kb and 22 kb proximal,
743 respectively. Gene ontology revealed these genes function as integral membrane components and
744 protein binding factors. Previous studies have reported QTL associated with flour protein on
745 6DL (Tsilo et al., 2011; Zhang et al., 2020) with the more recent study by Zhang et al. (2020)
746 identifying a region located 31.8 Mb to 44.3 Mb proximal to the regions identified in this study.
747 Enhancing baking quality in wheat is a priority for breeding programs. Research studies
748 aimed at identifying new genes and alleles underlying these traits is the first step towards
749 improving germplasm within the programs. The results of this study show that wild relatives of
750 wheat could be a source of potentially beneficial loci for improving end-use quality traits. Two

751 unique haplotypes from *Ae. tauschii* showed association with the bread-making traits in the
752 current population. The alleles at these regions are potential sources for improving baking quality
753 in the breeding program. However, because only six *T. aestivum* parents were included in this
754 study, there is still a chance that these alleles already exist in a broader range of bread wheat
755 germplasm. Development of markers and screening of diverse germplasm will need to be
756 performed to determine the frequency of these alleles in the breeding programs. Positive
757 haplotypes found only in *T. aestivum* parents suggest that breeding for end-use quality traits in
758 bread wheat selected for useful diversity outside of the mini-core set of *Ae. tauschii* lines used in
759 this study. While this core set of accessions captures a broad range of diversity from the wild
760 relative, untapped diversity in other germplasm pools of *Ae. tauschii* may still exist.
761

Acknowledgements: The generation of genomic data for this project was supported by the Agriculture and Food Research Initiative Competitive Grants 2019-67013-29017 and 2017–67007-25939 (WheatCAP) from the USDA National Institute of Food and Agriculture. We would like to thank KSU Integrated Genomics Facility for sequencing genomic libraries.

Author contribution: E.A. and M.N. contributed data from whole genome sequencing of parental genotypes, genotyping, imputation, and haplotype inference in the introgression population.

763 **Figure 1-1.** Violin plots showing the phenotypic distributions and median values of five end-use
764 quality traits (SRC, PQS, GPC, GPY, GTW) across four environments.

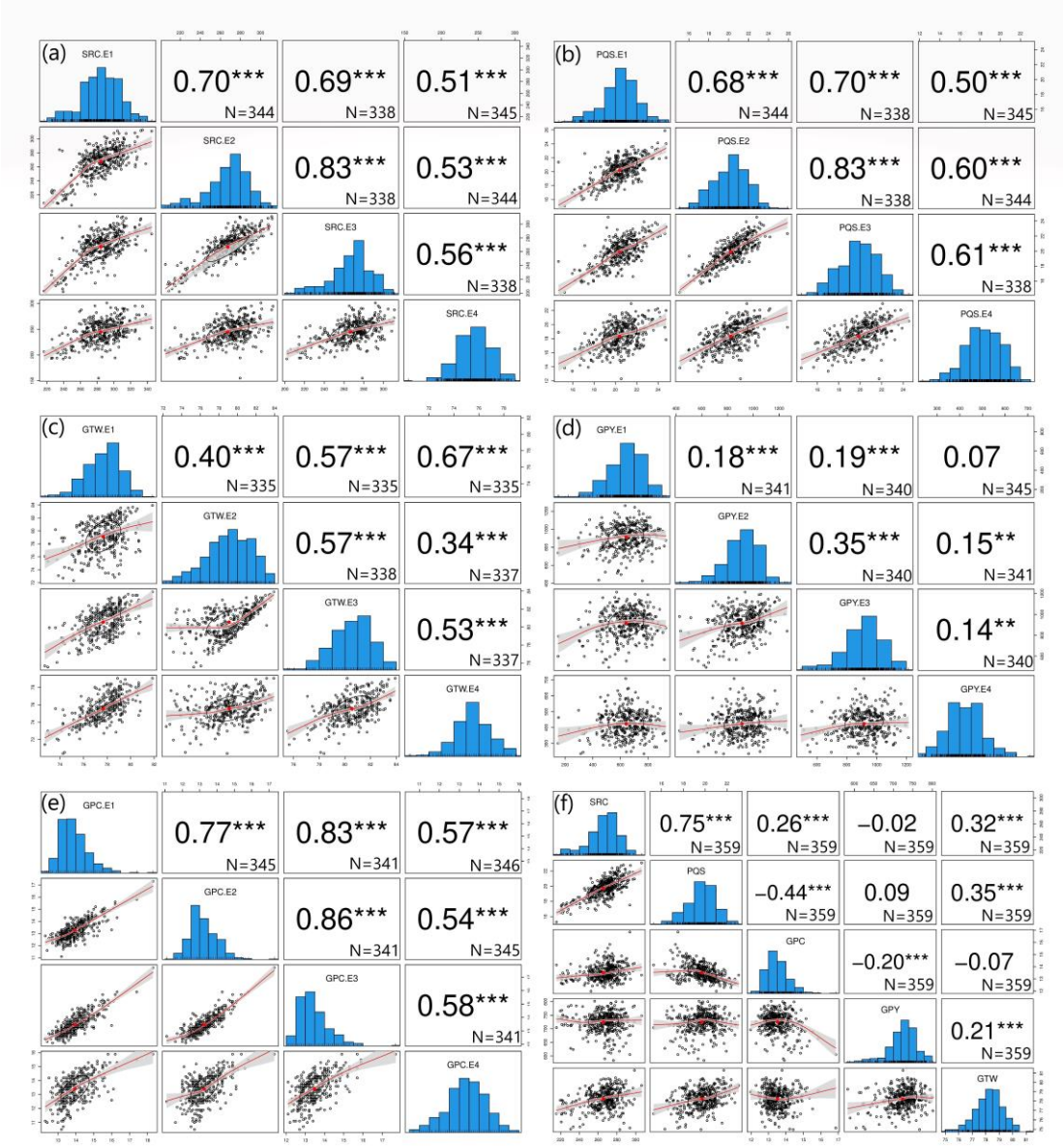

Figure 1-2. Scatterplot matrices (lower triangle), histograms (main diagonal) and Pearson correlations (upper triangle) of model estimates for each end-use quality trait between environments (A-E) and comparisons of BLUPs between each end-use quality trait (F). The diagonal shows the distribution of each variable as well as displaying the abbreviation for each end-use quality traits and the corresponding environment (E1, E2, E3, and E4). * ($P < 0.05$), ** ($P < 0.01$), *** ($P < 0.001$). The lower triangle displays bivariate scatter plots fitted with a LOESS curve.

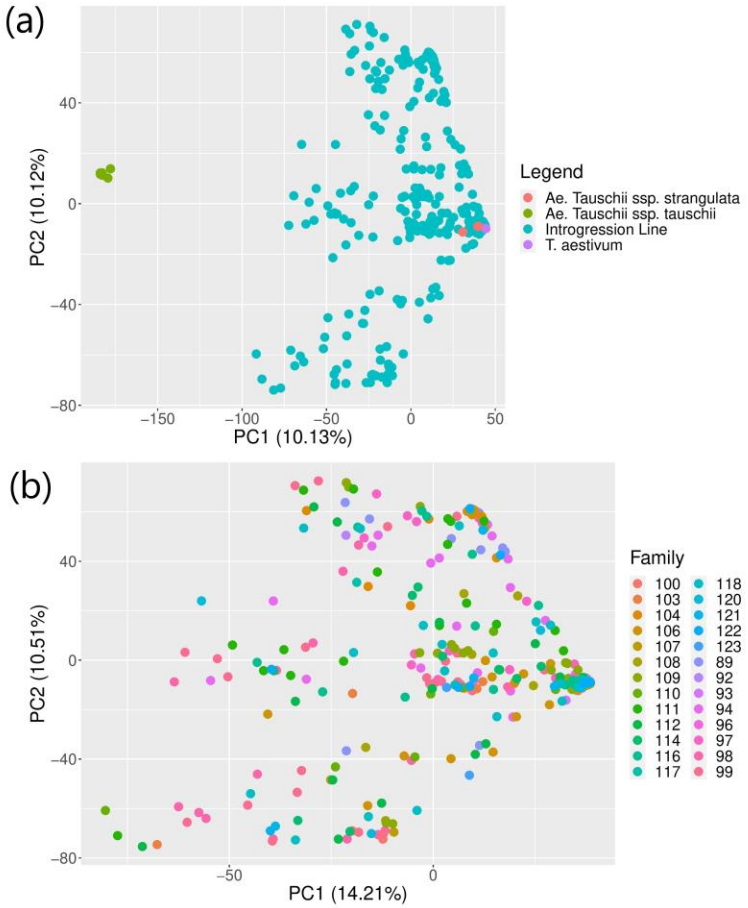

773 **Figure 1-3.** (A) Scatterplot displaying PC1 [of what?] on the X-axis and PC2 on the Y-axis.
774 Individual points represent genotypes with color differentiating introgression lines (blue), T.
775 aestivum parents (purple), Ae. tauschii ssp. strangulata parents (red), and Ae. tauschii ssp.
776 tauschii parents (green). (B) Scatterplot displaying PC1 on the X-axis and PC2 on the Y-axis.
777 Individual points represent only the introgression lines with color differentiating the 26 families.

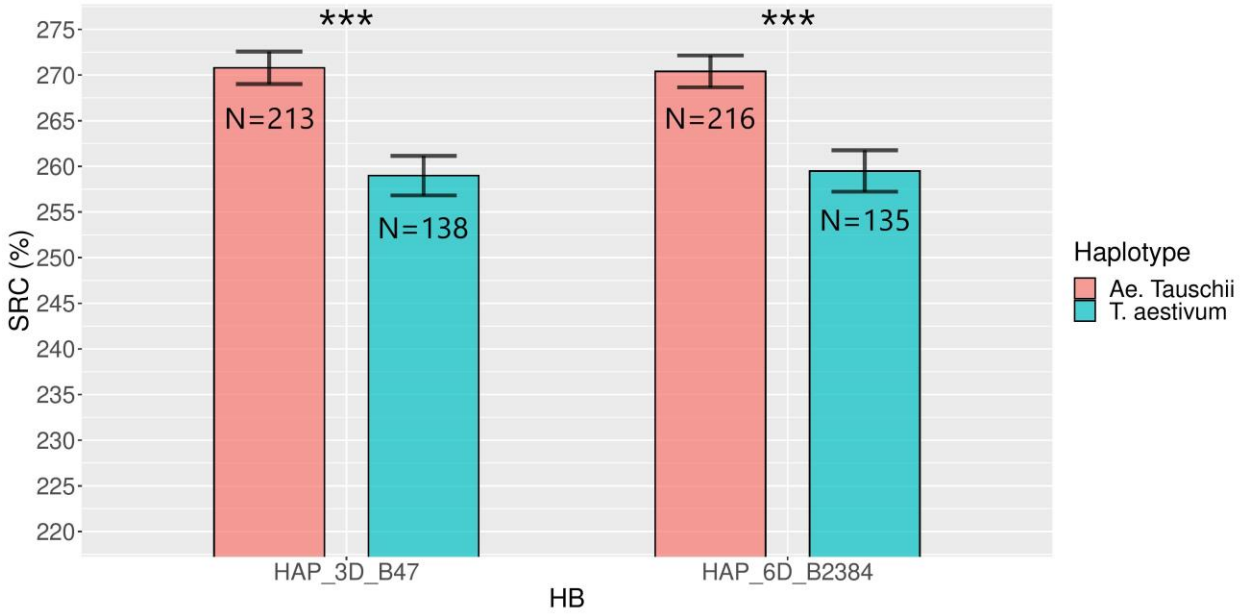

Figure 1-4. Bar chart figure displaying estimated means for solvent retention capacity (SRC %) of *Ae. tauschii* haplotype and *T. aestivum* haplotype for the haplotype blocks HAP_3D_B47 and HAP_6D_B2384. , * ($P < 0.05$), ** ($P < 0.01$), *** ($P < 0.001$)

Table 1-1. Estimated means of end-use quality traits for introgression lines (IL) and parents, as well as their differences, within each environment (ENV).

ENV	Trait	IL (Mean ± SEM)	Parent (Mean ± SEM)	Difference*	Standard Error Difference	*df*	Pr > |t|
E1	SRC	284.19 ± 1.18	262.09 ± 6.54	22.11	6.65	380	0.001
E1	PQS	20.41 ± 0.09	20.11 ± 0.47	0.30	0.48	377	0.5434
E1	PRO	13.96 ± 0.04	13.04 ± 0.23	0.93	0.24	377	<.0001
E1	GPY	641.39 ± 6.68	641.98 ± 36.83	-0.60	37.44	375	0.9874
E1	GTW	77.67 ± 0.08	78.39 ± 0.43	-0.73	0.44	365	0.0969
E2	SRC	267.46 ± 1.10	271.64 ± 5.10	-4.18	5.22	380	0.4246
E2	PQS	20.22 ± 0.09	21.14 ± 0.41	-0.92	0.43	380	0.0313
E2	PRO	13.27 ± 0.04	12.86 ± 0.19	0.41	0.20	381	0.0359
E2	GPY	912.45 ± 7.12	1025.65 ± 32.86	-113.20	33.63	377	0.0008
E2	GTW	79.1 ± 0.13	78.93 ± 0.58	0.18	0.6	379	0.7723
E3	SRC	266.66 ± 1.12	269.26 ± 5.00	-2.60	5.13	375	0.6123
E3	PQS	19.85 ± 0.93	20.91 ± 0.42	-1.06	0.43	375	0.0137
E3	PRO	13.47 ± 0.04	12.89 ± 0.18	0.59	0.18	378	0.0014
E3	GPY	915.54 ± 6.65	999.79 ± 29.80	-84.25	30.54	377	0.0061
E3	GTW	80.55 ± 0.08	80.61 ± 0.36	-0.07	0.38	375	0.8622
E4	SRC	244.69 ± 1.14	241.24 ± 5.29	3.46	5.41	381	0.5238
E4	PQS	18.33 ± 0.10	18.71 ± 0.44	-0.38	0.46	381	0.4055
E4	PRO	13.41 ± 0.05	13.00 ± 0.24	0.42	0.25	382	0.0894
E4	GPY	423.58 ± 4.14	485.24 ± 19.23	-61.66	19.67	382	0.0019
E4	GTW	58.38 ± 0.23	58.93 ± 1.07	-0.55	1.10	375	0.6177

* Postive values correspond to differences where the introgression population had a higher LSmean while negative values represent differences where the parents had a higher LSmean.

785 **Table 1-2.** Genotype Summary.

Chromosome	SNP Count	Distance (Mb)	Max SNP Density (Mb)	Average SNP Density (Mb)	HB Count	SNP Count per HB		HB Size (Mb)		HB Spacing (Mb)	
						Max	Average	Max	Average	Max	Average
1D	723324	491.11	5.10	0.00068	2,370	7,523	305.20	5.44	0.13	5.10	0.08
2D	672860	534.05	7.12	0.00079	2,218	4,293	297.60	4.97	0.14	10.48	0.10
3D	189535	533.28	17.13	0.00281	687	189,535	550.97	16.17	0.39	17.13	0.40
4D	1033061	509.50	5.16	0.00049	2,509	7,110	411.74	2.03	0.14	5.17	0.07
5D	844401	536.57	4.33	0.00064	2,496	6,627	338.30	2.71	0.14	4.34	0.09
6D	852905	470.73	3.52	0.00055	2,415	8,345	353.17	2.27	0.13	3.52	0.07
7D	891968	536.68	5.42	0.00060	3,177	5,259	280.76	3.83	0.12	5.42	0.06

786

Table 1-3. The twenty-one *Ae. tauschii* accessions and their respective subspecies classification. The two columns to the right show which accessions contain haplotypes unique to *Ae. tauschii* for the haplotype blocks HAP_3D_B47 and HAP_6D_B2384. Accessions labeled "*Ae. tauschii*" possess haplotypes unique to this species, while those labeled "*T. aestivum*" contain haplotypes that are also found in bread wheat and are therefore not unique to *Ae. tauschii*.

Accession	Subspecies	HAP_3D_B47	HAP_6D_B2384
TA10142	*strangulata*	*T. aestivum*	*Ae. tauschii*
TA1642	*strangulata*	*T. aestivum*	*T. aestivum*
TA2378	*strangulata*	*Ae. tauschii*	*Ae. tauschii*
TA10077	*tauschii*	*Ae. tauschii*	*Ae. tauschii*
TA10106	*tauschii*	*Ae. tauschii*	*Ae. tauschii*
TA10155	*tauschii*	*Ae. tauschii*	*Ae. tauschii*
TA10166	*tauschii*	*Ae. tauschii*	*Ae. tauschii*
TA10189	*tauschii*	*Ae. tauschii*	*Ae. tauschii*
TA10193	*tauschii*	*Ae. tauschii*	*Ae. tauschii*
TA1634	*tauschii*	*Ae. tauschii*	*Ae. tauschii*
TA2374	*tauschii*	*Ae. tauschii*	*Ae. tauschii*
TA2388	*tauschii*	*Ae. tauschii*	*Ae. tauschii*
TA2389	*tauschii*	*Ae. tauschii*	*T. aestivum*
TA2395	*tauschii*	*Ae. tauschii*	*Ae. tauschii*
TA2398	*tauschii*	*Ae. tauschii*	*T. aestivum*
TA2489	*tauschii*	*Ae. tauschii*	*Ae. tauschii*
TA2521	*tauschii*	*Ae. tauschii*	*Ae. tauschii*
TA2536	*tauschii*	*Ae. tauschii*	*Ae. tauschii*
TA2538	*tauschii*	*Ae. tauschii*	*Ae. tauschii*
TA2543	*tauschii*	*Ae. tauschii*	*Ae. tauschii*
TA2567	*tauschii*	*Ae. tauschii*	*Ae. tauschii*

Table 1-4. Details of 9 stable haplotype blocks associated with end-use quality traits.

Trait	HB[a]	Chr.	Start (bp)[b]	End (bp)[c]	GWAS Significance[d]	R^2 (%)[e]	Positive Source[f]
SRC	HAP_3D_B47	3D	26382902	26738476	**	5.09 – 6.62	*Ae. Tauschii*
SRC	HAP_6D_B2354	6D	454636091	454639980	**	6.03 – 7.18	*T. aestivum*
SRC	HAP_6D_B2384	6D	463775852	463809722	**	5.58 – 5.75	*Ae. Tauschii*
SRC	HAP_6D_B2393	6D	465141041	465177049	**	5.72 – 6.64	Both
PQS	HAP_1D_B2116	1D	414902844	414917687	**	6.05 – 12.18	Both
PQS	HAP_1D_B2117	1D	414917730	414929805	**	6.43 – 11.89	Both
PQS	HAP_1D_B2118	1D	414929899	414939966	**	6.12 – 8.4	Both
PQS	HAP_6D_B2354	6D	454636091	454639980	***	6.66 – 8.62	*T. aestivum*
GPC	HAP_6D_B2399	6D	467210863	467211385	*	5.62 – 6.74	Both

[a]Stable haplotype blocks associated with BLUPs calculated for end-use quality traits. [bc]Physical genetic interval of each HB in base pairs. [d]Significance of GWAS result for adjusted means using MLM following an FDR controlling procedure where * = ($P < 0.05$), ** = ($P < 0.01$), and *** = ($P < 0.001$). [e]Percent of phenotypic variance explained by each HB. [f]Parental species containing the beneficial haplotype associated with each trait.

References

Akhunov, E. D., Akhunova, A. R., Anderson, O. D., Anderson, J. A., Blake, N., Clegg, M. T., et al. (2010). Nucleotide diversity maps reveal variation in diversity among wheat genomes and chromosomes. *BMC genomics* 11, 702. doi:10.1186/1471-2164-11-702.

Altenbach, S. (2003). Temperature, water and fertilizer influence the timing of key events during grain development in a US spring wheat. *J. cereal sci.* 37, 9. doi:10.1006/jcrs.2002.0483.

Anderson, K. (2017). Protein is where the premium is; it could be as much as $36/acre. *Farm Progress*. Available at: https://www.farmprogress.com/wheat/protein-where-premium-it-could-be-much-36acre [Accessed July 13, 2020].

Avni, R., Zhao, R., Pearce, S., Jun, Y., Uauy, C., Tabbita, F., et al. (2013). Functional characterization of GPC-1 genes in hexaploid wheat. *Planta* 239, 313–324. doi:10.1007/s00425-013-1977-y.

Balfourier, F., Bouchet, S., Robert, S., Oliveira, R. D., Rimbert, H., Kitt, J., et al. (2019). Worldwide phylogeography and history of wheat genetic diversity. *Science Advances* 5, eaav0536. doi:10.1126/sciadv.aav0536.

Barrett, J. C., Fry, B., Maller, J., and Daly, M. J. (2004). Haploview: analysis and visualization of LD and haplotype maps. *Bioinformatics* 21, 263–265. doi:10.1093/bioinformatics/bth457.

Benjamini, Y., and Hochberg, Y. (1995). Controlling the False Discovery Rate: A Practical and Powerful Approach to Multiple Testing. *Journal of the Royal Statistical Society: Series B (Methodological)* 57, 289–300. doi:10.1111/j.2517-6161.1995.tb02031.x.

Bogard, M., Allard, V., Martre, P., Heumez, E., Snape, J. W., Orford, S., et al. (2012). Identifying wheat genomic regions for improving grain protein concentration independently of grain yield using multiple inter-related populations. *Molecular Breeding* 31, 587–599. doi:10.1007/s11032-012-9817-5.

Bonferroni, carlo e. (2008). (Springer New York), 50–51. doi:10.1007/978-0-387-32833-1$_{39}$.

Bonferroni, C. E. (1936). *Teoria statistica delle classi e calcolo delle probabilità*. Libreria internazionale Seeber Available at: https://books.google.com/books?id=3CY-HQAACAAJ.

Boyd, W. J. R., and Lee, J. W. (1967). The control of wheat gluten synthesis at the genome and chromosome levels. *Experientia* 23, 332–333. doi:10.1007/bf02144496.

Branlard, G., Lesage, Véronique S, Bancel, E., Martre, P., Méleard, B., and Rhazi, L. (2015). Coping with wheat quality in a changing environment: Proteomics evidence for stress caused by environmental changes. in, eds. Y. Ogihara, S. Takumi, and H. Handa (Springer Japan), 255–264.

Cabral, A. L., Jordan, M. C., Larson, G., Somers, D. J., Humphreys, D. G., and McCartney, C. A. (2018). Relationship between QTL for grain shape, grain weight, test weight, milling yield, and plant height in the spring wheat cross RL4452/"AC Domain." *PLOS ONE* 13, e0190681. doi:10.1371/journal.pone.0190681.

Carter, A. H., Garland-Campbell, K., Morris, C. F., and Kidwell, K. K. (2011). Chromosomes 3B and 4D are associated with several milling and baking quality traits in a soft white spring wheat (Triticum aestivum L.) population. *Theoretical and Applied Genetics* 124, 1079–1096. doi:10.1007/s00122-011-1770-x.

Chen, H., Bemister, D. H., Iqbal, M., Strelkov, S. E., and Spaner, D. M. (2020). Mapping genomic regions controlling agronomic traits in spring wheat under conventional and organic managements. *Crop Science* 60, 2038–2052. doi:10.1002/csc2.20157.

Chung, O. K., Ohm, J. B., Caley, M. S., and Seabourn, B. W. (2001). Prediction of Baking Characteristics of Hard Winter Wheat Flours Using Computer-Analyzed Mixograph Parameters. *Cereal Chemistry Journal* 78, 493–497. doi:10.1094/cchem.2001.78.4.493.

Cruppe, G., Silva, P., Lemes da Silva, C., Peterson, G., Pedley, K. F., Cruz, C. D., et al. (2020). Genome-wide association reveals limited benefits of pyramiding the 1B and 1D loci with the 2NvS translocation for wheat blast control. *Crop Science*. doi:10.1002/csc2.20397.

Dong, Z., Yang, Y., Li, Y., Zhang, K., Lou, H., An, X., et al. (2013). Haplotype Variation of

Glu-D1 Locus and the Origin of Glu-D1d Allele Conferring Superior End-Use Qualities in Common Wheat. *PLoS ONE* 8. doi:10.1371/journal.pone.0074859.

Earl, D. A., and vonHoldt, B. M. (2011). STRUCTURE HARVESTER: a website and program for visualizing STRUCTURE output and implementing the Evanno method. *Conservation Genetics Resources* 4, 359–361. doi:10.1007/s12686-011-9548-7.

Evanno, G., Regnaut, S., and Goudet, J. (2005). Detecting the number of clusters of individuals using the software structure: a simulation study. *Molecular Ecology* 14, 2611–2620. doi:10.1111/j.1365-294x.2005.02553.x.

Falush, D., Stephens, M., and Pritchard, J. K. (2003). Inference of Population Structure Using Multilocus Genotype Data: Linked Loci and Correlated Allele Frequencies. *Genetics* 164, 1567–1587. Available at: https://www.genetics.org/content/164/4/1567 [Accessed July 16, 2020].

Gabriel, S. B., Schaffner, S. F., Nguyen, H., Moore, J. M., Roy, J., Blumenstiel, B., et al. (2002). The Structure of Haplotype Blocks in the Human Genome. *Science* 296, 2225. doi:10.1126/science.1069424.

Gao, Y., An, K., Guo, W., Chen, Y., Zhang, R., Zhang, X., et al. (2021). The endosperm-specific transcription factor TaNAC019 regulates glutenin and starch accumulation and its elite allele improves wheat grain quality. *The Plant Cell*. doi:10.1093/plcell/koaa040.

Goel, S., Singh, K., Singh, B., Grewal, S., Dwivedi, N., Alqarawi, A. A., et al. (2019). Analysis of genetic control and QTL mapping of essential wheat grain quality traits in a recombinant inbred population. *PLOS ONE* 14, e0200669. doi:10.1371/journal.pone.0200669.

Guttieri, M. J., Baenziger, P. S., Frels, K., Carver, B., Arnall, B., Wang, S., et al. (2015). Prospects for Selecting Wheat with Increased Zinc and Decreased Cadmium Concentration in Grain. *Crop Science* 55, 1712–1728. doi:10.2135/cropsci2014.08.0559.

Guttieri, M. J., Bowen, D., Gannon, D., O'Brien, K., and Souza, E. (2001). Solvent Retention Capacities of Irrigated Soft White Spring Wheat Flours. *Crop Science* 41, 1054–1061.

874 doi:10.2135/cropsci2001.4141054x.

875 Guttieri, M. J., and Souza, E. (2003). Sources of Variation in the Solvent Retention Capacity
876 Test of Wheat Flour. *Crop Science* 43, 1628–1633. doi:10.2135/cropsci2003.1628.

877 Gwirtz, J. A., Willyard, M. R., and McFall, K. L. (2006). "Wheat Quality in the United States of
878 America," in *Future of Flour - A Compendium of Flour Improvement* (Kansas City:
879 Sosland Publishing Co.), 17–42.

880 Haudry, A., Cenci, A., Ravel, C., Bataillon, T., Brunel, D., Poncet, C., et al. (2007). Grinding up
881 Wheat: A Massive Loss of Nucleotide Diversity Since Domestication. *Molecular Biology*
882 *and Evolution* 24, 1506–1517. doi:10.1093/molbev/msm077.

883 He, S., Schulthess, A. W., Mirdita, V., Zhao, Y., Korzun, V., Bothe, R., et al. (2016). Genomic
884 selection in a commercial winter wheat population. *Theoretical and Applied Genetics*
885 129, 641–651. doi:10.1007/s00122-015-2655-1.

886 Henkrar, F., El-Haddoury, J., Iraqi, D., Bendaou, N., and Udupa, S. M. (2017). Allelic variation
887 at high-molecular weight and low-molecular weight glutenin subunit genes in Moroccan
888 bread wheat and durum wheat cultivars. *3 Biotech* 7. doi:10.1007/s13205-017-0908-1.

889 Nutall J.G., G.J. O'Leary, J.F. Panozzo, Walker, C. K., K.M. Barlow, and G.J. Fitzgerald (2017).
890 Models of grain quality in wheat—A review. *Field Crops Research* 202, 136–145.
891 doi:https://doi.org/10.1016/j.fcr.2015.12.011.

892 Jernigan, K. L., Godoy, Jayfred V, Huang, M., Zhou, Y., Morris, C. F., Garland-Campbell, K.
893 A., et al. (2018). Genetic dissection of end-use quality traits in adapted soft white winter
894 wheat. *Frontiers in Plant Science* 9, 271. doi:10.3389/fpls.2018.00271.

895 Jernigan, K. L., Morris, C. F., Zemetra, R., Chen, J., Garland-Campbell, K., and Carter, A. H.
896 (2017). Genetic analysis of soft white wheat end-use quality traits in a club by common
897 wheat cross. *Journal of Cereal Science* 76, 148–156. doi:10.1016/j.jcs.2017.06.005.

898 Joppa, L. R., Du, C., Hart, G. E., and Hareland, G. A. (1997). Mapping Gene(s) for Grain Protein
899 in Tetraploid Wheat (Triticum turgidum L.) Using a Population of Recombinant Inbred

Chromosome Lines. *Crop Science* 37, 1586–1589. doi:10.2135/cropsci1997.0011183x003700050030x.

Jordan, K. W., Wang, S., Lun, Y., Gardiner, L.-J., MacLachlan, R., Hucl, P., et al. (2015). A haplotype map of allohexaploid wheat reveals distinct patterns of selection on homoeologous genomes. *Genome Biology* 16. doi:10.1186/s13059-015-0606-4.

Kaler, A. S., Ray, J. D., Schapaugh, W. T., King, C. A., and Purcell, L. C. (2017). Genome-wide association mapping of canopy wilting in diverse soybean genotypes. *Theoretical and Applied Genetics* 130, 2203–2217. doi:10.1007/s00122-017-2951-z.

Kulwal, P., Kumar, N., Kumar, A., Gupta, R. K., Balyan, H. S., and Gupta, P. K. (2005). Gene networks in hexaploid wheat: interacting quantitative trait loci for grain protein content. *Functional & Integrative Genomics* 5, 254–259. doi:10.1007/s10142-005-0136-3.

Kumar, A., Jain, S., Elias, E. M., Ibrahim, M., and Sharma, L. K. (2018). An Overview of QTL Identification and Marker-Assisted Selection for Grain Protein Content in Wheat. *Eco-friendly Agro-biological Techniques for Enhancing Crop Productivity*, 245–274. doi:10.1007/978-981-10-6934-5_11.

Kweon, M., Slade, L., and Levine, H. (2011). Solvent Retention Capacity (SRC) Testing of Wheat Flour: Principles and Value in Predicting Flour Functionality in Different Wheat-Based Food Processes and in Wheat Breeding—A Review. *Cereal Chemistry Journal* 88, 537–552. doi:10.1094/cchem-07-11-0092.

Li, Q., Pan, Z., Gao, Y., Li, T., Liang, J., Zhang, Z., et al. (2020). Quantitative Trait Locus (QTLs) Mapping for Quality Traits of Wheat Based on High Density Genetic Map Combined With Bulked Segregant Analysis RNA-seq (BSR-Seq) Indicates That the Basic 7S Globulin Gene Is Related to Falling Number. *Frontiers in Plant Science* 11. doi:10.3389/fpls.2020.600788.

Liu, S., Rudd, J. C., Bai, G., Haley, S. D., Ibrahim, A. M. H., Xue, Q., et al. (2014). Molecular Markers Linked to Important Genes in Hard Winter Wheat. *Crop Science* 54, 1304–1321. doi:10.2135/cropsci2013.08.0564.

927 Liu, T., Liu, K., Wang, F., Zhang, Y., Li, Q., Zhang, K., et al. (2017). Conditional and
928 unconditional QTLs mapping of gluten strength in common wheat (Triticum aestivum
929 L.). *Journal of Integrative Agriculture* 16, 2145–2155. doi:10.1016/S2095-
930 3119(16)61564-2.

931 Luo, M.-C. ., Yang, Z.-L. ., You, F. M., Kawahara, T., Waines, J. G., and Dvorak, J. (2007). The
932 structure of wild and domesticated emmer wheat populations, gene flow between them,
933 and the site of emmer domestication. *Theoretical and Applied Genetics* 114, 947–959.
934 doi:10.1007/s00122-006-0474-0.

935 Moonen, J. H. E., Scheepstra, A., and Graveland, A. (1982). Use of the SDS-sedimentation test
936 and SDS-polyacrylamidegel electrophoresis for screening breeder's samples of wheat for
937 bread-making quality. *Euphytica* 31, 677–690. doi:10.1007/bf00039206.

938 Morris, G. P., Ramu, P., Deshpande, S. P., Hash, C. T., Shah, T., Upadhyaya, H. D., et al.
939 (2012). Population genomic anD-genome-wide association studies of agroclimatic traits
940 in sorghum. *Proceedings of the National Academy of Sciences* 110, 453–458.
941 doi:10.1073/pnas.1215985110.

942 Mourad, A. M. I., Belamkar, V., and Baenziger, P. S. (2020). Molecular genetic analysis of
943 spring wheat core collection using genetic diversity, population structure, and linkage
944 disequilibrium. *BMC Genomics* 21. doi:10.1186/s12864-020-06835-0.

945 Muqaddasi, Q. H., Brassac, J., Ebmeyer, E., Kollers, S., Korzun, V., Argillier, O., et al. (2020).
946 Prospects of GWAS and predictive breeding for European winter wheat's grain protein
947 content, grain starch content, and grain hardness. *Scientific Reports* 10, 12541.
948 doi:10.1038/s41598-020-69381-5.

949 Nakamura, H. (1999). Identification of alleles for complex gene loci Glu-A1, Glu-B1, and Glu-
950 FD1, which code for high molecular weight subunits of glutenin in Japanese hexaploid
951 wheat varieties. *Journal of Agricultural and Food Chemistry* 47, 5273–5277.
952 doi:10.1021/jf990151p.

953 Narasimhamoorthy, B., Gill, B. S., Fritz, A. K., Nelson, J. C., and Brown-Guedira, G. L. (2006).

Advanced backcross QTL analysis of a hard winter wheat × synthetic wheat population. *Theoretical and Applied Genetics* 112, 787–796. doi:10.1007/s00122-005-0159-0.

Nyine, M., Adhikari, E., Clinesmith, M., Jordan, K. W., Fritz, A. K., and Akhunov, E. (2020). Genomic Patterns of Introgression in Interspecific Populations Created by Crossing Wheat with Its Wild Relative. *G3: Genes, Genomes, Genetics* 10, 3651–3661. doi:10.1534/g3.120.401479.

Nyine, M., Adhikari, E., Clinesmith, M., Jordan, K., Fritz, A. K., and Akhunov, E. (2019). Understanding the introgression process from Aegilops tauschii into hexaploid wheat through identity by descent analysis and its effect on genetic diversity. *bioRxiv*, 855106. doi:10.1101/855106.

Payne, P. I., Jackson, E. A., Holt, L. M., and Law, C. N. (1984). Genetic linkage between endosperm storage protein genes on each of the short arms of chromosomes 1A and 1B in wheat. *Theoretical and Applied Genetics* 67, 235–243. doi:10.1007/bf00317044.

Payne, P. I., Law, C. N., and Mudd, E. E. (1980). Control by homoeologous group 1 chromosomes of the high-molecular-weight subunits of glutenin, a major protein of wheat endosperm. *TAG. Theoretical and applied genetics. Theoretische und angewandte Genetik* 58, 113–120. doi:10.1007/BF00263101.

Pena, R. J. (2007). *Wheat Production in Stressed Environments*. Dordrecht, The Netherlands: Springer Available at: https://link.springer.com/content/pdf/10.1007%2F1-4020-5497-1.pdf [Accessed May 12, 2020].

Pook, T., Schlather, M., Campos, G. de los, Mayer, M., Schoen, C. C., and Simianer, H. (2019). HaploBlocker: Creation of Subgroup-Specific Haplotype Blocks and Libraries. *Genetics* 212, 1045–1061. doi:10.1534/genetics.119.302283.

Pritchard, J. K., Stephens, M., and Donnelly, P. (2000). Inference of population structure using multilocus genotype data. *Genetics* 155, 945–959. Available at: https://www.genetics.org/content/155/2/945.

Purcell, S., Neale, B., Todd-Brown, K., Thomas, L., Ferreira, Manuel A. R., Bender, D., et al.

(2007). PLINK: A Tool Set for Whole-Genome Association and Population-Based Linkage Analyses. *American Journal of Human Genetics* 81, 559–575. Available at: https://www.ncbi.nlm.nih.gov/pmc/articles/PMC1950838/.

Qi, P. F., Wei, Y. M., Yue, Y. W., Yan, Z. H., and Zheng, Y. L. (2006). Biochemical and molecular characterization of gliadins. *Molecular Biology* 40, 713–723. doi:10.1134/s0026893306050050.

Raftery, A. E. (1995). Bayesian Model Selection in Social Research. *Sociological Methodology* 25, 111. doi:10.2307/271063.

Ruan, Y., Yu, B., Knox, R. E., Singh, A. K., DePauw, R., Cuthbert, R., et al. (2020). High Density Mapping of Quantitative Trait Loci Conferring Gluten Strength in Canadian Durum Wheat. *Frontiers in Plant Science* 11. doi:10.3389/fpls.2020.00170.

Seabourn, B. W., Xiao, Z. S., Tilley, M., Herald, T. J., and Park, S.-H. (2012). A Rapid, Small-Scale Sedimentation Method to Predict Breadmaking Quality of Hard Winter Wheat. *Crop Science* 52, 1306–1315. doi:10.2135/cropsci2011.04.0210.

Shewry, P. R., and Halford, N. G. (2002). Cereal seed storage proteins: structures, properties and role in grain utilization. *Journal of Experimental Botany* 53, 947–958. doi:10.1093/jexbot/53.370.947.

Shewry, P. R., Halford, N. G., and Lafiandra, D. (2003). Genetics of Wheat Gluten Proteins. *ScienceDirect* 49, 111–184. Available at: https://www.sciencedirect.com/science/article/pii/S0065266003010034 [Accessed March 3, 2021].

Shiferaw, B., Prasanna, B. M., Hellin, J., and Bänziger, M. (2011). Crops that feed the world 6. Past successes and future challenges to the role played by maize in global food security. *Food Security* 3, 307–327. doi:10.1007/s12571-011-0140-5.

Simons, K., Anderson, J. A., Mergoum, M., Faris, J. D., Klindworth, D. L., Xu, S. S., et al. (2012). Genetic Mapping Analysis of Bread-Making Quality Traits in Spring Wheat. *Crop Science* 52, 2182–2197. doi:10.2135/cropsci2012.03.0175.

1008 Singh, N. K., and Shepherd, K. W. (1988). Linkage mapping of genes controlling endosperm
1009 storage proteins in wheat. *Theoretical and Applied Genetics* 75, 628–641.
1010 doi:10.1007/BF00289132.

1011 Slade, L., and Levine, H. (1994). "Structure–function relationships of cookies and cracker
1012 ingredients," in *The Science of Cookies and Cracker Production* (New York: Chapman &
1013 Hall), 23–141.

1014 Smith, N., Guttieri, M., Souza, E., Shoots, J., Sorrells, M., and Sneller, C. (2011). Identification
1015 and Validation of QTL for Grain Quality Traits in a Cross of Soft Wheat Cultivars
1016 Pioneer Brand 25R26 and Foster. *Crop Science* 51, 1424–1436.
1017 doi:10.2135/cropsci2010.04.0193.

1018 Song, Y., and Zheng, Q. (2007). Dynamic rheological properties of wheat flour dough and
1019 proteins. *Trends in Food Science & Technology* 18, 132–138.
1020 doi:10.1016/j.tifs.2006.11.003.

1021 Souza, E. J., Sneller, C., Guttieri, M. J., Sturbaum, A., Griffey, C., Sorrells, M., et al. (2012).
1022 Basis for selecting soft wheat for end-use quality. *Crop Science* 52, 21–31.
1023 doi:10.2135/cropsci2011.02.0090.

1024 Sun, X., Marza, F., Ma, H., Carver, B. F., and Bai, G. (2009). Mapping quantitative trait loci for
1025 quality factors in an inter-class cross of US and Chinese wheat. *Theoretical and Applied*
1026 *Genetics* 120, 1041–1051. doi:10.1007/s00122-009-1232-x.

1027 Torbica, A., Antov, M., Mastilović, J., and Knežević, D. (2007). The influence of changes in
1028 gluten complex structure on technological quality of wheat (Triticum aestivum L.). *Food*
1029 *Research International* 40, 1038–1045. doi:10.1016/j.foodres.2007.05.009.

1030 Triboï, E., Martre, P., and Triboï-Blondel, A. (2003). Environmentally-induced changes in
1031 protein composition in developing grains of wheat are related to changes in total protein
1032 content. *Journal of Experimental Botany* 54, 1731–1742. doi:10.1093/jxb/erg183.

1033 Tsilo, T. J., Hareland, G. A., Chao, S., and Anderson, J. A. (2011). Genetic Mapping and QTL
1034 Analysis of Flour Color and Milling Yield Related Traits Using Recombinant Inbred

Lines in Hard Red Spring Wheat. *Crop Science* 51, 237–246. doi:10.2135/cropsci2009.12.0711.

USDA NASS (2020). USDA ERS - Wheat Data. *USDA.gov*. Available at: https://www.ers.usda.gov/data-products/wheat-data/ [Accessed May 12, 2020].

Utebayev, M., Dashkevich, S., Bome, N., Bulatova, K., and Shavrukov, Y. (2019). Genetic diversity of gliadin-coding alleles in bread wheat (Triticum aestivum L.) from Northern Kazakhstan. *PeerJ* 7. doi:10.7717/peerj.7082.

VanRaden, P. M. (2008). Efficient methods to compute genomic predictions. *Journal of Dairy Science* 91(11), 4414-4423. doi:10.3168/jds.2007-0980

Venske, E., dos Santos, R. S., Busanello, C., Gustafson, P., and Costa de Oliveira, A. (2019). Bread wheat: a role model for plant domestication and breeding. *Hereditas* 156. doi:10.1186/s41065-019-0093-9.

Wang, D., Li, F., Cao, S., and Zhang, K. (2020). Genomic and functional genomics analyses of gluten proteins and prospect for simultaneous improvement of end-use and health-related traits in wheat. *Theoretical and Applied Genetics* 133, 1521–1539. doi:10.1007/s00122-020-03557-5.

Wang, J., Luo, M.-C., Chen, Z., You, F. M., Wei, Y., Zheng, Y., et al. (2013). Aegilops tauschiisingle nucleotide polymorphisms shed light on the origins of wheat D-genome genetic diversity and pinpoint the geographic origin of hexaploid wheat. *New Phytologist* 198, 925–937. doi:10.1111/nph.12164.

Wang, J., and Zhang, Z. (2018). GAPIT Version 3:An Interactive Analytical Tool for Genomic Association and Prediction. Available at: https://github.com/jiabowang/GAPIT3 [Accessed July 30, 2020].

Wang, S., Wong, D., Forrest, K., Allen, A., Chao, S., Huang, B. E., et al. (2014). Characterization of polyploid wheat genomic diversity using a high-density 90 000 single nucleotide polymorphism array. *Plant Biotechnology Journal* 12, 787–796. doi:10.1111/pbi.12183.

Xiao, Y., Liu, H., Wu, L., Warburton, M., and Yan, J. (2017). Genome-wide Association Studies in Maize: Praise and Stargaze. *Molecular Plant* 10, 359–374. doi:10.1016/j.molp.2016.12.008.

Xue, C., Matros, A., Mock, H.-P., and Mühling, K.-H. (2019). Protein Composition and Baking Quality of Wheat Flour as Affected by Split Nitrogen Application. *Frontiers in Plant Science* 10. doi:10.3389/fpls.2019.00642.

Yang, X., Xu, H., Li, W., Li, L., Sun, J., Li, Y., et al. (2011). Screening and identification of seed-specific genes using digital differential display tools combined with microarray data from common wheat. *BMC Genomics* 12. doi:10.1186/1471-2164-12-513.

Yang, Y., Chai, Y., Zhang, X., Lu, S., Zhao, Z., Wei, D., et al. (2020). Multi-locus GWAS of quality traits in bread wheat: Mining more candidate genes and possible regulatory network. *Frontiers in Plant Science* 11, 1091. doi:10.3389/fpls.2020.01091.

Yu, J., Pressoir, G., Briggs, W. H., Vroh Bi, I., Yamasaki, M., Doebley, J. F., et al. (2005). A unified mixed-model method for association mapping that accounts for multiple levels of relatedness. *Nature Genetics* 38, 203–208. doi:10.1038/ng1702.

Yuan, J., Wang, X., Zhao, Y., Khan, N. U., Zhao, Z., Zhang, Y., et al. (2020). Genetic basis and identification of candidate genes for salt tolerance in rice by GWAS. *Scientific Reports* 10. doi:10.1038/s41598-020-66604-7.

Zhang, G., Chen, R. Y., Shao, M., Bai, G., and Seabourn, B. W. (2020). Genetic analysis of end-use quality traits in wheat. *Crop Science*. doi:10.1002/csc2.20411.

Zhang, W., Chao, S., Manthey, F., Chicaiza, O., Brevis, J. C., Echenique, V., et al. (2008). QTL analysis of pasta quality using a composite microsatellite and SNP map of durum wheat. *Theoretical and Applied Genetics* 117, 1361–1377. doi:10.1007/s00122-008-0869-1.

Zhang, Y.-M., Mao, Y., Xie, C., Smith, H., Luo, L., and Xu, S. (2005). Mapping Quantitative Trait Loci Using Naturally Occurring Genetic Variance Among Commercial Inbred Lines of Maize (Zea maysL.). *Genetics* 169, 2267–2275. doi:10.1534/genetics.104.033217.

Zhang, Z., Ersoz, E., Lai, C.-Q., Todhunter, R. J., Tiwari, H. K., Gore, M. A., et al. (2010). Mixed linear model approach adapted for genome-wide association studies. *Nature Genetics* 42, 355–360. doi:10.1038/ng.546.

Zhao, L., Zhang, K.-P., Liu, B., Deng, Z., Qu, H.-L., and Tian, J.-C. (2010). A comparison of grain protein content QTLs and flour protein content QTLs across environments in cultivated wheat. *Euphytica* 174, 325–335. doi:10.1007/s10681-009-0109-z.

Zheng, S., Byrne, P. F., Bai, G., Shan, X., Reid, S. D., Haley, S. D., et al. (2009). Association analysis reveals effects of wheat glutenin alleles and rye translocations on dough-mixing properties. *Journal of Cereal Science* 50, 283–290. doi:10.1016/j.jcs.2009.06.008.

Zhou, Z., Zhang, Z., Jia, L., Qiu, H., Guan, H., Liu, C., et al. (2021). Genetic Basis of Gluten Aggregation Properties in Wheat (Triticum aestivum L.) Dissected by QTL Mapping of GlutoPeak Parameters. *Frontiers in Plant Science* 11. doi:10.3389/fpls.2020.611605.

Zörb, C., Ludewig, U., and Hawkesford, M. J. (2018). Perspective on Wheat Yield and Quality with Reduced Nitrogen Supply. *Trends in plant science* 23, 1029–1037. doi:10.1016/j.tplants.2018.08.012.

Chapter 2 - Genomic Regions Associated with Adult Plant Resistance to Leaf Rust in Wheat Cultivars Everest and WB-Cedar

Marshall Clinesmith[1*], Allan Fritz[1*], Cristiano Lemes da Silva[2], Robert Bowden[3], Nora M. Bello[4], Mary Guttieri[3], Eduard Ahkunov[5], Jessica Noller[5]

[1] Department of Agronomy, Kansas State University, Manhattan, KS 66502

[2] Corteva Agriscience, Westfield, IN

[3] USDA, Agricultural Research Service, Center for Grain and Animal Health Research, Hard Winter Wheat Genetics Research Unit

[4] Department of Animal Sciences, The Ohio State University, Columbus, OH

[5] Department of Plant Pathology, Kansas State University, Manhattan, KS 66506

Abstract

Leaf rust, caused by *Puccinia triticina,*is an important foliar disease in wheat with significant impacts on grain yield. Primary control of leaf rust is through fungicide applications and the deployment of resistant cultivars. The objective of this study was to search for genomic regions associated with adult plant resistance (APR) to leaf rust in the hard winter wheat cultivars Everest and WB-Cedar using a doubled haploid (DH) population consisting of 159 lines. The DH population and parents were initially screened for leaf rust infection at seedling stage using artificial inoculation with four common races. Adult plant stage screening was then performed in a greenhouse using artificial inoculation with the leaf rust race TFBJQ determined to be virulent on both parents at the seedling stage. Adult plant screening was also conducted at Castroville, TX under natural inoculum. For WB-Cedar, resistance alleles were identified in three genomic regions on chromosomes 2AS, 5AL and 7DS. Specifically, *QLr.ksu-7DS* was associated with the

largest effect for both infection type and severity and was confirmed to be the APR race non-specific gene *Lr34*. For Everest, resistance alleles were identified in six genomic regions on chromosomes 1BL, 2AL, 2BS, 3BL, 4DL, and 7BL. Specifically, *QLr.ksu-2AL* was observed in multiple datasets and was associated with the largest effect of any QTL in Everest, while *QLr.ksu-7BL* was confirmed to be the slow rusting APR gene *Lr68*. These findings suggest the resistance to leaf rust observed in WB-Cedar is due in part to the larger effect of the APR gene *Lr34* while Everest appears to be controlled by multiple APR genes of smaller effect.

Introduction

Leaf rust, (also known as brown rust) caused by the fungal pathogen *Puccinia triticina* Erikss. (Pt) is an important foliar disease in wheat (Browder, 1971a; Bolton et al., 2008). Leaf rust is more prevalent than other rust pathogens of wheat, occurring worldwide in all regions where the crop is grown (Kolmer, 2005; McCallum et al., 2021). Yield losses associated with leaf rust can be significant depending on environmental conditions, varietal selections, and management practices, with light to moderate losses typically observed in the Great Plains (Bolton et al., 2008; Kolmer et al., 2019). Severe infections can cause considerable loss of flag leaves, which are responsible for around 75% of photosynthesis for grain fill (Lindsey et al., 2017). Leaf rust inoculum can survive between winter wheat crops on volunteer plants, later causing infections in the fall when the new crop emerges (Kolmer, 2013). Overwintering uredinia and mycelium are considered a source of inoculum for spring infections (Kolmer, 2021); however, they are not usually problematic in Kansas as the pathogen does not typically survive the winter (DeWolf & Lollato, 2019). Spring infections in the Northern Great Plains can be increased by wind-blown urediniospores that survive the winter on fall-seeded wheat crops in

the southern U.S. and Mexico. These spores can travel hundreds of miles and are carried north from Mexico to Canada along the "Puccinia Pathway*"* (Bokore et al., 2020).

Fungicide applications can provide sufficient levels of protection depending on application timing and length of residual (Joshi et al., 2017). Environmental factors can reduce the usefulness of fungicides if applications are delayed due to heavy rainfall or wind (Figueroa et al., 2017). The deployment of genetically resistant cultivars is considered the most sustainable method of control (McIntosh, Wellings, et al., 1995; Wiesner-Hanks & Nelson, 2016). To date, around 80 designated leaf rust resistance (Lr) genes have been discovered in wheat (Pinto da Silva et al., 2018; Dinh et al., 2020; Kumar et al., 2021). Leaf rust resistance in wheat is divided into two categories based on the stage at which resistance is observed, namely seedling resistance (also known as all-stage resistance (ASR), due to genes effective at all plant stages) and adult plant resistance (APR) effective only at the adult plant stage (McIntosh et al., 2014). The majority of designated Lr genes provide ASR (Feuillet et al., 2003; Kolmer, 2013). These genes are often considered race-specific and only provide resistance against isolates of the pathogen that carry corresponding avirulence genes (Lowe et al., 2010; Pinto da Silva et al., 2018). Consequently, resistance built solely on ASR genes is not typically durable (Pinto da Silva et al., 2018) as high rates of mutation and broad transport of newly selected races can quickly overcome deployed resistance (Lowe et al., 2010).

In turn, APR resistance is associated with a slow rusting response effective only at the adult stage of the plant life cycle. APR genes are typically considered quantitative in nature and have minor effects relative to ASR genes, thus considered as conveyors of incomplete or partial resistance to the pathogen (Ellis et al., 2014). Some APR genes show race-specificity similar to ASR genes while others, such as *Lr34*, are considered race non-specific, with no known

pathogen isolates showing virulence (Rinaldo et al., 2017). The loss of ASR effectiveness of many race-specific Lr genes has limited their use in breeding programs (Chu et al., 2009). Strategies to pyramid multiple ASR genes together for enhanced durability can also fall short since it is difficult to prevent other breeders from releasing cultivars containing single genes.

Combining both APR and ASR genes has been shown to potentially improve durability of genetic resistance in wheat (Figlan et al., 2020). Indeed, previous reports have shown positive interactions between Lr genes conferring complete resistance and APR genes with partial effects (Kloppers & Pretorius, 1997; Kolmer et al., 2007; Vanzetti et al., 2011). Observed complementation between genes from both categories has shown effective levels of broad-spectrum resistance.

Genetic mapping of leaf rust resistance genes in elite breeding lines is important for developing a strategy for durable resistance. In particular, the hard red winter wheat (HRWW) cultivar Everest (PI 659807) is of interest as it has shown high levels of adult plant resistance to leaf rust with little to no loss of effectiveness while grown over extensive acreage across Kansas for the past decade. Everest was developed by Kansas State University under the experimental designation KS970093-8-9-#1 and released in 2009 through the Kansas Wheat Alliance. The pedigree of Everest is HBK1064-3/JaggerW//X960103 (NPGS, 2017). Kansas State University Research and Extension designates Everest as moderatley resistant to leaf rust (DeWolf et al., 2017). Data from the Southern Regional Performance Nursery (SRPN) in 2007, 2008, and 2009 showed Everest had high levels of leaf rust susceptibility at the seedling stage to the majority of isolates used (*Research : USDA ARS*, 2021). In turn, adult plant screening in the field showed high levels of resistance. This suggests that Everest may carry APR genes for leaf rust. SRPN

marker data suggests that Everest does not carry the resistance alleles for *Lr19, Lr21, Lr24, Lr34, Lr37, Lr39, Lr41*, or *Lr50*.

WB-Cedar (PI 661996) was developed by WestBred under the experimental designation HV9W96-1383R and released in 2011. The pedigree of WB-Cedar is TAM-302/PIONEER-2180//EXP (NPGS, 2017). WB-Cedar is designated as intermediate in resistance to leaf rust by Kansas State University Research and Extension (DeWolf et al., 2017). This suggests it also carries alleles for leaf rust resistance. A better understanding of the genetic architecture underlying resistance of the cultivars Everest and WB-Cedar will aid in the development of future breeding strategies aimed at maintaining durable resistance. The objectives of this study were to 1) develop a mapping population between the cultivars Everest and WB-Cedar; 2) screen the parents and population for leaf rust resistance at the adult plant stage utilizing both greenhouse and field studies; 3) obtain molecular markers for the parents and population; 4) use the genotypic and phenotypic data to search for regions associated with APR resistance to leaf rust.

Material and Methods

Plant Materials

Plant materials consisted of a doubled haploid (DH) population containing 159 lines generated using F_1 seeds from a cross between HRWW cultivars Everest and WB-Cedar.

Assessment of Resistance at Seedling Stage

The parental lines, Everest, and WB-Cedar, along with the DH population were screened for seedling resistance according to (Kolmer, 2017) using four races of leaf rust (TBBGS, BBBBD, TNRJJ, and MBDSD) available at the USDA Cereal Disease Lab in St. Paul, Minnesota**.** The races and their virulence profiles are provided below as well as in Table 2-1.

TBBGS is the most common race in the Northern Plains spring wheat region (South Dakota, North Dakota, and Minnesota) being virulent to *Lr1*, *Lr2a*, *Lr2c*, *Lr3*, *Lr10*, *Lr21*, *Lr28*, and *Lr39* (Kolmer, 2019). Race BBBBD is avirulent to nearly all seedling genes excluding Lr39 (U.S. Department of Agriculture, Agricultural Research Service, 2016; Kolmer, Bernardo, et al., 2018). Race TNRJJ is virulent to *Lr1, Lr2a, Lr2c, Lr3, Lr9, Lr10, Lr11, Lr24, Lr3ka, Lr30, Lr14a, Lr28, Lr39* (U.S. Department of Agriculture, Agricultural Research Service, 2013; Kolmer et al., 2006) while race MBDSD is virulent to *Lr1*, *Lr3*, *Lr10*, *Lr14a*, *Lr17*, *Lr39*, and *LrB* (U.S. Department of Agriculture, Agricultural Research Service, 2023; Aoun et al., 2016). Seedlings of each line were grown in small 3.5 cm by 3.5 cm plastic pots filled with vermiculite. Each line had 5 seeds planted into the corner of a single pot, resulting in four lines planted per pot. Pots were placed into plastic trays holding six pots each resulting in a total of 24 lines per tray. Seedlings were inoculated eight days after planting when the primary leaf was fully expanded. A mixture of rust urediniospores and Soltrol 170 (Chevron Phillips Chemical Company, The Woodlands, TX, USA) was atomized at XX bar onto the seedlings. The inoculated pots were fertilized with 20-20-20 NPK and placed in a mist chamber overnight at 100% humidity. Plants were removed at 24 h and placed on a greenhouse bench at 18-22 C, with 16 hrs of supplemental lighting per day. Infection types (IT) were read at 10 days after inoculation (dai) by taking an average rating of all 4 plants per line. Initial leaf rust IT were converted to Stakman IT scores on a linear scale using the formula proposed by Zhang et al., (2014), where IT 0, 1-, 1, 1+, 2-, 2, 2+, 3-, 3, and 3+ were converted to IT 0, 1, 2, 3, 4, 5, 6, 7, 8, and 9, respectively.

Selection of *Puccinia triticina* Race for Adult Plant Screening

An initial assessment was performed to identify a race showing virulence on both parents at the seedling stage. Since the current study is focused on identifying durable APR resistance, races showing virulent reactions on both parents at the seedling stage help control against identifying genomic regions conferring all-stage resistance. Initially we inoculated the parental cultivars "Everest' and WB-Cedar with three individual races of leaf rust based on SRPN data, namely MLDSD, TNRJ, and TFBJQ (obtained from Dr. John Fellers, USDA-ARS). The races and their virulence profiles are provided below as well as in Table 2-1. MLDSD is virulent to *Lr1, Lr3, Lr9, Lr10, Lr14a, Lr17, Lr39,* and *LrB* (USDA-ARS, 2016). TNRJ is virulent on genes *Lr1*, *Lr2a*, *Lr2c*, *Lr3*, *Lr9*, *Lr24*, *Lr3ka*, *Lr17*, *Lr30*, *Lr10*, *Lr14a*, *Lr28*, *Lr39*, *Lr14b*, *Lr20*, *and Lr28 (Fellers et al., 2020b). TFBJQ is virulent on Lr3, Lr2a, Lr2c, Lr10, Lr14a, Lr21, Lr24, Lr26, and Lr28 (U.S. Department of Agriculture, Agricultural Research Service, 2016; Aoun et al., 2016).* Each race was used to inoculate a tray containing 4 plants of each parent cultivar. Inoculations were performed following the protocol by (Browder, 1971) whereby inocula was heat-shock treated for 6 minutes at 42°C, suspended in Soltrol 170 light oil (Chevron Phillips Chemical Company, The Woodlands, TX, USA), and applied to leaves using an atomizer. Seedlings were placed in a dew chamber at 22°C for 18 hours. Trays containing the plants were then transferred to a growth chamber set for 14 h of light and constant temperature of 20°C. Trays were removed from the chamber at 18 h and returned to the greenhouse set for 14 h of light with constant daytime temperature of 20°C and nighttime temperature of 16°C. Response to leaf rust infection was evaluated 14 dai. To avoid leaves that escaped inoculation, the leaf showing the highest level of infection from each plant was selected for evaluation and one

observation was recorded per leaf. Leaves were visually examined for pustule severity and appearance of hypersensitive response.

Assessment of Resistance at Adult Plant Stage

The parental cultivars, Everest and WB-Cedar, the DH population, and a resistant ('Overley') (PI634974) and susceptible ('Jagger') (PI593688) check were used to assess leaf rust resistance at the adult plant stage in both controlled greenhouse conditions as well as in the field.

Greenhouse assessment was performed using artificial inoculation with race TFBJQ shown to be virulent on both parents at the seedling stage (Figure B-1). The study was conducted as a randomized complete block design with subsampling in a greenhouse at Kansas State University in Manhattan, Kansas and was repeated through three greenhouse cycles (blocking factor) from 2019 to 2020 designated GH19S, GH19F, and GH20S. Within a greenhouse cycle, each genotype was randomly assigned to a single pot with two vernalized seedlings planted per pot (i.e. subsamples). Inoculations were performed at the adult plant stage using the same protocol as the seedling screening. Limited dew chamber space within cycles required lines to be placed into three groups based on their heading date. Each group was inoculated when >75% of plants were at or past Feekes stage 10. Lines were not consistently assigned to the same group across greenhouse cycles due to within-cycle maturity differences. Response to leaf rust infection were recorded 14 dai with measurements conducted on the flag leaf of each plant. Leaf rust IT was recorded on a 0-9 scale according to Zhang et al., (2014), where IT 0, 1, 2, 3, 4, 5, 6, 7, 8, and 9 correspond to IT 0, 1-, 1, 1+, 2-, 2, 2+, 3-, 3, and 3+, respectively. Visual severity (VSEV) of leaf rust was recorded as percent of diseased leaf area using the modified Cobb scale (Peterson et al., 1948). The modified Cobb scale is a diagrammatic scale with drawings of leaves showing different percentages of leaf rust sporulation used to approximate the amount of rust on

live samples. One flag leaf from each pot was selected and removed for image analysis immediately after visual scoring. Leaves were scanned using an Epson Perfection 3170 photo scanner. Images were edited to improve contrast, apply black backgrounds, and crop out individual leaves. Each leaf image was then processed using the Leaf Doctor app (Pethybridge & Nelson, 2015) to determine the percent of diseased leaf area, termed image severity (ISEV).

The DH population, parents, and checks were planted in the field under natural leaf rust infection at the Texas Agrilife Research Nursery near Castroville, TX during the 2020 growing season designated CV20S. Field trials were conducted using a randomized complete block design (RCBD) which consisted of genotypes assigned to 1-meter rows planted in two blocks. A single value for IT and VSEV was recorded for each row based on observations from individual leaves.

Statistical Modeling

Data were analyzed using a general linear mixed model. For adult plant screening in the greenhouse, this model was fitted to response variables IT, VSEV, and ISEV.

Adult Plant Screening – Greenhouse Experiment

$$y_{ijkl} = \eta + b_i + a_{j(i)} + c_{k(ij)} + g_l + bg_{il} + e_{ijklm}$$

where y_{ijkl} is the observed response of the l^{th} line assigned to the k^{th} chamber in the j^{th} group within the i^{th} block, n is the intercept, b_i is the differential effect of the i^{th} cycle assumed independent and identically distributed (i.i.d.) $b_i \sim N(0, \sigma_b^2)$, $a_{j(i)}$ is the differential effect of the j^{th} group within the i^{th} cycle assumed independent and identically distributed (i.i.d.) $a_{j(i)} \sim N(0, \sigma_a^2)$, $c_{k(ij)}$ is the differential effect of the k^{th} chamber in the j^{th} group within the i^{th} cycle assumed independent and identically distributed (i.i.d.) $c_{k(ij)} \sim N(0, \sigma_c^2)$, g_l is the differential effect of the l^{th} genotype assumed independent and identically distributed (i.i.d.)

$g_l \sim N(0, \sigma_g^2)$, bg_{il} is the differential effect of the combination of the lth genotype and ith cycle assumed independent and identically distributed (i.i.d.) $bg_{il} \sim N(0, \sigma_{bg}^2)$, and e_{ijklm} is the leftover random residual corresponding to the mth plant from the lth genotype assigned to the kth chamber in the jth group within the ith block assumed independent and identically distributed (i.i.d.) $e_{ijklm} \sim N(0, \sigma_e^2)$.

Adult Plant Screening - Field Experiment

$$y_{il} = n + b_i + g_l + e_{il}$$

Where y_{il} is the observed response of the lth genotype in the ith block, n is the intercept, b_i is the differential effect of the ith block assumed independent and identically distributed (i.i.d.) $b \sim N(0, \sigma_b^2)$, g_l is the differential effect of the lth genotype assumed independent and identically distributed (i.i.d.) $g \sim N(0, \sigma_g^2)$, and e_{il} is the leftover random residual corresponding to the lth genotype in the ith block assumed independent and identically distributed (i.i.d.) $e \sim N(0, \sigma_e^2)$.

Restricted maximum likelihood was used to estimate variance components. Plots of studentized residuals were used to evaluate model assumptions. The responses VSEV and ISEV recorded in the greenhouse experiment, along with VSEV recorded in the Castroville experiment were log transformed to meet model assumptions. Pairwise comparisons were performed for IT, VSEV, and ISEV between each DH line and parent lines to assess if transgressive segregation had occurred in the population. A Dunnett adjustment was performed to control for Type I error. Estimated means and confidence intervals were backtransformed to the original scales following inference. The model was fitted using the GLIMMIX procedure of SAS (Version 9.4, SAS Institute, Cary, NC).

Broad-sense heritability (H^2) was estimated in the adult plant greenhouse experiment across cycles for each trait using the following equation:

$$H^2 = \hat{\sigma}_g^2 \,/\, (\hat{\sigma}_g^2 + \frac{\hat{\sigma}_{bg}^2}{r} + \frac{\hat{\sigma}_e^2}{r})$$

where $\hat{\sigma}_g^2$, $\hat{\sigma}_{bg}^2$, and $\hat{\sigma}_e^2$ are the variance of the lines, line by cycle interaction, and residuals, respectively, and *r* is the number of cycles (He et al. 2016). Broad-sense heritability (H^2) was estimated in the adult plant field experiment across blocks for each trait using the following equation:

$$\hat{H}^2 = \hat{\sigma}_g^2 \,/\, (\hat{\sigma}_g^2 + \frac{\hat{\sigma}_e^2}{B})$$

where $\hat{\sigma}_g^2$, and $\hat{\sigma}_e^2$ are the variance of the lines, and residuals, respectively, and *B* is the number of blocks (He et al. 2016). Pearson's correlation coefficients of adjusted means were calculated for adult plant experiments on each phenotype, IT, VSEV, and ISEV between the three greenhouse cycles and the field data at Castroville using the rcorr package in R (R Core Team, 2017). Pearson's correlation coefficient of adjusted means was also calculated between greenhouse VSEV and ISEV data.

Lr34 and *Lr68* Marker Screening

The 159 DH lines along with the two parents were screened for the presence of *Lr34* and *Lr68* resistance alleles using Kompetitive allele-specific polymerase chain reaction (KASP) markers. Four µl of KASP assay master mix containing $MgCl_2$, 2× KASP buffer, and primer was used to resuspend 50 to 100 ng of DNA dried in a 384-well plate. Two separate primers were used for *Lr34* (Table B-1), Lr34Exon11-KASP (Lagudah et al., 2009) was used to confirm the presence of the *Lr34* resistance allele and Lr34JagExon22-KASP was used to control for false positives. The primer used for *Lr68* was *Lr68*-2-KASP (Herrera-Foessel et al., 2012). Polymerase chain reactions (PCR) were conducted using the following thermal cycler conditions according to Fellers et al. (2020). For Lr34Exon11-KASP*,* 94 °C for 15 min, 97 °C for 15 sec, 68

°C for 1 min with a change of -0.8 °C per cycle for 10 cycles, 97 °C for 20 sec, 60 °C for 1 min for 30 cycles, 59 °C for 30 sec at -1.0 °C per cycle for 34 cycles, with a final cool down of 10 °C for 5 min. For Lr34JagExon22-KASP, 94 °C for 15 min, 94 °C for 20 sec, 60 °C for 1 min for 30 cycles, with a cool down of 10 °C for 5 min. For *Lr68*-2-KASP, 94 °C for 15 min, 94 °C for 20 sec, 65 °C for 1 min with a change of -0.8 °C per cycle for 10 cycles, 94 °C for 20 sec, 57 °C for 1 min for 50 cycles, 56 °C for 30 sec with a change of -1.0 °C per cycle for 32 cycles, with a cool down of 10 °C for 5 min. PCR reactions were run on a GeneAmp Systems 9700 (Applied Biosystems). Plates were read using a FLUOstar Omega SNP reader (BMG Labtech). KASP assay results were analyzed using Klustercaller (LGC Biosearch Technologies).

SNP Genotyping and Linkage Map Construction

Leaf tissue was collected from each DH line and the parents at the two-leaf stage. Tissue was freeze dried at −51°C for 48 h using a Labconco Freezone 6. Dried tissue was ground in a Retsch mm400 tissue grinder set at 25 cycles s−1. DNA purification was performed using the BS96 DNA Plant protocol for the Biosprint 96 workstation and the Biosprint 96 DNA plant kit (Qiagen). Genotyping-by-sequencing (GBS; Elshire et al., 2011) was performed according to (Poland et al., 2012). The restriction enzymes *PstI* and *MspI* were used for DNA sample digestion. An Illumina Hiseq 2000 was used for sequencing following DNA amplification.

Raw GBS sequence data was processed into single nucleotide polymorphisms (SNPs) using the TASSEL-GBS bioinformatics pipeline implemented in TASSEL 5.0. Physical positions of SNPs within the genome were determined through alignment of GBS sequences to the Chinese Spring (CS) reference genome v.1 (Appels et al., 2018). SNPs were then filtered to < 20% missing data and a minor allele frequency ≥ 0.05 using a custom script in Rstudio V

1.3.959. Missing data was imputed using Beagle (Browning et al., 2018). A linkage map was constructed using the Kosambi mapping function (Kosambi, 1943) in JoinMap 4.1 (Van Ooijen, 2006) which groups SNPs into linkage groups using a maximum likelihood mapping procedure. Marker data from the GBS SNPs, *Lr34*, and *Lr68* KASP assays was used to generate the linkage map. Physical positions of SNPs obtained from alignment with the CS reference genome were included in the name of each SNP and used to confirm correct positioning of SNPs within the genetic map. SNPs with the same genetic position due to tight linkage were ordered within linkage blocks based on their physical position.

QTL Mapping

QTL mapping for all traits was conducted using the R/qtl package (Broman et al., 2003) in R (R Core Team, 2017). All analyses were performed using Haley-Knott regression (Haley & Knott, 1992). This method was chosen as it has been shown to give similar results to standard interval mapping and multiple imputation when there are low levels of missing data and is more computationally efficient for larger marker datasets (Broman & Sen, 2009). The genome-wide LOD thresholds for each trait were estimated using a permutation test with 1,000 permutations to determine the significance of QTL at $P < 0.05$. The initial search for QTL was conducted using simple interval mapping (SIM). The results from SIM were used to obtain markers closely positioned to significant QTL. These markers were then used as covariates to search for additional QTL via composite interval mapping. Composite interval mapping (CIM) was implemented using forward selection of marker covariates and an infinite window size which omits marker covariates residing on the chromosome of the position being tested. Linkage of multiple QTL and epistatic interactions between QTL were investigated using the scantwo

function in R/qtl. The results from these analyses were used in multiple qtl mapping (MQM) to fit a multiple fixed effect QTL model according to (Broman & Sen, 2009) using the model

$$y = u + \sum_{j} \beta_j q_j + \sum_{j,k} \beta_{jk} q_j q_k + e$$

where y is the observed response, u is the overall mean, $\sum_j \beta_j q_j$ is the sum of QTL main effects, $\sum_{j,k} \beta_{jk} q_j q_k$ is the sum of QTL interaction effects, and e is the residual random error. MQM was used to further test the significance of each QTL, refine the position of the QTL, and estimate the percent phenotypic variance explained by the QTL.

Identification of Candidate Genes

Identification of potential candidate genes was conducted using Basic Local Alignment Search Tool (BLAST). Nucleotide sequences of known *Lr* genes, if available, were BLAST against the Chinese Spring reference genome, IWGSC RefSeq v1.0, in the Ensemble Plants window browser (http://plants.ensembl.org/index.html). The physical positions were obtained from the BLAST analysis and compared against the physical position of the peak marker for each QTL.

Results

Phenotypic Data

Seedling screening of the population and parents for IT response revealed one race, TBBGS, showing a varied response for the parents and segregation in the population. (Table 2-2; Figure 2-1a). The other three races, BBBBD, TNRJJ, and MBDSD, showed avirulent, virulent, and virulent responses on both parents, respectively. Everest showed a highly resistant response to race TBBGS whereas WB-Cedar showed a higher infection response.[This needs elaboration and reporting of details…]

The response of the DH lines and parents to leaf rust race TFBJQ at the adult plant stage varied across the different experimental runs in the greenhouse (Table 2-2; Figure 2-1b-d). Heritability values were moderately high to high at 0.60, 0.70, and 0.73 for ISEV, VSEV, and IT, respectively. Lower leaf rust pressure was observed during the spring of 2019 relative to the other experimental runs. The greatest amount of disease pressure was present during the fall experiment in 2019 where the mean response of the population to IT, VSEV, and ISEV were 5.29, 20.81%, and 38.19%, respectively. The data for VSEV was normally distributed while ISEV was skewed to the right. Continuous variation for leaf rust traits was also observed under natural inoculum pressure in the field experiment at Castroville (Table 2-2; Figure 2-1b,c). Heritability values were slightly lower under natural inoculum pressure in the field experiment at Castroville relative to greenhouse experiments with IT and VSEV having values of 0.51 and 0.65, respectively.

The three phenotypes, IT, VSEV, and ISEV each showed a significant positive correlation ($P<0.001$) across the three greenhouse cycles (Figure 2-2a). Positive correlations for IT were also significant ($P<0.01$ and $P<0.001$) between the CV20S dataset and greenhouse cycles GH19F and GH20S, respectively. Additionally, VSEV data from CV20S showed significant positive correlation ($P<0.05$) with greenhouse cycle GH20S. Severity data of BLUPs was significantly positively correlated ($P<0.001$) between the visual and image methods used for measurement.

Transgressive segregation was observed for leaf rust traits in the DH population. Mean comparisons were performed using BLUPs from the greenhouse experiments and field data at Castroville, TX. No significant mean differences ($P<0.05$) were observed between Everest and WB-Cedar. Everest showed a slightly lower mean value for all traits in the greenhouse while at

Castroville the parents scored the same for IT, and WB-Cedar showed a slightly lower mean for VSEV compared to Everest. Four lines showed significantly lower IT than WB-Cedar in greenhouse experiments; however, no lines were significantly lower than Everest. Eleven and ten lines were significantly more resistant than WB-Cedar for VSEV and ISEV, respectively. Four lines showed significantly lower ISEV compared to Everest, while no lines were statistically better for VSEV.

SNP Genotypes

A total of 4,171 SNP markers spanning a genetic distance of 3,628.13 cM were retained after filtering for missing data and MAF (Table 2-3, Figure B-2). Distribution of the SNPs across the wheat genome was consistent with previous observations. Most SNPs were observed on the A and B genomes with only ~11% of the markers present on the D genome chromosomes. Average marker spacing was 0.72 cM, 0.66 cM, and 2.31 cM for the A, B, and D genomes, respectively. Plotting genetic versus physical position for each chromosome revealed several regions with low marker coverage on chromosomes 4B, 4D, and 5D (Figure B-2). The short arm of chromosome 4D contained a single marker while the short arm of 5D was completely absent.

QTL Analysis

Nine leaf rust resistance QTL were identified across all experimental trials (Figure 2-3; Figure B-3). The QTL conferring the strongest effect was contributed by WB-Cedar, while Everest contributed a higher number of QTL of smaller effects (Table 2-4; Table B-2). Five QTL were considered as stable associations being significant in more than one environment or in one environment and the BLUP. Genetic positions of peak markers were mostly consistent across datasets for stable QTL; however, most QTL fell within large confidence intervals resulting partly from limited recombination in the DH population. Six QTL were contributed by Everest

on chromosomes 1B, 2A, 2B, 3B, 4D, and 7B. *QLr.ksu-1BL* was only detected for ISEV in the GH19F experiment and expressed a relatively weak effect on severity. The peak marker for this QTL was located at a genetic position of 97.40 cM and explained 8.40% of the phenotypic variance (PV). *QLr.ksu-2AL* was among the most effective and stable QTL with peak markers located in a genomic region between 114.99 cM and 142.89 cM. The most consistent marker was snp-2A-630461249 located at 127.20 cM. This QTL was associated with IT in the GH19F, GH20S, and GHBLUP datasets where it explained 9.39% to 13.55% of the PV, VSEV in the GH19F, GH20S, and GHBLUP datasets where it explained 8.00% to 13.51%, and ISEV in the GH19S and GH19F datasets where it explained 7.36% to 9.73%. It was also the only QTL associated with IT at the seedling stage, explaining 7.48% of the PV. *QLr.ksu-2BS* was a moderately strong QTL detected in the GH19S and GHBLUP datasets with peak markers located at 85.49 cM and 97.67 cM, respectively. This was the only QTL associated solely with IT where it explained 7.55% to 9.06% of the PV. *QLr.ksu-3BL* conferred a moderate effect for ISEV from the GHBLUP dataset, where it explained 8.05% of the PV, respectively. The peak marker for this QTL was located at 60.30 cM. Additional peaks for this QTL were observed in other severity datasets falling just short of the significance thresholds. *QLr.ksu-4DL* was among the smallest effective QTL detected being associated with VSEV in the GH19F and GHBLUP datasets where it explained 4.07% to 6.78% of the PV. Peak markers placed this QTL around 46.23 cM to 50.16 cM. *QLr.ksu-7BL* was the only QTL detected under natural infection at Castroville with a resistance allele provided by Everest. It provided a minor effect in this environment for VSEV explaining 7.15% of the PV. This QTL was not detected in any other dataset. The peak marker for this QTL was snp-7B-730113648 located at 185.75 cM. Alignment of the KASP primer for *Lr68* with the Chinese Spring reference genome placed this marker at a

physical position of 734.2 Mb and linkage analysis placed it at a genetic position of 192.012 cM The *Lr68* marker was not significantly associated with any phenotypic data.

WB-Cedar contributed resistance alleles for three leaf rust QTL on chromosomes 2AS, 5AL, and 7DS (Table 2-4; Table B-2). The QTL on chromosomes 2AS and 5AL was only detected under natural infection at Castroville while the QTL on 7DS was detected in all datasets except the seedling IT and Castroville IT datasets. *QLr.ksu-2AS* explained 9.56% of the PV for VSEV with the peak marker located at 55.00 cM on the short arm of chromosome 2AS. The exact position of this QTL is difficult to determine as a large confidence interval was observed spanning across the centromere and overlapping with the region on 2AL containing the QTL from Everest observed in greenhouse and seedling experiments. Two peaks were initially observed, one at 55.00 cM on the short arm, and one at 134.43 cM on the long arm with WB-Cedar contributing the resistance allele for both. Results of the scantwo analysis for detection of multiple linked QTL did not support the hypothesis that two QTL were present on chromosome 2A. Furthermore, addition of both QTL into the MQM model resulted in the QTL on the long arm falling below the significance level. This QTL was then removed from the model and the QTL on the short arm remained above the threshold for significance. *QLr.ksu-5AL* had a moderately strong impact on VSEV under natural infection at Castroville. This QTL was located at 67.11 cM and explained 9.37% of the PV. *QLr.ksu-7DS* was the most consistent QTL being detected for all traits in each greenhouse dataset as well as for VSEV in the field experiment. It consistently mapped to either the *Lr34* marker or snp-7D-53700222, with the peak position varying from 79.40 cM to 85.82 cM. This QTL exhibited the largest effect for all traits explaining PV of 11.77% to 27.55% for greenhouse IT, 12.33% to 39.59% for greenhouse VSEV, 14.64% to 33.74% for greenhouse ISEV, and 18.34% for VSEV at Castroville.

Discussion

The current study investigated the association of genomic regions with leaf rust resistance in winter wheat adapted to the Great Plains. Multiple measurements were used to quantify the amount of leaf rust spores present on flag leaves of wheat plant. Along with visual rating of leaf rust severity we also applied an imaging technique using the Leaf Doctor app to calculate the percent of the leaf area covered with urediniospores using an algorithm. It can be difficult to maintain consistency in visual rating of disease; therefore, a rating system based on images and algorithms could improve the quality of data collected. The strong positive correlation between the VSEV and ISEV data provides evidence that the Leaf Doctor app analysis can be a viable method of measuring leaf rust. During the GH19S cycle where we experienced the lowest average infection, VSEV had a higher average severity compared to ISEV. During cycles with higher infection, ISEV had a higher average severity relative to VSEV. This could suggest that when infection is low our visual rating tends to be an overestimate of the true rating and when infection is high our visual rating is underestimated. Comparing the QTL mapped between the two traits we see that both VSEV and ISEV both identified the two major QTL on 2A and 7D as well as a minor QTL on chromosome 3B. They each also identified a unique QTL, VSEV on 4D and ISEV on 1B. These results suggest that visual severity ratings were accurate enough in the current study to identify the major QTL given the trait in question and the genetic architecture underlying this trait.

The detection of multiple leaf rust resistance QTL of varying effects in the current study were consistent with expectations based on the continuous distributions observed in the phenotypic data. Distributions ranged from normal to slightly skewed to the right signifying segregation of multiple loci. The presence of lines showing significant transgressive segregation

towards resistance compared to the parents suggested that both parents were contributing resistance alleles which was confirmed through the results of QTL mapping. The alignment of GBS markers with the CS reference genome allowed comparison between physical positions of the QTL identified in this study with potential candidate genes and QTL detected in other studies (Table B-3). Primer sequences for markers closely linked to QTL identified in previous studies were used to blast again the CS reference for comparison.

Everest contributed the highest number of resistance loci in the doubled haploid population. These QTL include *QLr.ksu-1BL, QLr.ksu-2AL, QLr.ksu-2BS, QLr.ksu-3BL, QLr.ksu-4DL*, and *QLr.ksu-7BL.* The majority of QTL from Everest were associated with smaller effects than those of WB-Cedar. *QLr.ksu-2AL* was one exception as it conferred the second largest effect of any QTL. The peak marker for *QLr.ksu-1BL* was snp-1B-499556038 located at 499.6 Mb on the distal end of chromosome 1BL. This QTL was associated with leaf rust severity at the adult plant stage for race TFBJQ. Several leaf rust resistance genes have been discovered on chromosome 1BL. *Lr33* and *Lr44* have previously been located to the proximal region of 1BL close to the centromere (Dyck et al., 1987; Dyck & Sykes, 1994; Zhou et al., 2013). *Lr46* is a slow rusting gene on the distal end of the long arm of chromosome 1B (Singh et al., 1998). A recent study placed this gene in a physical region ~170 Mb distal to the QTL detected in this study at 672.6 Mb to 673.8 Mb (Yuan et al., 2020). *Lr51* originated from *Aegilops speltoides* and was transferred into common wheat (Dvořák, 1977). This gene has not been widely deployed likely due to negative agronomic effects from linkage drag of the introgressed segment (Helguera et al., 2005). The inconsistency in position with *QLr.ksu-1BL* and previously reported genes on chromosome 1BL could suggest the detection of a novel locus associated with leaf rust; however, it was only detected in one dataset so further investigation will be needed.

QLr.ksu-2AL was contributed by Everest and was present under artificial inoculum at the seedling stage with race TBBGS and at the adult plant stage with race TFBJQ. Race TFBJQ was selected for adult plant screening due to strong initial seedling virulence shown on Everest and WB-Cedar; however, subsequent inoculum increases grown on the parents revealed a weak avirulent response from "Everest' suggesting some genetic seedling resistance could be present. Peak markers for this QTL were in a physical region between 513.8 Mb and 678.0 Mb. Marker snp-2A-630461249 was the most consistent marker associated with this QTL observed in three of the datasets. Two genes, *Lr38* and *LrTt1,* have been associated with seedling leaf rust resistance on the long arm of chromosome 2A. *Lr38* was originally detected in *Agropyron intermedium* and was transferred to several wheat chromosomes including 2A (Wienhues, 1966; Wienhues, 1973; Friebe et al., 1993; Friebe et al., 1996; McCallum et al., 2012) while *LrTt1* originated from *Triticum timopheevii* (Leonova et al., 2010). It is unknown whether Everest contains these translocations; however, these are unlikely candidates as linkage drag for yield has limited their adoption (Mebrate et al., 2007). Several QTL associated with leaf rust have been identified on chromosome 2AL including *QLr.sfr-2AL* (Schnurbusch et al., 2004), *QLr.ubo-2AL* (Maccaferri et al., 2008), *QLr.cimmyt-2AL* (Rosewarne et al., 2012), and *QLr.hebau-2AL* (Zhang et al., 2017). The exact physical position of these QTL regarding the QTL discovered in this study is unknown. *QLr.ubo-2AL* was located on the distal end of the 2AL genetic map making it a potential candidate for *QLr.ksu-2AL* (Maccaferri et al., 2008; Li et al., 2014).

QLr.ksu-2BS associated with adult plant resistance to IT of race TFBJQ was identified on the short arm of chromosome 2B with peak markers located at 65.7 Mb and 94.1 Mb. To date seven leaf rust resistance genes have been identified on this chromosome arm including *Lr13, Lr16, Lr23, Lr35, Lr48, Lr73,* and *LrZH22* (Seyfarth et al., 1999; Li et al., 2014; Park et al.,

2014; Nsabiyera et al., 2016; Wang et al., 2016; Zhang et al., 2017). *Lr13* was initially labeled as an APR gene; however, it has also been shown to be effective at the seedling stage (Pretorious et al., 1984). It was recently placed ~ 60 Mb to 90 Mb proximal to *QLr.ksu-2BS* in a physical region between 157.7 Mb and 158.0 Mb (Qiu et al., 2020). A recent study developed KASP markers for *Lr16* placing this gene on the distal end in a physical region at 5 Mb to 6 Mb (Kassa et al., 2017). *Lr16* is an ASR resistance gene and virulence data suggests that both TBBGS and TFBJQ are avirulent for *Lr16* (Kolmer, 2021). No peak was observed at the seedling stage in this region providing further evidence this gene is not a candidate. *Lr35* was transferred into wheat from *Ae. speltoides* (Kerber & Dyck, 1990) but has not been widely adopted in breeding programs (McIntosh et al., 1995). *Lr73* was mapped to the distal end of chromosome 2BS (Park et al., 2014) placing it away from the region identified in this study. Blasting of primer sequences for genetic markers linked to *Lr23* and *Lr48* placed them both at a physical position of ~93 Mb to 94 Mb very near one of the peak markers detected for *QLr.ksu-2BS* (Nsabiyera et al., 2016; Chhetri et al., 2017). *Lr23* is an ASR gene that was transferred from durum wheat into common wheat (Watson & Luig, 1961; McIntosh & Dyck, 1975). Pathogen virulence to this gene has limited its effectiveness and could have prevented it from being detected at the seedling stage in this experiment. *Lr48* is an APR gene initially discovered in and the Australian line CSP44 (Saini et al., 2002).

QLr.ksu-3BL showed resistance to race TFBJQ for leaf rust severity. Peak markers for this QTL were located between 512.2 and 544.6 Mb. Two known Lr genes, *Lr77* and *Lr79*, are located on 3BL, along with three leaf rust QTL (Messmer et al., 2000; Chu et al., 2009; Kolmer et al., 2018; Qureshi et al., 2018; Zhang et al., 2019). *Lr77* is an APR gene originally discovered in the HRWW cultivar Santa Fe (Kolmer et al., 2018) and located in a physical region near 743.2

Mb (Qureshi et al., 2018). KASP assay for *Lr77* revealed that Everest does not carry the resistance allele at this locus. *Lr79* is an ASR gene initially mapped in a durum landrace and positioned slightly distal to *Lr77* at 752.6 Mb (Qureshi et al., 2018). *QLr.hebau-3BL* mapped to a similar region, 761.3 Mb to 761.6 Mb, at the distal end of 3BL (Zhang et al., 2019). *QLr.fcu-3BL* was detected as an ASR QTL in the synthetic hexaploid wheat line TA4152-60 (Chu et al., 2009). This QTL was positioned near the centromere at a physical position of 586.5 Mb (Zhang et al., 2019). *QLr.sfrs-3B* was detected in the Swiss winter wheat cultivar Forno and was located on chromosome 3BL in a region close to the centromere approximately 5 cM proximal to *QLr.fcu-3BL* (Messmer et al., 2000; Li et al., 2014). This suggests *QLr.sfrs-3B* is a potential candidate for *QLr.ksu-3BL*.

QLr.ksu-4DL provided a minor affect for leaf rust severity for race TFBJQ. Chromosome 4D showed the lowest marker coverage, consistent with previous results. The interval for this QTL was large representing most of the mapped long arm with peak markers placed at 485.4 Mb and 504.2 Mb. Nine genomic regions associated with leaf rust have been previously identified on chromosome 4D (Pinto da Silva et al., 2018). *Lr67* is an APR gene on 4DL transferred into Thatcher from the common wheat accession PI250413 (Herrera-Foessel et al., 2010; Hiebert et al., 2010). Blast alignment of KASP markers linked to *Lr67* (Milne et al., 2019) placed this gene at 405 Mb. Three QTL, *QLr.fcu-4DL, QLr.hebau-4D,* and *QLr.jki-4D.1*, were in a similar region with physical locations of 412.7 Mb, 428.6 Mb, and 465.0 Mb, respectively (Chu et al., 2009; Zhang et al., 2019; Rollar et al., 2020). Limited marker density resulting in positional uncertainty makes it difficult to discern a potential candidate for the QTL detected in this study.

QLr.ksu-7BL was the only locus contributed by Everest showing an effect against native races at Castroville. This QTL was located at 730 Mb on the distal end of chromosome 7BL. A

number of studies have reported QTL on chromosome 7B with the majority mapping near the three designated leaf rust genes *Lr14, Lr19,* and *Lr68* (Faris et al., 1999; Messmer et al., 2000; Herrera-Foessel et al., 2012; Soriano & Royo, 2015). *Lr14* is an ASR gene with two alleles, *Lr14a* and *Lr14b* showing variation in their race specification (Mcintosh et al., 1967; Dyck & Samborski, 1970). Race TBBGS is considered avirulent for *Lr14a*, while TFBJQ is considered virulent. The absence of a peak on 7B at the seedling stage with TBBGS suggests *QLr.ksu-7BL* is not allelic to *Lr14a* while the absence of a peak in greenhouse experiments is consistent with the virulence to race TFBJQ. Blasting of KASP marker sequence placed the position of *Lr14* in a potential physical position of 739.9 Mb on the distal end of 7BL (Terracciano et al., 2013). *Lr68* is a slow rusting APR gene first detected in a CIMMYT spring wheat cultivar (Herrera-Foessel et al., 2012). Sequence alignment also placed this gene at the distal end of 7BL at 734.2 Mb. KASP assay for *Lr68* confirmed that Everest carries the resistance allele at this locus making this gene a likely candidate for the QTL detected in this study. However, *Lr68* is described as being race non-specific (Herrera-Foessel et al., 2012) which is interesting as we only detected it under natural inoculum in the field. The peak marker for this QTL was positioned 4.1 Mb away from the KASP marker for *Lr68.*

We detected three QTL with resistance alleles contributed by WB-Cedar. Two QTL, *QLr.ksu-2AS* and *QLr.ksu-5AL,* were detected in a single dataset at Castroville under natural leaf rust infection with native races. *QLr.ksu-7DS* explained the largest percent of phenotypic variance of leaf rust traits and was the most consistent QTL detected. *QLr.ksu-2AS* was effective for leaf rust severity under natural infection at Castroville and located at a physical position of 24.0 Mb. While the strongest peak for this QTL was on the short arm a second peak was in the region on 2AL associated with resistance to TFBJQ from Everest providing some uncertainty

about the true position of the QTL. Results did not indicate that two QTL were present in this region for any of the analyzed datasets. This could suggest that each parent carries a separate locus associated with race specific resistance and the large linkage blocks associated with the DH population, especially in the centromeric region, make it difficult to accurately differentiate these loci. Five Lr genes have been identified on chromosome 2AS (Wang et al., 2010; Mcintosh et al., 2013; Darino et al., 2015). *Lr17* is an ASR gene with two alleles, *Lr17a* and *Lr17b*. This gene is located on the distal end of 2AS in a physical interval between 3.6 Mb and 6.1 Mb (Xue et al., 2018). *Lr37* is an APR gene located on a non-recombinant chromosomal segment that was transferred into wheat from *Aegilops ventricosa* (Helguera et al., 2003). This segment, designated 2NS, is not present in either parent (unpublished data). *Lr45* is an ASR gene that was transferred into wheat from *Secale cereale* (McIntosh, Friebe, et al., 1995). To our knowledge this gene was not utilized in breeding programs when the cultivar WB-Cedar was released (Naik et al., 2015). Sapkota et al. (2020) identified a QTL, *QLr.ags-2AS*, conferring APR resistance to leaf rust and located at a genetic position of 62 cM. Further information is needed to determine the relationship between *QLr.ksu-2AS* and previously detected loci.

QLr.ksu-5AL was associated with leaf rust severity under natural infection at Castroville with the most significant marker located near the centromere at 395.7 Mb on the long arm of chromosome 5AL. Visual rating of leaf rust phenotypes in the field using natural inoculation can be affected by differences in plant maturity (Hickey et al., 2011). Plant maturity is controlled in part by the vernalization gene *Vrn-1*. The gene *Vrn-A1* controlling spring versus winter growth habit in wheat is located on chromosome 5A at approximately 587.4 Mb (Yan et al., 2003; Royo et al., 2020). The parental cultivars “Everest’ and WB-Cedar share the same allele at this locus so this gene is an unlikely candidate for the QTL detected in this study (*Research : USDA ARS*,

2021). Currently no labeled Lr genes have been discovered on chromosome 5A (Pinto da Silva et al., 2018). Two QTL, *QLr.hebau-5AL* and *QLr.cimmyt-5AL* have been previously detected on 5AL (Rosewarne et al., 2012; Zhang et al., 2019; Gebrewahid et al., 2020). *QLr.hebau-5AL* was detected in two different studies in the Chinese spring wheat Fuyu 3. Zhang et al. (2019) placed this QTL ~200 Mb distal to *QLr.ksu-5AL* in a physical interval between 589.3 Mb and 591.5 Mb. The study by Gebrewahid et al. (2020) positioned this QTL closer to the one detected in the current study around 436.1 Mb to 441.1 Mb. *QLr.cimmyt-5AL* was discovered in the Australian wheat line Avocet. This QTL was considered closely linked to the vernalization gene Vrn-A1 at 587.0 Mb (Rosewarne et al., 2012; Zhang et al., 2019). To our knowledge no leaf rust QTL have been detected in the pericentromeric region of chromosome 5AL suggesting *QLr.ksu-5AL* could be a novel QTL.

QLr.ksu-7DS was a large effect QTL on the short arm of chromosome 7D showing APR to race TFBJQ and native races at Castroville. It consistently mapped to either the marker for *Lr34* or snp-7D-53700222. Alignment with the CS reference places *Lr34* at 47.4 Mb while snp-7D-53700222 is located at 53.7 Mb. *Lr34* has shown durable, broad-spectrum resistance to all known races throughout several decades of deployment (Dyck, 1987; Sawhney, 1992; Singh & Huerta-Espino, 2003; Krattinger et al., 2015).

We identified nine QTL associated with leaf rust with three of these being uniquely detected using the field data from Castroville and one being detected using both field and greenhouse data. The detection of *Lr34* via single race inoculation with TFBJQ as well as in the field under natural race pressure was consistent with the non-race specific effect of this gene. *Lr68* is another race specific gene carried by Everest and was only detected in the field at Castroville. It is possible that this gene was not observed during the TFBJQ inoculations due to

the background effect of other race-specific Everest resistance QTL that were effective against this individual race but not against the natural races seen in the field.

In the present study we detected six potential QTL in Everest showing small to moderate effects for leaf rust resistance. This suggests the durability of resistance shown in Everest is due to an oligogenic combination of multiple genes providing individual effects. Limited seedling data limits our ability to confirm resistance type for these loci; however, it appears that the resistance in Everest is likely a combination of both ASR and APR genes. This study also confirmed the presence of *Lr34* in WB-Cedar which to our knowledge was previously unknown. The addition of this gene to the Everest package could provide increased levels of leaf rust protection and improve the durability of resistance in HRWW germplasm.

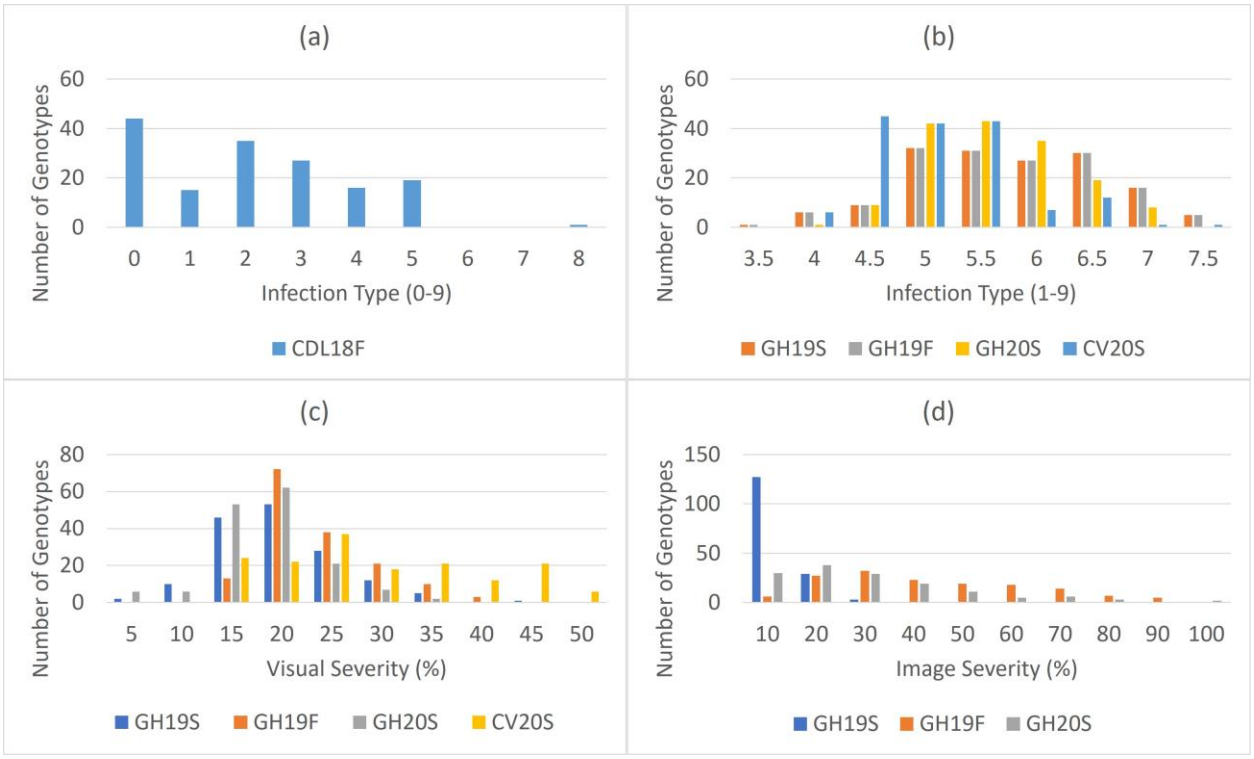

Figure 2-1. Empirical distributions of the DH lines for (a) infection type at the seedling stage, (b) infection type at the adult plant stage in the GH using race TFBJQ and under natural infection in the field at CV, (c) visual severity at the adult plant stage in the greenhouse using race TFBJQ and under natural infection in the field at CV, and (d) image severity at the adult plant stage in the greenhouse using race TFBJQ. The legends display datasets where CDL18F is the greenhouse experiment conducted at the USDA Cereal Disease Lab in St. Paul, Minnesota with race TBBGS, GH19S, GH19F, and GH20S are the three greenhouse experiments conducted at Kansas State University in Manhattan, KS with race TFBJQ, and CV20S is the field study conducted under natural inoculum in CV.

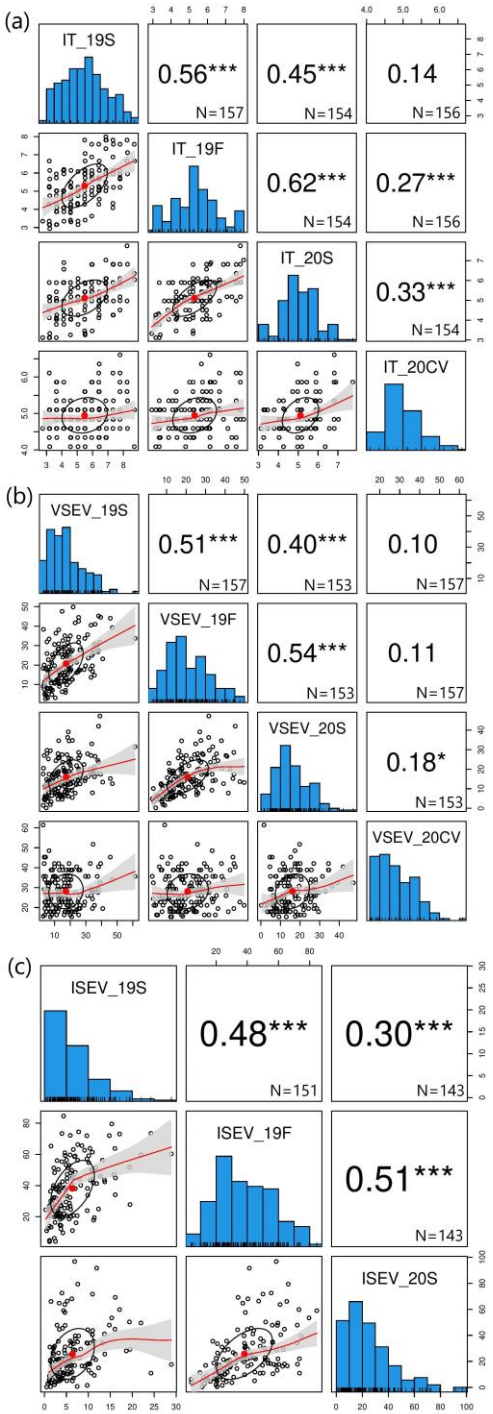

Figure 2-2. Scatterplot matrices showing comparisons of raw phenotypic values for (a) Infection type, (b) visual severity, and (c) image severity. The diagonal shows the distribution of each variable as well as displaying the abbreviation for each trait and the corresponding dataset (19S, 19F, 20S, and 20CV). The boxes in the top of the diagonal contain Pearson's correlation coefficients with asterisks displaying the significance of correlation, * ($P < 0.05$), ** ($P < 0.01$), *** ($P < 0.001$). The number in the lower right of the boxes corresponds to the number of data points used in each comparison. The boxes below the diagonal display the bivariate scatter plots fitted with a LOESS curve.

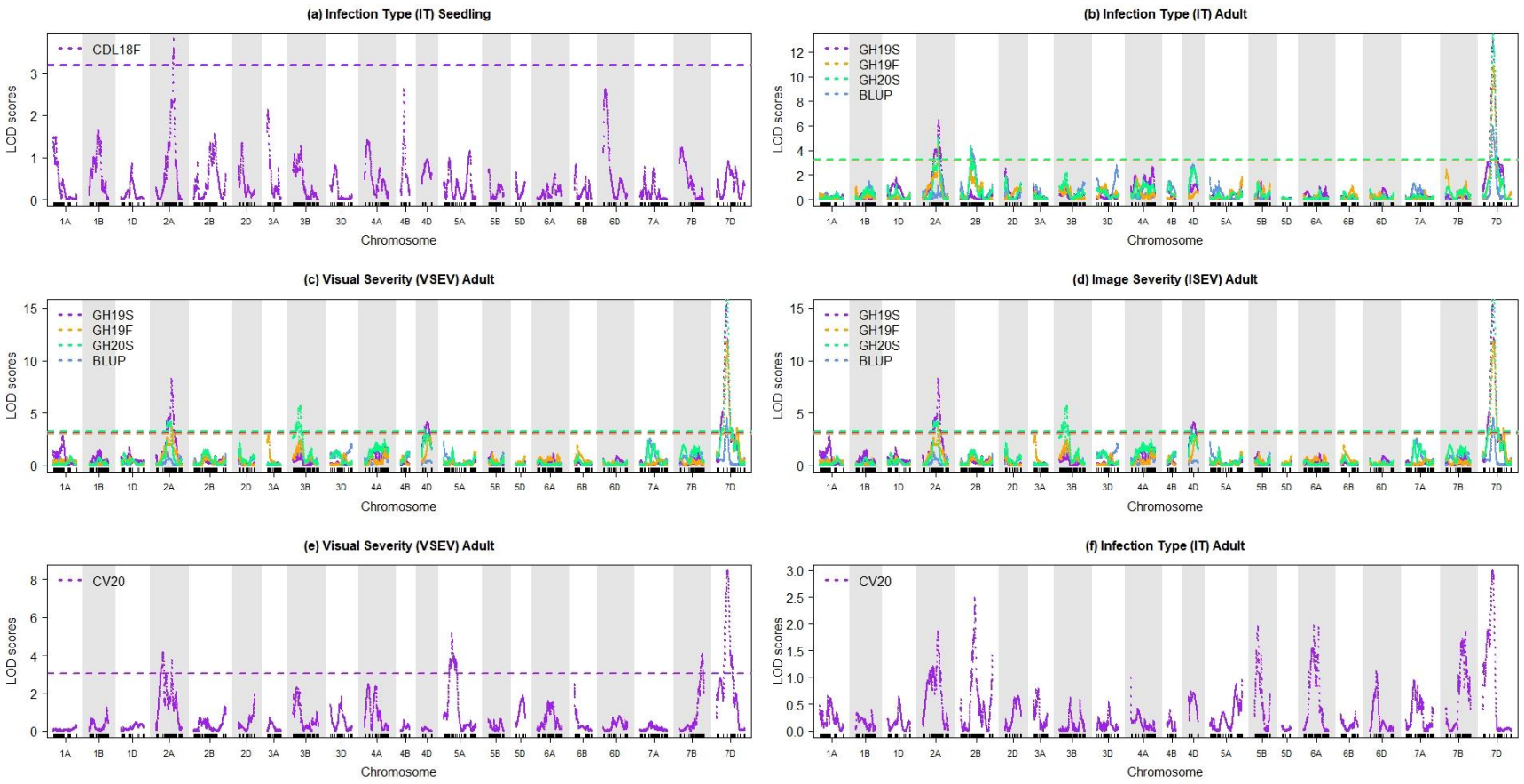

Figure 2-3. Genome-wide logarithm of the odds (LOD) values obtained from composite interval mapping of the DH population for (a) infection type at the seedling stage, (b) infection type at the adult plant stage in the greenhouse using race TFBJQ, (c) visual severity at the adult plant stage in the greenhouse using race TFBJQ, (d) image severity at the adult plant stage in the greenhouse using race TFBJQ, (e) visual severity at the adult plant stage under natural infection in the field at Castroville, TX, and (f) infection type at the adult plant stage under natural infection in the field at Castroville, TX.. Individual points on the LOD curve represent SNPs. Horizontal dashed lines represent the genome-wide LOD thresholds ($P<0.05$).

1731 **Table 2-1.** Virulence profiles of the 7 *Puccinia triticina* races.

Race	Virulence profile	Source
TBBGS	1, 2a, 2c, 3, 10, 21, 28, 39	Kolmer, 2019
BBBBD	39	USDA-ARS, 2016; Kolmer, Bernardo, et al., 2018
TNRJJ	1, 2a, 2c, 3, 9, 24, 3ka, 11, 30, 10, 14a, 28, 39	USDA-ARS, 2013; Kolmer et al., 2006
MBDSD	1, 3, 10, 14a, 17, 39, B	USDA-ARS, 2023; Aoun et al., 2016
MLDSD	1, 3, 9, 10, 14a, 17, 39, B	USDA-ARS, 2016
TNRJ	1, 2a, 2c, 3, 9, 24, 3ka, 17, 30, 10, 14a, 28, 39, 14b, 20, 28	Fellers et al., 2020b
TFBJQ	1, 2a, 2c, 3, 10, 14a, 14b, 20, 21, 24, 26, 28	USDA-ARS, 2016; Aoun et al., 2016

1732

Table 2-2. Descriptive statistics of leaf rust traits for Everest, Cedar, and the DH population for seedling screening, adult plant greenhouse screening, and adult plant field screening. Broad sense heritability was calculated for each trait across cycles or blocks for greenhouse and field experiments, respectively.

Trait	Experiment	Stage*	Race¥	Parents		DH Lines			H^2
				Everest	Cedar	Mean	MIN	MAX	
IT	CDL18F	Seedling	TBBGS	0	5	2	0	8	-
IT	GH19F	Adult	TFBJQ	4	5	6	2	9	0.7
	GH19F	Adult	TFBJQ	5	5	5	3	8	
	GH20S	Adult	TFBJQ	5	5	5	2	8	
VSEV	GH19S	Adult	TFBJQ	8.7%	11.5%	17.5%	3.4%	40.1%	0.7
	GH19F	Adult	TFBJQ	17.7%	25.9%	20.8%	12.0%	38.9%	
	GH20S	Adult	TFBJQ	20.6%	23.8%	19.5%	2.5%	31.0%	
ISEV	GH19S	Adult	TFBJQ	2.5%	4.2%	6.4%	0.1%	29.4%	0.6
	GH19F	Adult	TFBJQ	23.3%	52.7%	38.2%	3.8%	89.5%	
	GH20S	Adult	TFBJQ	28.3%	35.0%	25.7%	0.4%	96.8%	
IT	CV20S	Adult	Native	4	4	5	1	8	0.5
VSEV	CV20S	Adult	Native	22.8%	21.0%	23.4%	2.0%	90.0%	0.7

* Plant growth stage at which leaf rust measurements were recorded.

¥ Leaf rust race used for artificial inoculation. Natural pressure in field experiments is designated at 'Native'.

Table 2-3. Summary of SNP marker data for all 21 wheat chromosomes.

Chromosome/Genome	Number of SNPs	Genetic Length (cM)	Map Density (cM/SNPs)	SNP Density (SNPs/cM)
1A	358	188.83	0.53	1.90
2A	338	209.63	0.62	1.61
3A	187	112.27	0.60	1.67
4A	224	196.89	0.88	1.14
5A	184	263.11	1.43	0.70
6A	330	199.92	0.61	1.65
7A	329	223.99	0.68	1.47
A Genome	1950	1394.63	0.72	1.40
1B	232	160.54	0.69	1.45
2B	395	259.02	0.66	1.52
3B	458	204.78	0.45	2.24
4B	51	71.18	1.40	0.72
5B	198	123.51	0.62	1.60
6B	133	137.81	1.04	0.97
7B	282	201.20	0.71	1.40
B Genome	1749	1158.04	0.66	1.51
1D	96	185.59	1.93	0.52
2D	69	135.27	1.96	0.51
3D	106	175.49	1.66	0.60
4D	15	77.22	5.15	0.19
5D	31	76.52	2.47	0.41
6D	80	194.22	2.43	0.41
7D	75	231.16	3.08	0.32
D Genome	472	1075.47	2.28	0.44
Total	4171	3628.13	0.87	1.15

Table 2-4. Summary of quantitative trait loci associated with BLUPs estimated for leaf rust resistance traits. Logorithm of the odds (LOD) values obtained from composite interval mapping (CIM) and multiple QTL mapping (MQM) are presented for each significant association. The percent variance (R2) explained by each QTL is provided.

QTL	Trait	Data Set	Race	Peak Marker*	Alleles	Genetic Position (cM)	1.5 LOD Interval (cM)	LOD Threshold$^{\varphi}$	LOD-CIM	LOD-MQM	Variance Explained	Source‡
QLr.ksu-2AS	VSEV	CV20S	Native	snp-2A-24002490	G/C	55.00	15.76-134.43	3.09	4.13	5.50	9.56	WB-Cedar
QLr.ksu-2AL	IT	GHBLUP	TFBJQ	snp-2A-630461249	C/T	127.19	120.89-134.43	3.21	4.93	5.51	9.39	Everest
QLr.ksu-2AL	VSEV	GHBLUP	TFBJQ	snp-2A-630461249	C/T	127.19	120.89-131.96	3.17	4.10	5.84	8.75	Everest
QLr.ksu-2BS	IT	GHBLUP	TFBJQ	snp-2B-65685562	C/T	85.49	67.78-107.83	3.21	4.28	4.49	7.55	Everest
QLr.ksu-3BL	ISEV	GHBLUP	TFBJQ	snp-3B-512203483	T/C	60.30	0.76-79.40	3.23	5.15	4.24	8.05	Everest
QLr.ksu-4DL	VSEV	GHBLUP	TFBJQ	snp-4D-504199409	C/T	48.00	19.64-72.47	3.17	3.42	4.58	7.07	Everest
QLr.ksu-5AL	VSEV	CV20S	Native	snp-5A-395681178	G/C	67.11	45.05-105.70	3.09	5.09	5.40	9.37	WB-Cedar
QLr.ksu-7BL	VSEV	CV20S	Native	snp-7B-730113648	C/T	185.70	156.84-201.20	3.09	4.07	4.19	7.15	Everest
QLr.ksu-7DS	VSEV	CV20S	Native	snp-7D-53700222	C/T	83.00	57.31-114.13	3.09	8.44	9.86	18.34	WB-Cedar
QLr.ksu-7DS	IT	GHBLUP	TFBJQ	*Lr34*	A/T	82.00	57.31-114.13	3.21	13.73	13.73	26.59	WB-Cedar
QLr.ksu-7DS	VSEV	GHBLUP	TFBJQ	*Lr34*	A/T	82.00	57.31-114.13	3.17	19.11	20.11	39.59	WB-Cedar
QLr.ksu-7DS	ISEV	GHBLUP	TFBJQ	*Lr34*	A/T	81.00	57.31-114.13	3.23	15.62	15.05	33.74	WB-Cedar

* Labels for markers contain the chromosome and the physical position in bp anchored to the Chinese Spring reference genome. φ LOD thresholds for each trait-environment combination derived from 1,000 permutations at P≤0.05. ‡ The source of the QTL associated with IT, VSEV, and ISEV corresponds with the resistance alleles.

References

Appels, R., Eversole, K., Stein, N., Feuillet, C., Keller, B., Rogers, J., Pozniak, C. J., Choulet, F., Distelfeld, A., Poland, J., Ronen, G., Sharpe, A. G., Barad, O., Baruch, K., Keeble-Gagnère, G., Mascher, M., Ben-Zvi, G., Josselin, A.-A., Himmelbach, A., & Balfourier, F. (2018). Shifting the limits in wheat research and breeding using a fully annotated reference genome. *Science*, *361*(6403), eaar7191. https://doi.org/10.1126/science.aar7191

Bokore, F. E., Knox, R. E., Cuthbert, R. D., Pozniak, C. J., McCallum, B. D., N'Diaye, A., DePauw, R. M., Campbell, H. L., Munro, C., Singh, A., Hiebert, C. W., McCartney, C. A., Sharpe, A. G., Singh, A. K., Spaner, D., Fowler, D. B., Ruan, Y., Berraies, S., & Meyer, B. (2020). Mapping quantitative trait loci associated with leaf rust resistance in five spring wheat populations using single nucleotide polymorphism markers. *PLOS ONE*, *15*(4), e0230855. https://doi.org/10.1371/journal.pone.0230855

Bolton, M. D., Kolmer, J. A., & Garvin, D. F. (2008). Wheat leaf rust caused by Puccinia triticina. *Molecular Plant Pathology*, *9*(5), 563–575. https://doi.org/10.1111/j.1364-3703.2008.00487.x

Broman, K. W., Wu, H., Sen, S., & Churchill, G. A. (2003). R/qtl: QTL mapping in experimental crosses. *Bioinformatics*, *19*(7), 889–890. https://doi.org/10.1093/bioinformatics/btg112

Broman, K., & Sen, S. (2009). A Guide to QTL Mapping with R/qtl. In *www.springer.com*. Springer-Verlag. https://www.springer.com/gp/book/9780387921242

Browder, L. E. (1971a). Pathogenic specialization in cereal rust fungi, especially Puccinia recondita f. sp. tritici : Concepts, methods of study, and application. *Naldc.nal.usda.gov*. https://naldc.nal.usda.gov/catalog/CAT71328703

Browder, L. E. (1971b). *Pathogenic specialization in cereal rust fungi, especially Puccinia recondita f. sp. tritici: Concepts, methods of study, and application* (Vol. 1424). US Agricultural Research Service.

Browder, L. E. (1972). Designation of Two Genes for Resistance to Puccinia Recondita in Triticum Aestivum 1. *Crop Science*, *12*(5), 705–706. https://doi.org/10.2135/cropsci1972.0011183x001200050049x

Browning, B. L., Zhou, Y., & Browning, S. R. (2018). A One-Penny Imputed Genome from Next-Generation Reference Panels. *The American Journal of Human Genetics*, *103*(3), 338–348. https://doi.org/10.1016/j.ajhg.2018.07.015

Calvo-Salazar, V., Singh, R. P., Huerta-Espino, J., Cruz-Izquierdo, S., Lobato-Ortiz, R., Sandoval-Islas, S., Vargas-Hernández, M., German, S., Silva, P., Basnet, B. R., Lan, C. X., & Herrera-Foessel, S. A. (2015). Genetic Analysis of Resistance to Leaf Rust and Yellow Rust in Spring Wheat Cultivar Kenya Kongoni. *Plant Disease*, *99*(8), 1153–1160. https://doi.org/10.1094/pdis-07-14-0718-re

Che, M., Hiebert, C. W., McCartney, C. A., Zhang, Z., & McCallum, B. D. (2019). Mapping and DNA marker development for Lr33 from the leaf rust resistant line KU168-2. *Euphytica*, *215*(2). https://doi.org/10.1007/s10681-019-2343-3

Chhetri, M., Bariana, H., Wong, D., Sohail, Y., Hayden, M., & Bansal, U. (2017). Development of robust molecular markers for marker-assisted selection of leaf rust resistance gene Lr23 in common and durum wheat breeding programs. *Molecular Breeding*, *37*(3). https://doi.org/10.1007/s11032-017-0628-6

Chu, C.-G. ., Friesen, T. L., Xu, S. S., Faris, J. D., & Kolmer, J. A. (2009). Identification of novel QTLs for seedling and adult plant leaf rust resistance in a wheat doubled haploid

population. *Theoretical and Applied Genetics*, *119*(2), 263–269. https://doi.org/10.1007/s00122-009-1035-0

Darino, M. A., Dieguez, M. J., Singh, D., Ingala, L. R., Pergolesi, M. F., Park, R. F., McIntosh, R. A., & Sacco, F. (2015). Detection and location of Lr11 and other leaf rust resistance genes in the durably resistant wheat cultivar Buck Poncho. *Euphytica*, *206*(1), 135–147. https://doi.org/10.1007/s10681-015-1486-0

DeWolf, E. D., Lollato, R., & Whitworth, R. J. (2017). *Wheat Variety Disease and Insect Ratings 2017*. Kansas State University.

DeWolf, E., & Lollato, R. (2019, November 2). *Wheat leaf rust establishes a foothold in Kansas*. Webapp.agron.ksu.edu. https://webapp.agron.ksu.edu/agr_social/m_eu_article.throck?article_id=2026

Dinh, H. X., Singh, D., Periyannan, S., Park, R. F., & Pourkheirandish, M. (2020). Molecular genetics of leaf rust resistance in wheat and barley. *Theoretical and Applied Genetics*, *133*(7), 2035–2050. https://doi.org/10.1007/s00122-020-03570-8

Dvořák, J. (1977). Transfer of leaf rust resistance from Aegilops speltoides to Trticum aestivum. *Canadian Journal of Genetics and Cytology*, *19*(1), 133–141. https://doi.org/10.1139/g77-016

Dyck, P. L. (1977). Genetics of leaf rust reaction in three introductions of common wheat. *Canadian Journal of Genetics and Cytology*, *19*(4), 711–716. https://doi.org/10.1139/g77-077

Dyck, P. L. (1987). The association of a gene for leaf rust resistance with the chromosome 7D suppressor of stem rust resistance in common wheat. *Genome*, *29*(3), 467–469. https://doi.org/10.1139/g87-081

1810 Dyck, P. L., Kerber, E. R., & Lukow, O. M. (1987). Chromosome location and linkage of a new
1811 gene (Lr33) for reaction to Puccinia recondita in common wheat. *Genome*, *29*(3), 463–
1812 466. https://doi.org/10.1139/g87-080
1813 Dyck, P. L., & Samborski, D. J. (1970). The genetics of two alleles for leaf rust resistance at the
1814 Lr14 locus in wheat. *Canadian Journal of Genetics and Cytology*, *12*(4), 689–694.
1815 https://doi.org/10.1139/g70-091
1816 Dyck, P. L., & Sykes, E. E. (1994). Genetics of leaf-rust resistance in three spelt wheats.
1817 *Canadian Journal of Plant Science*, *74*(2), 231–233. https://doi.org/10.4141/cjps94-047
1818 Ellis, J. G., Lagudah, E. S., Spielmeyer, W., & Dodds, P. N. (2014). The past, present and future
1819 of breeding rust resistant wheat. *Frontiers in Plant Science*, *5*.
1820 https://doi.org/10.3389/fpls.2014.00641
1821 Elshire, R. J., Glaubitz, J. C., Sun, Q., Poland, J. A., Kawamoto, K., Buckler, E. S., & Mitchell,
1822 S. E. (2011). A Robust, Simple Genotyping-by-Sequencing (GBS) Approach for High
1823 Diversity Species. *PLoS ONE*, *6*(5), e19379.
1824 https://doi.org/10.1371/journal.pone.0019379
1825 Faris, J. D., Li, W. L., Liu, D. J., Chen, P. D., & Gill, B. S. (1999). Candidate gene analysis of
1826 quantitative disease resistance in wheat. *Theoretical and Applied Genetics*, *98*(2), 219–
1827 225. https://doi.org/10.1007/s001220051061
1828 Fellers, J. P., Matthews, A., Fritz, A. K., Rouse, M. N., Grewal, S., Hubbart-Edwards, S., King,
1829 I. P., & King, J. (2020). Resistance to wheat rusts identified in wheat/Amblyopyrum
1830 muticum chromosome introgressions. *Crop Science*, *60*(4), 1957–1964.
1831 https://doi.org/10.1002/csc2.20120

1832 Feuillet, C., Travella, S., Stein, N., Albar, L., Nublat, A., & Keller, B. (2003). Map-based
1833 isolation of the leaf rust disease resistance gene Lr10 from the hexaploid wheat (Triticum
1834 aestivum L.) genome. *Proceedings of the National Academy of Sciences*, *100*(25),
1835 15253–15258. https://doi.org/10.1073/pnas.2435133100
1836 Figlan, S., Ntushelo, K., Mwadzingeni, L., Terefe, T., Tsilo, T. J., & Shimelis, H. (2020).
1837 Breeding Wheat for Durable Leaf Rust Resistance in Southern Africa: Variability,
1838 Distribution, Current Control Strategies, Challenges and Future Prospects. *Frontiers in*
1839 *Plant Science*, *11*. https://doi.org/10.3389/fpls.2020.00549
1840 Figueroa, M., Hammond-Kosack, K. E., & Solomon, P. S. (2017). A review of wheat diseases-a
1841 field perspective. *Molecular Plant Pathology*, *19*(6), 1523–1536.
1842 https://doi.org/10.1111/mpp.12618
1843 Friebe, B., Jiang, J., Gill, B. S., & Dyck, P. L. (1993). Radiation-induced nonhomoeologous
1844 wheat-Agropyron intermedium chromosomal translocations conferring resistance to leaf
1845 rust. *Theoretical and Applied Genetics*, *86-86*(2-3), 141–149.
1846 https://doi.org/10.1007/bf00222072
1847 Friebe, B., Jiang, J., Raupp, W. J., McIntosh, R. A., & Gill, B. S. (1996). Characterization of
1848 wheat-alien translocations conferring resistance to diseases and pests: current status.
1849 *Euphytica*, *91*(1), 59–87. https://doi.org/10.1007/bf00035277
1850 Gebrewahid, T. W., Zhang, P., Zhou, Y., Yan, X., Xia, X., He, Z., Liu, D., & Li, Z. (2020). QTL
1851 mapping of adult plant resistance to stripe rust and leaf rust in a Fuyu 3/Zhengzhou 5389
1852 wheat population. *The Crop Journal*, *8*(4), 655–665.
1853 https://doi.org/10.1016/j.cj.2019.09.013

German, S. E., & Kolmer, J. A. (1992). Effect of gene Lr34 in the enhancement of resistance to leaf rust of wheat. *Theoretical and Applied Genetics*, *84*(1-2), 97–105. https://doi.org/10.1007/bf00223987

Haley, C. S., & Knott, S. A. (1992). A simple regression method for mapping quantitative trait loci in line crosses using flanking markers. *Heredity*, *69*(4), 315–324. https://doi.org/10.1038/hdy.1992.131

He, S., Schulthess, A. W., Mirdita, V., Zhao, Y., Korzun, V., Bothe, R., Ebmeyer, E., Reif, J. C., & Jiang, Y. (2016). Genomic selection in a commercial winter wheat population. *Theoretical and Applied Genetics*, *129*(3), 641–651. https://doi.org/10.1007/s00122-015-2655-1

Helguera, M., Khan, I. A., Kolmer, J., Lijavetzky, D., Zhong-qi, L., & Dubcovsky, J. (2003). PCR Assays for the Lr37-Yr17-Sr38 Cluster of Rust Resistance Genes and Their Use to Develop Isogenic Hard Red Spring Wheat Lines. *Crop Science*, *43*(5), 1839–1847. https://doi.org/10.2135/cropsci2003.1839

Helguera, M., Vanzetti, L., Soria, M., Khan, I. A., Kolmer, J., & Dubcovsky, J. (2005). PCR Markers for Triticum speltoides Leaf Rust Resistance Gene Lr51 and Their Use to Develop Isogenic Hard Red Spring Wheat Lines. *Crop Science*, *45*(2), 728–734. https://doi.org/10.2135/cropsci2005.0728

Herrera-Foessel, S. A., Lagudah, E. S., Huerta-Espino, J., Hayden, M. J., Bariana, H. S., Singh, D., & Singh, R. P. (2010). New slow-rusting leaf rust and stripe rust resistance genes Lr67 and Yr46 in wheat are pleiotropic or closely linked. *Theoretical and Applied Genetics*, *122*(1), 239–249. https://doi.org/10.1007/s00122-010-1439-x

Herrera-Foessel, S. A., Singh, R. P., Huerta-Espino, J., Rosewarne, G. M., Periyannan, S. K., Viccars, L., Calvo-Salazar, V., Lan, C., & Lagudah, E. S. (2012). Lr68: a new gene conferring slow rusting resistance to leaf rust in wheat. *Theoretical and Applied Genetics*, *124*(8), 1475–1486. https://doi.org/10.1007/s00122-012-1802-1

Hiebert, C. W., Thomas, J. B., McCallum, B. D., Humphreys, D. G., DePauw, R. M., Hayden, M. J., Mago, R., Schnippenkoetter, W., & Spielmeyer, W. (2010). An introgression on wheat chromosome 4DL in RL6077 (Thatcher*6/PI 250413) confers adult plant resistance to stripe rust and leaf rust (Lr67). *Theoretical and Applied Genetics*, *121*(6), 1083–1091. https://doi.org/10.1007/s00122-010-1373-y

Joshi, K. D., Ullah, G., Rehman, A. U., Javaid, M. M., Ahmad, J., Hussain, M., Pacheco, A., Khalil, I. A., & Baloch, A. (2017). Wheat Yield Response to Foliar Fungicide Application against Leaf Rust Caused by Puccinia triticina. *Journal of Agricultural Science and Technology*, *7*(3). https://doi.org/10.17265/2161-6256/2017.03.003

Kassa, M. T., You, F. M., Hiebert, C. W., Pozniak, C. J., Fobert, P. R., Sharpe, A. G., Menzies, J. G., Humphreys, D. G., Rezac Harrison, N., Fellers, J. P., McCallum, B. D., & McCartney, C. A. (2017). Highly predictive SNP markers for efficient selection of the wheat leaf rust resistance gene Lr16. *BMC Plant Biology*, *17*(1). https://doi.org/10.1186/s12870-017-0993-7

Kerber, E. R., & Dyck, P. L. (1990). Transfer to hexaploid wheat of linked genes for adult-plant leaf rust and seedling stem rust resistance from an amphiploid of Aegilops speltoides × Triticum monococcum. *Genome*, *33*(4), 530–537. https://doi.org/10.1139/g90-079

Kloppers, F. J., & Pretorius, Z. A. (1997). Effects of combinations amongst genes Lr13 , Lr34 and Lr37 on components of resistance in wheat to leaf rust. *Plant Pathology*, *46*(5), 737–750. https://doi.org/10.1046/j.1365-3059.1997.d01-58.x

Kolmer, J. (2013). Leaf Rust of Wheat: Pathogen Biology, Variation and Host Resistance. *Forests*, *4*(1), 70–84. https://doi.org/10.3390/f4010070

Kolmer, J. (2021, January 11). *Wheat leaf rust : USDA ARS*. Www.ars.usda.gov. https://www.ars.usda.gov/midwest-area/stpaul/cereal-disease-lab/docs/cereal-rusts/wheat-leaf-rust/

Kolmer, J. A. (2005). Tracking wheat rust on a continental scale. *Current Opinion in Plant Biology*, *8*(4), 441–449. https://doi.org/10.1016/j.pbi.2005.05.001

Kolmer, J. A. (2009). Genetics of Leaf Rust Resistance in the Soft Red Winter Wheat "Caldwell." *Crop Science*, *49*(4), 1187. https://doi.org/10.2135/cropsci2008.10.0598

Kolmer, J. A. (2017). Genetics of Leaf Rust Resistance in the Hard Red Winter Wheat Cultivars Santa Fe and Duster. *Crop Science*, *57*(5), 2500–2505. https://doi.org/10.2135/cropsci2016.12.1029

Kolmer, J. A. (2019). Virulence of Puccinia triticina, the Wheat Leaf Rust Fungus, in the United States in 2017. *Plant Disease*, *103*(8), 2113–2120. https://doi.org/10.1094/pdis-09-18-1638-sr

Kolmer, J. A., Jin, Y., & Long, D. L. (2007). Wheat leaf and stem rust in the United States. *Australian Journal of Agricultural Research*, *58*(6), 631–638. https://doi.org/10.1071/AR07057

Kolmer, J. A., Su, Z., Bernardo, A., Bai, G., & Chao, S. (2018). Mapping and characterization of the new adult plant leaf rust resistance gene Lr77 derived from Santa Fe winter wheat.

Theoretical and Applied Genetics, *131*(7), 1553–1560. https://doi.org/10.1007/s00122-018-3097-3

Kolmer, J. A., Su, Z., Bernardo, A., Bai, G., & Chao, S. (2019). A Backcross Line of Thatcher Wheat with Adult Plant Leaf Rust Resistance Derived from Duster Wheat has Lr46 and Lr77. *Phytopathology®*, *109*(1), 127–132. https://doi.org/10.1094/phyto-06-18-0184-r

Kosambi, D. D. (1943). The estimation of map distances from recombination values. *Annals of Eugenics*, *12*(1), 172–175. https://doi.org/10.1111/j.1469-1809.1943.tb02321.x

Krattinger, S. G., Sucher, J., Selter, L. L., Chauhan, H., Zhou, B., Tang, M., Upadhyaya, N. M., Mieulet, D., Guiderdoni, E., Weidenbach, D., Schaffrath, U., Lagudah, E. S., & Keller, B. (2015). The wheat durable, multipathogen resistance geneLr34confers partial blast resistance in rice. *Plant Biotechnology Journal*, *14*(5), 1261–1268. https://doi.org/10.1111/pbi.12491

Kumar, S., Bhardwaj, S. C., Gangwar, O. P., Sharma, A., Qureshi, N., Kumaran, V. V., Khan, H., Prasad, P., Miah, H., Singh, G. P., Sharma, K., Verma, H., Forrest, K. L., Trethowan, R. M., Bariana, H. S., & Bansal, U. K. (2021). Lr80: A new and widely effective source of leaf rust resistance of wheat for enhancing diversity of resistance among modern cultivars. *Theoretical and Applied Genetics*, *134*(3), 849–858. https://doi.org/10.1007/s00122-020-03735-5

Lagudah, E. S., Krattinger, S. G., Herrera-Foessel, S., Singh, R. P., Huerta-Espino, J., Spielmeyer, W., Brown-Guedira, G., Selter, L. L., & Keller, B. (2009). Gene-specific markers for the wheat gene Lr34/Yr18/Pm38 which confers resistance to multiple fungal pathogens. *Theoretical and Applied Genetics*, *119*(5), 889–898. https://doi.org/10.1007/s00122-009-1097-z

Leonova, I., Budashkina, E., Flath, K., Weidner, A., Börner, A., & Röder, M. (2010). Microsatellite mapping of a leaf rust resistance gene transferred to common wheat fromTriticum timopheevii. *Cereal Research Communications*, *38*(2), 211–219. https://doi.org/10.1556/crc.38.2010.2.7

Li, Z., Lan, C., He, Z., Singh, R. P., Rosewarne, G. M., Chen, X., & Xia, X. (2014). Overview and Application of QTL for Adult Plant Resistance to Leaf Rust and Powdery Mildew in Wheat. *Crop Science*, *54*(5), 1907–1925. https://doi.org/10.2135/cropsci2014.02.0162

Lindsey, L., Paul, P., & Lentz, E. (2017, October). *Wheat Growth Stages and Associated Management: Feekes 7, 8, and 9 | Agronomic Crops Network*. Agcrops.osu.edu. https://agcrops.osu.edu/newsletter/corn-newsletter/2017-10/wheat-growth-stages-and-associated-management-feekes-7-8-and-9

Lowe, I., Cantu, D., & Dubcovsky, J. (2010). Durable resistance to the wheat rusts: integrating systems biology and traditional phenotype-based research methods to guide the deployment of resistance genes. *Euphytica*, *179*(1), 69–79. https://doi.org/10.1007/s10681-010-0311-z

Maccaferri, M., Mantovani, P., Tuberosa, R., DeAmbrogio, E., Giuliani, S., Demontis, A., Massi, A., & Sanguineti, M. C. (2008). A major QTL for durable leaf rust resistance widely exploited in durum wheat breeding programs maps on the distal region of chromosome arm 7BL. *Theoretical and Applied Genetics*, *117*(8), 1225–1240. https://doi.org/10.1007/s00122-008-0857-5

McCallum, B. D., Reimer, E., McNabb, W., Foster, A., Rosa, S., & Xue, A. (2021). Physiologic specialization of Puccinia triticina, the causal agent of wheat leaf rust, in Canada in 2015-

2019. *Canadian Journal of Plant Pathology*. https://doi.org/10.1080/07060661.2021.1888156

McCallum, B., Hiebert, C., Huerta-Espino, J., & Cloutier, S. (2012). Wheat leaf rust. In *Disease resistance in wheat* (pp. 33–62). Cabi.

McIntosh, R. A., Dubcovsky, J., Rogers, W. J., Morris, F. C., Appels, R., & Xia, X. (2014). Catalogue of gene symbols for wheat: 2013-14 Supplement. *Annual Wheat Newsletter*, *vol. 58*. https://digital.cic.gba.gob.ar/handle/11746/6438

McIntosh, R. A., Friebe, B., Jiang, J., The, D., & Gill, B. S. (1995). Cytogenetical studies in wheat XVI. Chromosome location of a new gene for resistance to leaf rust in a Japanese wheat-rye translocation line. *Euphytica*, *82*(2), 141–147. https://doi.org/10.1007/bf00027060

McIntosh, R. A., Wellings, C. R., & Park, R. F. (1995). Wheat Rusts: An Atlas of Resistance Genes. In *www.springer.com*. Springer Netherlands. https://www.springer.com/gp/book/9789401040419

McIntosh, R., & Dyck, P. (1975). Cytogenetical Stndies in Wheat. VII Gene Lr23 for Reaction to Puccinia recondita in Gabo and Related Cultivars. *Australian Journal of Biological Sciences*, *28*(2), 201. https://doi.org/10.1071/bi9750201

Mcintosh, R., Luig, N., & Baker, E. (1967). Genetic and Cytogenetic Studies of Stem Rust, Leaf Rust, and Powdery Mildew Resistances in Hope and Related Wheat Cultivars. *Australian Journal of Biological Sciences*, *20*(6), 1181. https://doi.org/10.1071/bi9671181

Mcintosh, R., Yamazaki, Y., Dubcovsky, J., Rogers, J., Morris, C., Appels, R., & Xia, X. (2013). *Catalog of Gene Symbols for Wheat*.

https://wheat.pw.usda.gov/GG3/sites/default/files/Catalogue%20of%20Gene%20Symbols%20for%20Wheat%20-%202013%20edition.pdf

Mebrate, S. A., Oerke, E. C., Dehne, H. W., & Pillen, K. (2007). Mapping of the leaf rust resistance gene Lr38 on wheat chromosome arm 6DL using SSR markers. *Euphytica*, *162*(3), 457–466. https://doi.org/10.1007/s10681-007-9615-z

Messmer, M. M., Seyfarth, R., Keller, M., Schachermayr, G., Winzeler, M., Zanetti, S., Feuillet, C., & Keller, B. (2000). Genetic analysis of durable leaf rust resistance in winter wheat. *Theoretical and Applied Genetics*, *100*(3-4), 419–431. https://doi.org/10.1007/s001220050055

Milne, R. J., Dibley, K. E., Schnippenkoetter, W., Mascher, M., Lui, A. C. W., Wang, L., Lo, C., Ashton, A. R., Ryan, P. R., & Lagudah, E. S. (2019). The Wheat Lr67 Gene from the Sugar Transport Protein 13 Family Confers Multipathogen Resistance in Barley1[OPEN]. *Plant Physiology*, *179*(4), 1285–1297. https://doi.org/10.1104/pp.18.00945

Naik, B. K., Vinod, Sharma, J. B., Sivasamy, M., Prabhu, K. V., Tomar, R. S., & Tomar, S. M. S. (2015). Molecular mapping and validation of the microsatellite markers linked to the Secale cereale-derived leaf rust resistance gene Lr45 in wheat. *Molecular Breeding*, *35*(2). https://doi.org/10.1007/s11032-015-0234-4

Nsabiyera, V., Qureshi, N., Bariana, H. S., Wong, D., Forrest, K. L., Hayden, M. J., & Bansal, U. K. (2016). Molecular markers for adult plant leaf rust resistance gene Lr48 in wheat. *Molecular Breeding*, *36*(6). https://doi.org/10.1007/s11032-016-0488-5

Park, R. F., Mohler, V., Nazari, K., & Singh, D. (2014). Characterisation and mapping of gene Lr73 conferring seedling resistance to Puccinia triticina in common wheat. *Theoretical and Applied Genetics*, *127*(9), 2041–2049. https://doi.org/10.1007/s00122-014-2359-y

Peterson, R. F., Campbell, A. B., & Hannah, A. E. (1948). A DIAGRAMMATIC SCALE FOR ESTIMATING RUST INTENSITY ON LEAVES AND STEMS OF CEREALS. *Canadian Journal of Research*, *26c*(5), 496–500. https://doi.org/10.1139/cjr48c-033

Pethybridge, S. J., & Nelson, S. C. (2015). Leaf Doctor: A New Portable Application for Quantifying Plant Disease Severity. *Plant Disease*, *99*(10), 1310–1316. https://doi.org/10.1094/pdis-03-15-0319-re

Pinto da Silva, G. B., Zanella, C. M., Martinelli, J. A., Chaves, M. S., Hiebert, C. W., McCallum, B. D., & Boyd, L. A. (2018). Quantitative Trait Loci Conferring Leaf Rust Resistance in Hexaploid Wheat. *Phytopathology®*, *108*(12), 1344–1354. https://doi.org/10.1094/phyto-06-18-0208-rvw

Poland, J. A., Brown, P. J., Sorrells, M. E., & Jannink, J.-L. (2012). Development of High-Density Genetic Maps for Barley and Wheat Using a Novel Two-Enzyme Genotyping-by-Sequencing Approach. *PLoS ONE*, *7*(2), e32253. https://doi.org/10.1371/journal.pone.0032253

Pretorious, Z. A., Wilcoxson, R. D., Long, D. L., & Schafer, J. F. (1984). Detecting wheat leaf rust resistance gene Lr 13 in seedlings. *Detecting Wheat Leaf Rust Resistance Gene Lr 13 in Seedlings*, *68*(7), 585–586. https://pascal-francis.inist.fr/vibad/index.php?action=getRecordDetail&idt=8915320

Qiu, L., Wang, H., Li, Y., Wang, W., Liu, Y., Mu, J., Geng, M., Guo, W., Hu, Z., Ma, J., Sun, Q., & Xie, C. (2020). Fine Mapping of the Wheat Leaf Rust Resistance Gene LrLC10 (Lr13) and Validation of Its Co-segregation Markers. *Frontiers in Plant Science*, *11*. https://doi.org/10.3389/fpls.2020.00470

Qureshi, N., Bariana, H., Kumran, V. V., Muruga, S., Forrest, K. L., Hayden, M. J., & Bansal, U. (2018). A new leaf rust resistance gene Lr79 mapped in chromosome 3BL from the durum wheat landrace Aus26582. *Theoretical and Applied Genetics*, *131*(5), 1091–1098. https://doi.org/10.1007/s00122-018-3060-3

Research : USDA ARS. (2021). Www.ars.usda.gov. https://www.ars.usda.gov/plains-area/lincoln-ne/wheat-sorghum-and-forage-research/docs/hard-winter-wheat-regional-nursery-program/research/

Rinaldo, A., Gilbert, B., Boni, R., Krattinger, S. G., Singh, D., Park, R. F., Lagudah, E., & Ayliffe, M. (2017). The Lr34 adult plant rust resistance gene provides seedling resistance in durum wheat without senescence. *Plant Biotechnology Journal*, *15*(7), 894–905. https://doi.org/10.1111/pbi.12684

Rollar, S., Serfling, A., Geyer, M., Hartl, L., Mohler, V., & Ordon, F. (2020). QTL mapping of adult plant and seedling resistance to leaf rust (Puccinia triticina Eriks.) in a multiparent advanced generation intercross (MAGIC) wheat population. *Theoretical and Applied Genetics*, *134*(1), 37–51. https://doi.org/10.1007/s00122-020-03657-2

Rosewarne, G. M., Singh, R. P., Huerta-Espino, J., Herrera-Foessel, S. A., Forrest, K. L., Hayden, M. J., & Rebetzke, G. J. (2012). Analysis of leaf and stripe rust severities reveals pathotype changes and multiple minor QTLs associated with resistance in an Avocet × Pastor wheat population. *Theoretical and Applied Genetics*, *124*(7), 1283–1294. https://doi.org/10.1007/s00122-012-1786-x

Saini, R. G., Kaur, M., Singh, B., Sharma, S., Nanda, G. S., Nayar, S. K., Gupta, A. K., & Nagarajan, S. (2002). Genes Lr48 and Lr49 for hypersensitive adult plant leaf rust

resistance in wheat (Triticum aestivum L.). *Euphytica*, *124*(3), 365–370. https://doi.org/10.1023/a:1015762812907

Sapkota, S., Mergoum, M., Kumar, A., Fiedler, J. D., Johnson, J., Bland, D., Lopez, B., Sutton, S., Ghimire, B., Buck, J., Chen, Z., & Harrison, S. (2020). A novel adult plant leaf rust resistance gene Lr2K38 mapped on wheat chromosome 1AL. *The Plant Genome*, *13*(3). https://doi.org/10.1002/tpg2.20061

Sawhney, R. N. (1992). The role of Lr34 in imparting durable resistance to wheat leaf rust through gene interaction. *Euphytica*, *61*(1), 9–12. https://doi.org/10.1007/bf00035541

Schnurbusch, T., Paillard, S., Schori, A., Messmer, M., Schachermayr, G., Winzeler, M., & Keller, B. (2003). Dissection of quantitative and durable leaf rust resistance in Swiss winter wheat reveals a major resistance QTL in the Lr34 chromosomal region. *Theoretical and Applied Genetics*, *108*(3), 477–484. https://doi.org/10.1007/s00122-003-1444-4

Seyfarth, R., Feuillet, C., Schachermayr, G., Winzeler, M., & Keller, B. (1999). Development of a molecular marker for the adult plant leaf rust resistance gene Lr35 in wheat. *Theoretical and Applied Genetics*, *99*(3-4), 554–560. https://doi.org/10.1007/s001220051268

Singh, N. K., Shepherd, K. W., & McIntosh, R. A. (1990). Linkage mapping of genes for resistance to leaf, stem and stripe rusts and ω-secalins on the short arm of rye chromosome 1R. *Theoretical and Applied Genetics*, *80*(5), 609–616. https://doi.org/10.1007/bf00224219

Singh, R. P., & Huerta-Espino, J. (2003). Effect of leaf rust resistance gene Lr34 on components of slow rusting at seven growth stages in wheat. *Euphytica*, *129*(3), 371–376. https://doi.org/10.1023/a:1022216327934

Singh, R. P., Mujeeb-Kazi, A., & Huerta-Espino, J. (1998). Lr46: A Gene Conferring Slow-Rusting Resistance to Leaf Rust in Wheat. *Phytopathology®*, *88*(9), 890–894. https://doi.org/10.1094/phyto.1998.88.9.890

Soriano, J. M., & Royo, C. (2015). Dissecting the Genetic Architecture of Leaf Rust Resistance in Wheat by QTL Meta-Analysis. *Phytopathology®*, *105*(12), 1585–1593. https://doi.org/10.1094/phyto-05-15-0130-r

Terracciano, I., Maccaferri, M., Bassi, F., Mantovani, P., Sanguineti, M. C., Salvi, S., Simková, H., Doležel, J., Massi, A., Ammar, K., Kolmer, J., & Tuberosa, R. (2013). Development of COS-SNP and HRM markers for high-throughput and reliable haplotype-based detection of Lr14a in durum wheat (Triticum durum Desf.). *TAG. Theoretical and Applied Genetics. Theoretische Und Angewandte Genetik*, *126*(4), 1077–1101. https://doi.org/10.1007/s00122-012-2038-9

U.S. Department of Agriculture, Agricultural Research Service. (2016). Number and frequency of *Puccinia triticina* virulence phenotypes and isolates in the United States in 2016 (Tables 1 & 2). *Cereal Rusts Report, 2016 Wheat Leaf Rust*. Retrieved from https://www.ars.usda.gov/ARSUserFiles/50620500/Cerealrusts/2016wlr/WLR%202016%20Table%201_2.pdf

U.S. Department of Agriculture, Agricultural Research Service. (2013). Number and frequency of *Puccinia triticina* virulence phenotypes and isolates in the United States in 2013 (Tables 1 & 2). *Cereal Rusts Report, 2013 Wheat Leaf Rust*. Retrieved from https://www.ars.usda.gov/ARSUserFiles/50620500/Cerealrusts/2013wlr_tables_1_2.pdf

U.S. Department of Agriculture, Agricultural Research Service. (2023). Number and frequency of *Puccinia triticina* virulence data in the United States in 2023 (Table 3). *Cereal Rusts Report, 2023 Wheat Leaf Rust*. Retrieved from https://www.ars.usda.gov/ARSUserFiles/50620500/Cerealrusts/2023%20WLR%20survey/2023%20WLR%20Table%203.xlsx

Van Ooijen, J. (2006). *JoinMap 4: Software for the calculation of genetic linkage maps in experimental populations*. Kyazma BV, Wageningen.

Vanzetti, L. S., Campos, P., Demichelis, M., Lombardo, L. A., Aurelia, P. R., Vaschetto, L. M., Bainotti, C. T., & Helguera, M. (2011). Identification of leaf rust resistance genes in selected Argentinean bread wheat cultivars by gene postulation and molecular markers. *Electronic Journal of Biotechnology*, *14*(3), 9–9. https://scielo.conicyt.cl/scielo.php?pid=S0717-34582011000300009&script=sci_arttext

Wang, C., Yin, G., Xia, X., He, Z., Zhang, P., Yao, Z., Qin, J., Li, Z., & Liu, D. (2016). Molecular mapping of a new temperature-sensitive gene LrZH22 for leaf rust resistance in Chinese wheat cultivar Zhoumai 22. *Molecular Breeding*, *36*(2). https://doi.org/10.1007/s11032-016-0437-3

Wang, Y., Peng, H., Liu, G., Xie, C., Ni, Z., Yang, T., Liu, Z., & Sun, Q. (2010). Identification and molecular mapping of a leaf rust resistance gene in spelt wheat landrace Altgold. *Euphytica*, *174*(3), 371–375. https://doi.org/10.1007/s10681-010-0134-y

Watson, I. A., & Luig, N. H. (1961). Leaf rust on Wheat in Australia: a systematic scheme for the classification of strains. *Proceedings of the Linnean Society of New South Wales*, *86*(2(396)), 241–250.

Wienhues, A. (1966). Transfer of rust resistance of Agropyron to wheat by addition, substitution and translocation. In J. MacKey (Ed.), *Proceedings of the Second International Wheat Genetics Symposium* (pp. 328–341). [Mendelian Society of Lund]; WorldCat.org.

Wienhues, A. (1973). Translocations between wheat chromosomes and an Agropyron chromosome conditioning rust resistance. In E. Sears & L. Sears (Eds.), *Proceedings of the Fourth international wheat genetics symposium* (pp. 201–207). University of Missouri, Columbia.

Wiesner-Hanks, T., & Nelson, R. (2016). Multiple Disease Resistance in Plants. *Annual Review of Phytopathology*, *54*(1), 229–252. https://doi.org/10.1146/annurev-phyto-080615-100037

Xue, S., Kolmer, J. A., Wang, S., & Yan, L. (2018). Mapping of Leaf Rust Resistance Genes and Molecular Characterization of the 2NS/2AS Translocation in the Wheat Cultivar Jagger. *G3 Genes|Genomes|Genetics*, *8*(6), 2059–2065. https://doi.org/10.1534/g3.118.200058

Yuan, C., Singh, R. P., Liu, D., Randhawa, M. S., Huerta-Espino, J., & Lan, C. (2020). Genome-Wide Mapping of Adult Plant Resistance to Leaf Rust and Stripe Rust in CIMMYT Wheat Line Arableu#1. *Plant Disease*, *104*(5), 1455–1464. https://doi.org/10.1094/pdis-10-19-2198-re

Zhang, D., Bowden, R. L., Yu, J., Carver, B. F., & Bai, G. (2014). Association Analysis of Stem Rust Resistance in U.S. Winter Wheat. *PLoS ONE*, *9*(7), e103747. https://doi.org/10.1371/journal.pone.0103747

Zhang, P., Li, X., Gebrewahid, T.-W., Liu, H., Xia, X., He, Z., Li, Z., & Liu, D. (2019). QTL Mapping of Adult-Plant Resistance to Leaf and Stripe Rust in Wheat Cross SW

8588/Thatcher using the Wheat 55K SNP Array. *Plant Disease*, *103*(12), 3041–3049. https://doi.org/10.1094/pdis-02-19-0380-re

Zhang, P., Yin, G., Zhou, Y., Qi, A., Gao, F., Xia, X., He, Z., Li, Z., & Liu, D. (2017). QTL Mapping of Adult-Plant Resistance to Leaf Rust in the Wheat Cross Zhou 8425B/Chinese Spring Using High-Density SNP Markers. *Frontiers in Plant Science*, *8*. https://doi.org/10.3389/fpls.2017.00793

Zhang, W., Lukaszewski, A. J., Kolmer, J., Soria, M. A., Goyal, S., & Dubcovsky, J. (2005). Molecular characterization of durum and common wheat recombinant lines carrying leaf rust resistance (Lr19) and yellow pigment (Y) genes from Lophopyrum ponticum. *Theoretical and Applied Genetics*, *111*(3), 573–582. https://doi.org/10.1007/s00122-005-2048-y

Zhou, Y., Xia, X., He, Z., Li, X., Li, Z., & Liu, D. (2013). Fine Mapping of Leaf Rust Resistance Gene LrZH84 Using Expressed Sequence Tag and Sequence-Tagged Site Markers, and Allelism with Other Genes on Wheat Chromosome 1B. *Phytopathology®*, *103*(2), 169–174. https://doi.org/10.1094/phyto-08-12-0186-r

Chapter 3 - Genomic Regions Conferring Leaf Tip Necrosis in Wheat and their Association with Leaf Rust Resistance

Marshall Clinesmith[1*], Allan Fritz[1*], Cristiano Lemes da Silva[2], Robert Bowden[3], Nora Bello[4], Mary Guttieri[3], Eduard Akhunov[5], Jessica Noller[5]

[1] Department of Agronomy, Kansas State University, Manhattan, KS 66502

[2] Corteva Agriscience, Westfield, IN

[3] USDA, Agricultural Research Service, Center for Grain and Animal Health Research, Hard Winter Wheat Genetics Research Unit

[4] Department of Statistics, Kansas State University, Manhattan, KS 66506

[5] Department of Plant Pathology, Kansas State University, Manhattan, KS 66506

Abstract

Plant breeding strategies aimed at improving resistance to leaf rust in wheat (*Tritcum aestivum* L.) have benefited tremendously from the use of adult plant resistance genes. The genes are considered partial effect genes, as they do not provide complete protection for the plant, which necessitates stacking of multiple genes into single cultivars. This is further complicated by the association of several of these genes with expression of leaf tip necrosis (LTN) on flag leaves, which can result in undesirable yield reductions. A greenhouse experiment was performed to phenotype LTN traits on a DH population between the cultivars Everest and 'Cedar' each carrying multiple loci for leaf rust resistance including *Ltn4*/*Lr68* (7BL) and *Ltn1*/*Lr34* (7DS), respectively. Five QTL associated with LTN were detected on chromosomes 1D, 2A, 4D, 5A, and 7D. The QTL on 2A was previously associated with an all-stage resistance (ASR) gene for leaf rust. *Ltn1/Lr34* contributed the greatest effect on LTN expression, whereas

no evidence for association was detected in the region containing *Ltn4*/*Lr68*. Results in the current study suggest that lines carrying higher numbers of leaf rust resistance alleles also show more extensive LTN expression.

Introduction

Leaf rust, caused by the fungal pathogen *Puccinia triticina* Eriks., is a major disease of wheat that occurs worldwide in all wheat growing areas (Browder, 1971). Leaf rust is more prominent and wide-spread than other rust diseases of wheat making it a significant issue for producers, as it is typically present each growing season (Huerta-Espino et al., 2011). Breeding programs have made use of extensive genetic resistance to mitigate losses associated with the disease. Historically, all-stage resistance (ASR) genes have been deployed to combat leaf rust. While highly effective, these genes have been shown to be mostly race-specific and have been overcome by pathogen evolution resulting in virulence (McIntosh, Wellings, et al., 1995; Lowe et al., 2010). This has led to a transition in breeding efforts to focus on race-non-specific resistance sources characterized by partial, small effect genes effective at the adult plant stage (APR) and considered to be more durable (Johnson, 1984). The *Lr34/Yr18/Sr57/Pm38/Ltn1* locus (hereafter designated *Lr34)* is located on chromosome 7DS and has been one of the most widely deployed and effective APR genes for leaf rust resistance showing exceptional durability over several decades (German & Kolmer, 1992; Ellis et al., 2014).

Lr34 encodes an ABC transporter rather than the typical nucleotide binding leucine rich repeat (NBS-LRR) class associated with many ASR genes (Krattinger et al., 2009). This gene provides resistance to multiple pathogens including leaf rust (Dyck et al., 1966), stripe rust (McIntosh, 2007), stem rust (Dyck, 1987; Liu & Kolmer, 1998), powdery mildew (Spielmeyer et al., 2005), and barley yellow-dwarf virus (Singh, 1992). Cultivars containing *Lr34* are also

associated with the phenotype leaf tip necrosis (LTN), expressed as necrosis of flag leaf tips on adult plants (Dyck, 1991; Singh, 1992). Cloning of *Lr34* showed the ABC transporter has a pleiotropic effect for leaf rust, stripe rust, stem rust, powdery mildew, and LTN (Krattinger et al., 2009). Three other APR genes have been previously associated with LTN. *Lr46* on chromosome 1BL (Singh et al., 1998; Rosewarne et al., 2005), *Lr67* on chromosome 4DL (Dyck & Samborski, 1979; Hiebert et al., 2010; Herrera-Foessel et al., 2014), and *Lr68* on chromosome 7BL (Herrera-Foessel et al., 2012) are associated with LTN genes *Ltn2, Ltn3, and Ltn4,* respectively. LTN expression is quantitative and has been shown to be highly variable depending on environmental conditions and genetic background with studies reporting QTL for LTN on chromosomes 1A, 1B, 2A, 2B, 2D, 3A, 3B, 4A, 4B, 4D, 5A, 5B, 5D, 6A, 7B, and 7D. (Messmer et al., 2000; Rosewarne et al., 2005; Singh et al., 2014; Juliana et al., 2015).

In a previous study, we identified several QTL for leaf rust resistance in a doubled haploid population (DH) derived from the cultivars Everest and WB-Cedar (Clinesmith et al., unpublished). Everest was developed by Kansas State University and released in 2009 through the Kansas Wheat Alliance. The pedigree of Everest (PI 659807) is HBK1064-3/JaggerW//X960103 (NPGS, 2017). WB-Cedar (PI 661996) was developed by WestBred and released in 2011. The pedigree of WB-Cedar is TAM-302/PIONEER-2180//EXP (NPGS 2017). Everest was confirmed to carry *Lr68,* while WB-Cedar was shown to carry *Lr34*; however, LTN expression of Everest and WB-Cedar in this study appeared to be low while segregation of LTN was observed in the population (Clinesmith et al., unpublished). The strong LTN effect typically associated with *Lr34* suggested that WB-Cedar could potentially carry a suppressor for LTN. The objectives of the current study were to evaluate LTN in Everest, WB-Cedar, and the DH population in the absence of leaf rust infection and map regions associated with LTN to gain a

2230 better understanding of the genetic relationship between leaf rust resistance and LTN expression
2231 and to determine if a suppressor of LTN existed in WB-Cedar.

2232 ## Materials and Methods

2233 ### Plant Materials

2234 A doubled haploid (DH) population containing 159 lines was generated using F_1 seeds
2235 from a cross between the HRWW cultivars Everest and WB-Cedar.

2236 ### SNP Genotyping and Linkage Map Construction

2237 Leaf tissues was collected from each DH line and the parents at the two-leaf stage. Tissue
2238 was freeze dried at −51°C for 48 h using a Labconco Freezone 6. Dried tissue was ground in a
2239 Retsch mm400 tissue grinder set at 25 cycles s−1. DNA purification was performed using the
2240 "BS96 DNA Plant" protocol for the Biosprint 96 workstation and the Biosprint 96 DNA plant kit
2241 (Qiagen). Genotyping-by-sequencing (GBS; Elshire et al., 2011) was performed according to
2242 (Poland et al., 2012). The restriction enzymes *PstI* and *MspI* were used for DNA sample
2243 digestion. An Illumina Hiseq 2000 was used for sequencing following DNA amplification.
2244 Raw GBS sequence data was processed into single nucleotide polymorphisms (SNPs)
2245 using the TASSEL-GBS bioinformatics pipeline implemented in TASSEL 5.0. Physical
2246 positions of SNPs within the genome were determined through alignment of GBS sequences to
2247 the Chinese Spring reference genome (Appels et al., 2018). SNPs were then filtered to < 20%
2248 missing data and a minor allele frequency ≥ 0.05 using a custom script in Rstudio V 1.3.959. A
2249 linkage map was constructed using the Kosambi mapping function (Kosambi, 1943) in JoinMap
2250 4.1 (Van Ooijen, 2006) which groups SNPs into linkage groups using a maximum likelihood
2251 mapping procedure. Physical positions of SNPs were used to confirm correct positioning of
2252 SNPs within the genetic map.

Experimental Design and Data Collection

DH lines, the parents, Everest and WB-Cedar, as well as the variety 'KS Hatchett', which was observed to express high levels of LTN in the greenhouse, were planted in square pots in a greenhouse at Kansas State University, Manhattan, KS for three cycles between the spring of 2020 (20SG) and fall of 2020 (20FG and 20FD). Each cycle consisted of an unreplicated design where one genotype was randomly assigned to a pot and two plants were planted in each pot. This resulted in a randomized complete block design with subsampling across cycles where cycle served as the blocking factor. Within each cycle, checks were replicated with each check being planted in three pots with two plants per pot.

LTN was measured on the flag leaf of adult plants at 4 weeks post anthesis. Two measuring techniques were used to evaluate extent of LTN. 1) Visual estimation was performed using a ruler to measure the extent of LTN in centimeters from the tip of the leaf to the point in the center of the leaf along the midrib where LTN stopped, denoted LTNC, as well as the point on the margin of the leaf where LTN stopped, denoted LTNM. 2) Flag leaves were harvested at 4 weeks post anthesis and scanned into a computer using an Epson Perfection 3170 Photo scanner. Leaf images were edited to improve brightness, contrast, and to apply a black background around the leaf area. Images were loaded onto a Sony Xperia tablet running Android 6.0.1 and the application Leaf Doctor (Pethybridge & Nelson, 2015) was used to determine percent of leaf area expressing LTN denoted LTNI.

Statistical Modeling

Data were analyzed using a general linear mixed model fitted to each response variable:

$$y_{ijk} = \eta + b_i + g_j + bg_{ij} + e_{ijk}$$

where, y_{ij} is the observed response of the kth plant from the jth genotype within the ith experimental run, η is the intercept, b_i is the differential effect of the ith experimental run assumed independent and identically distributed (i.i.d.) $b_i \sim N(0, \sigma_b^2)$, g_j is the differential effect of the jth genotype assumed independent and identically distributed (i.i.d.) $g_j \sim N(0, \sigma_g^2)$, bg_{ij} is the differential effect of the pot, identified by the crossproduct between the ith experimental run and the jth genotype, and assumed independent and identically distributed (i.i.d.) $bg_{ij} \sim N(0, \sigma_{bg}^2)$, and e_{ijk} is the leftover random residual corresponding to the kth plant of the jth genotype within the ith experimental run assumed independent and identically distributed (i.i.d.) $e_{ijk} \sim N(0, \sigma_e^2)$.

Restricted maximum likelihood was used to estimate variance components. Plots of studentized residuals were used to evaluate model assumptions. A normal distribution was assumed and responses showing deviation from the normal distribution were log transformed to meet this assumption. Pairwise comparisons were performed between the two parents and 'KS Hatchett', and also between each DH line and parent lines to assess if transgressive segregation had occurred in the population. A Dunnett adjustment was performed to control the experiment-wise Type I error at 5%. Estimated means were back-transformed to the original scales following inference. The GLIMMIX procedure in SAS (Version 9.4, SAS Institute, Cary, NC) was used to fit the model.

Broad-sense heritability (H^2) was estimated across cycles for each trait using the following equation:

$$H^2 = \sigma_g^2 \,/\, (\sigma_g^2 + \frac{\sigma_{bg}^2}{r} + \frac{\sigma_e^2}{r})$$

where σ_g^2, σ_{bg}^2, and σ_e^2 are the variance of the genotypes, genotype by environment interaction, and residuals, respectively, and r is the number of cycles (He et al. 2016).

QTL Mapping

QTL mapping for all traits was conducted using the R/qtl package (Broman et al., 2003) in R (R Core Team, 2017). All analyses were performed using Haley-Knott regression (Haley & Knott, 1992). This method was chosen as it has been shown to give similar results to standard interval mapping and multiple imputation when there are low levels of missing data and is more computationally efficient for larger marker datasets (Broman & Sen, 2009). The genome-wide LOD thresholds for each trait were estimated using a permutation test with 1,000 permutations to determine the significance of QTL at $P < 0.05$. The initial search for QTL was conducted using simple interval mapping (SIM). The results from SIM were used to obtain markers closely positioned to significant QTL. These markers were then used as covariates to search for additional QTL via composite interval mapping. Composite interval mapping (CIM) was implemented using forward selection of marker covariates and an infinite window size which omits marker covariates residing on the chromosome of the position being tested. Linkage of multiple QTL and epistatic interactions between QTL were investigated using the scantwo function in R/qtl. The results from these analyses were used in multiple QTL mapping (MQM) to fit a multiple fixed effect QTL model according to (Broman & Sen, 2009) using the model

$$y = u + \sum_j \beta_j q_j + \sum_{j,k} \beta_{jk} q_j q_k + e$$

where y is the observed response, u is the overall mean, $\sum_j \beta_j q_j$ is the sum of QTL main effects, $\sum_{j,k} \beta_{jk} q_j q_k$ is the sum of QTL interaction effects, and e is the residual random error.

MQM was used to further test the significance of each QTL, refine the position of the QTL, and estimate the percent phenotypic variance explained by the QTL.

Comparison of physical position of QTL detected in this study with known genes and QTL identified in previous studies was conducted using Basic Local Alignment Search Tool (BLAST). Nucleotide sequences of known genes and QTL, if available, were BLAST against the Chinese Spring reference genome, IWGSC RefSeq v1.0, in the Ensemble Plants window browser (http://plants.ensembl.org/index.html). The physical positions were obtained from the BLAST analysis and compared against the physical position of the peak marker for each QTL.

QTL Pyramid Effect

Estimation of the effect on LTN expression from stacking multiple QTL within individual genotypes was performed by placing lines into haplotype groups based on the number of resistance alleles they carried for the LTN QTL detected in this study and leaf rust QTL detected in Clinesmith et al., (unpublished). Three QTL were unique to the LTN study. The QTL *Qltn.ksu-2A*, *Qltn.ksu-4DL*, and *Qltn.ksu-7DS* were associated with both LTN and leaf rust while five QTL were detected solely for leaf rust. The mean and 95% confidence intervals were calculated for each group using the following model:

$$y_{ijk} = n + h_i + g_{j(i)} + bg_{ij} + e_{ijk}$$

where y_{ij} is the observed response of the kth plant of the jth genotype within the ith haplotype group, n is the intercept, h_i is the differential effect of the ith haplotype group, $g_{j(i)}$ is the differential effect of the jth genotype nested within the ith haplotype group assumed independent and identically distributed (i.i.d.) $g_j \sim N(0, \sigma_g^2)$, and e_{ijk} is the leftover random residual corresponding to the kth plant of the jth genotype within the ith haplotype group assumed independent and identically distributed (i.i.d.) $e_{ijk} \sim N(0, \sigma_e^2)$.

Pairwise comparisons were performed between groups for each of the three LTN traits using a Bonferroni adjustment at $P<0.05$.

KASP Marker Screening

'KS Hatchett' was screened for the presence of the *Lr77* resistance allele using Kompetitive allele-specific polymerase chain reaction (KASP) markers. Four µl of KASP assay master mix containing $MgCl_2$, 2× KASP buffer, and primer was used to resuspend 50 to 100 ng of DNA dried in a 384-well plate. Two primers, *Lr77-3B-23680-KASP* and *Lr77*-3B-73555-KASP (Kolmer et al., 2019), were used to confirm the presence of the *Lr77* resistance allele. Polymerase chain reactions (PCR) were conducted using the following thermal cycler conditions. *Lr77-3B-23680-KASP* and *Lr77*-3B-73555-KASP, 94 °C for 15 min, 94 °C for 20 sec, 65 °C for 1 min for 10 cycles, 94 °C for 20 sec, 57 °C for 1 min for 40 cycles, with a final cool down of 10 °C for 5 min.

Results

Phenotypic Data

The phenotypic distributions of LTN traits LTNC, LTNM, and LTNI evaluated throughout the different cycles are shown in Figure 3-1a-c. Distributions were skewed to the right for all traits in 20SG and 20FD, while 20FG showed a more symmetric distribution for all traits. Significant ($P<0.001$) positive correlations were observed between cycles for each of the three LTN traits (Figure 3-2) as well as between traits within individual cycles (Figure C-1) and between the BLUPs (Figure 3-3). Estimated responses of the DH population, parents, and 'KS Hatchett' within individual cycles for the three traits are shown in Table 1. Broad-sense heritability across experimental runs was moderately high for all three traits at 0.77, 0.73, and

0.72 for LTNC, LTNM, and LTNI, respectively (Table 1). Pairwise comparisons among Everest, WB-Cedar, and "KS Hatchett' are displayed as bar charts in Figure 3-4 and Figure C-3, respectively. 'KS Hatchett' showed significantly higher levels of LTN for all traits relative to both parents (Figure 3-4). WB-Cedar showed a significantly higher expression for LTNM relative to Everest. Significant positive and negative transgressive segregation was observed within the population. DH lines showing significantly higher LTN values relative to either parent were observed for all three traits. Lines showing lower LTN relative to WB-Cedar were also observed for all three traits.

QTL Mapping

Five QTL were detected for three LTN traits on chromosomes 1D, 2A, 4A, 4D, 5A, and 7D (Table 2; Figure 3-5; Table C-1). Everest contributed alleles associated with higher LTN on chromosomes 2A, 4D, and 5A, while alleles from WB-Cedar were associated with higher LTN on chromosomes 1D and 7D. LOD scores for all QTL, excluding 7D, ranged from 2.44 – 4.94 explaining 4.82 – 6.19% of the phenotypic variance. The major QTL on chromosome 7D had LOD scores ranging from 7.18 – 29.25 and explained 20.83 – 54.17% of the phenotypic variance. The majority of QTL showed a minor effect on LTN traits. Two QTL, *Qltn.ksu-2A* and *Qltn.ksu-7DS*, were considered stable QTL associations being detected in multiple experimental runs. *Qltn.ksu-7DS* on chromosome 7D was the most stable and was considered a major effect QTL.

Qltn.ksu-1DL was detected for LTNM and was positioned on the long arm of chromosome 1D at 78.8 cM (Table 2; Figure 3-5b). The LOD score based on CIM fell below the genome-wide threshold (Figure 3-5b); however, the LOD score based on inclusion in the MQM model was above the threshold (Table 2). This QTL explained 3.64 – 8.27% of the phenotypic

variance for LTNM with an additive effect of 0.06 cm. The allele conferring higher LTN response was contributed by WB-Cedar.

Qltn.ksu-2A was detected for all LTN traits (Table 2; Figure 3-5). The position of this QTL varied slightly between the three traits with the peak markers located on the long arm in a genetic interval between 77.0 – 131.0 cM. This QTL explained 6.19 – 8.05%, 5.37 – 6.00%, and 7.36 – 9.73% of the phenotypic variance with additive effects of 0.08 – 0.11 cm, 0.07 – 0.13 cm, and 0.09 – 0.16% for LTNC, LTNM, and LTNI, respectively. The parent Everest contributed the allele associated with higher LTN values.

Qltn.ksu-4DL was associated with LTNC (Table 2; Figure 3-5a). This QTL was located at a genetic position of 56 cM on the long arm of chromosome 4D and explained 4.62% of the phenotypic variance with an additive effect of 0.10 cm. Everest contributed the allele associated with higher LTN.

Qltn.ksu-5AL was associated with LTNM, located at 188.0 cM on the long arm of chromosome 5A (Table 2; Figure 3-5b). This QTL explained 4.13% of the phenotypic variance with an additive effect of 0.09 cm. The allele conferring a higher value of LTN was contributed by Everest.

Qltn.ksu-7DS was the most stable QTL observed in the study being detected for all trait-environment combinations (Table 2; Figure 3-5; Table C-1). All datasets mapped to the marker for *Lr34* located in a genetic interval between 78.0 – 81.0 cM on the short arm of chromosome 7D with the 1.5 LOD interval located between 57.31 – 85.81 cM. This QTL also conferred the largest effect of all QTL explaining 32.60 – 54.17%, 20.83 – 47.07%, and 23.66 – 49.89% of the phenotypic variance with additive effects of 0.16 – 0.23 cm, 0.08 – 0.27 cm, and 0.16 – 0.43%

for LTNC, LTNM, and LTNI, respectively. The allele conferring higher LTN response was contributed by WB-Cedar.

QTL Pyramid Effect

We compared differences of means between groups of lines carrying differing numbers of alleles for the five LTN QTL detected in this study (Figure 3-6) and the eight QTL detected in Clinesmith et al., (unpublished) (Figure C-4). For LTN QTL, only one line was shown to carry zero alleles for LTN expression, while four lines contained alleles for LTN expression from all five QTL. Fewer significant differences were observed for lines containing lower numbers of alleles. Lines containing five alleles were significantly different than all other groups for all three traits. For the leaf rust QTL, only one line carried zero resistance alleles for leaf rust. This likely contributed to the large observed confidence intervals for this group where no significant differences between means of LTN were observed when compared to other groups. Eighteen lines carried five resistance alleles. An increasing trend in mean LTN was observed for lines containing higher numbers of leaf rust QTL; however, fewer significant differences were observed.

Discussion

Identification and deployment of durable leaf rust resistance packages is a priority for many wheat breeding programs as pathogen evolution has resulted in virulence to many major resistance genes deployed individually in cultivars (Kolmer, 2005, 2019). Genes conferring race-non-specific partial resistance at the adult plant stage through a slow-rusting phenotype have provided adequate and durable protection when deployed in combination with other resistance genes (Huerta-Espino et al., 2020). Major genes in this category include *Lr34* (Ellis et al., 2014), *Lr46* (Singh et al., 1998; Rosewarne et al., 2005), *Lr67* (Dyck & Samborski, 1979; Hiebert et al.,

2010; Herrera-Foessel et al., 2014), and *Lr68* (Herrera-Foessel et al., 2012). However, these genes have been associated with the undesirable morphological trait LTN which has limited their use in certain breeding programs due to yield penalties.

In a previous study we identified eight QTL associated with leaf rust resistance in an Everest x WB-Cedar DH population and confirmed the presence of the APR genes *Lr68* in Everest and *Lr34* in WB-Cedar (Clinesmith et al., unpublished). The presence of both genes was interesting as they have previously been associated with expression of LTN and minimal LTN had been observed on these cultivars previously; although, no studies aimed primarily at investigating LTN had been conducted. The aim of the current study was to identify the genomic regions associated with LTN in the Everest x WB-Cedar DH population where we detected QTL associated with LTN traits on chromosomes 1D, 2A, 4A, 4D, 5A, and 7D. Two of these QTL, located on chromosomes 2A and 7D were considered stable being detected for multiple traits across multiple cycles.

We identified a stable QTL associated with LTN expression on the distal end of the long arm of chromosome 2A. The interval for this QTL overlapped with the QTL for leaf rust resistance identified in our previous study (Clinesmith et al., unpublished) suggesting a potential pleiotropic effect for the two traits. Singh et al. (2014) identified a QTL in the Canadian spring wheat AC Cadillac associated with LTN on chromosome 2AL. The closest marker to this QTL was wPt-665330 located at 111.8 cM. Blasting of the marker sequence against the Chinese Spring reference genome positioned this marker at 633.8 Mb which falls within the confidence interval of the QTL detected in the current study. We had previously suggested *QLr.ubo-2AL* (Maccaferri et al., 2008; Li et al., 2014) as a potential candidate for the QTL associated with leaf rust resistance in this region. This suggests that the QTL identified in these three studies could all

be controlled by the same underlying locus controlling both leaf rust resistance and LTN expression. The association of this QTL with LTN is interesting because we observed an effect on leaf rust resistance at the seedling stage, suggesting this gene confers an ASR effect. All leaf rust genes currently associated with LTN are categorized as APR genes (William et al., 2003; Singh et al., 2010; Herrera-Foessel et al., 2012; Herrera-Foessel et al., 2014; Huerta-Espino et al., 2020). In recent studieshowever, *Lr34* has been shown to provide detectable levels of resistance at the seedling stage when transferred to durum wheat (Rinaldo et al., 2017) and in seedlings exposed to low temperatures in hexaploid wheat (McCallum et al., 2021). These results suggest the expression of LTN at this locus could be contributed by either an individual APR or ASR gene, or perhaps the presence of multiple genes located in close proximity. The race for the leaf rust experiment was chosen on the basis of a high reaction on the seedlings of both parents. However, subsequent inoculum increases suggested the race was not fully virulent on Everest. Further investigation will need to be done to confirm the genetic architecture underlying leaf rust resistance and LTN in this region.

The QTL identified on chromosome 7D conferred the largest effect on LTN traits and was the most stable being detected for all traits in all datasets. The genomic region for this QTL mapped to the marker for *Lr34* which matched results from the previous study (Clinesmith et al., unpublished). The variation in LTN response of the cultivar WB-Cedar is consistent with previous observations showing a high environmental effect on the expression of LTN associated with *Lr34* (Dyck, 1987; Drijepondt & Pretorius, 1989).

The cultivar Everest carrying *Lr68* showed lower levels of LTN relative to WB-Cedar and “KS-Hatchett’, both of which carry *Lr34*. Interestingly, no significant peaks were detected for LTN on chromosome 7B, where *Lr68* is located. This gene has been previously shown to

have a lower expression of LTN relative to *Lr34, Lr46*, and *Lr67* (Juliana et al., 2015; Huerta-Espino et al., 2020) which could have limited our ability to parse out its effect in the current population. KASP marker analysis showed that the check cultivar "KS Hatchett' carries SNPs associated with *Lr77.* Marker data from the Southern Regional Performance Nursery (SRPN) also confirmed the presence of *Lr34* and *Lr37* in 'KS Hatchett'. 'KS Hatchett' carries the spring wheat cultivar 'Amadina' in its pedigree which has been shown to contain multiple alleles for APR resistance to leaf rust, not including *Lr34* (Nyori, 2010). It is possible that 'KS Hatchett' inherited some of these alleles. The higher expression of LTN in 'KS Hatchett' relative to WB-Cedar could be due to the presence of other loci contributing an additive effect to LTN and/or interactions between these loci and *Lr34*. Apart from *Lr34*, only one other QTL for LTN was detected in WB-Cedar and was associated with relatively minor effect. The limited expression of LTN previously observed for WB-Cedar could be a result of a low number of loci contributing to the trait as well as the combination of genetic background and specific environmental conditions.

In the current study, we observed several loci controlling LTN expression without a significant effect on leaf rust resistance. This could be due to expression of LTN by loci that were not effective against the races used in the leaf rust experiments. The effect and stability of associations between these loci and LTN were also low making it difficult to draw meaningful conclusions from the data. Further studies will be needed to confirm these results. Increases in the level of LTN expression were observed in lines carrying higher numbers of LTN QTL. A similar increase in LTN expression was observed for lines carrying more leaf rust resistance alleles. These results suggest efforts to combine several resistance genes into single cultivars may result in increased levels of LTN expression, potentially leading to reduced yields. Use of race non-specific resistance is an effective strategy which can prevent boom and bust cycles that

are difficult for producers to manage and can harm genetic gain in breeding programs by encouraging the discard of otherwise useful lines. The choice of gene combinations that provide effective resistance and minimize LTN will likely be the most effective strategy. Though *Lr68* has been associated with LTN, it was not significant in the present study, suggesting combinations with Lr68 may be highly useful. Everest contains Lr68 and has remained resistant to leaf rust even though it led Kansas in acreage for six consecutive years and expresses minimal LTN in the field. With the threat of newly identified leaf rust races overcoming current resistance genes, continued efforts to uncover new sources of resistance and characterize their effect on LTN expression will be needed to maintain adequate levels of disease protection without compromising competitive levels of grain yield.

2511

2512

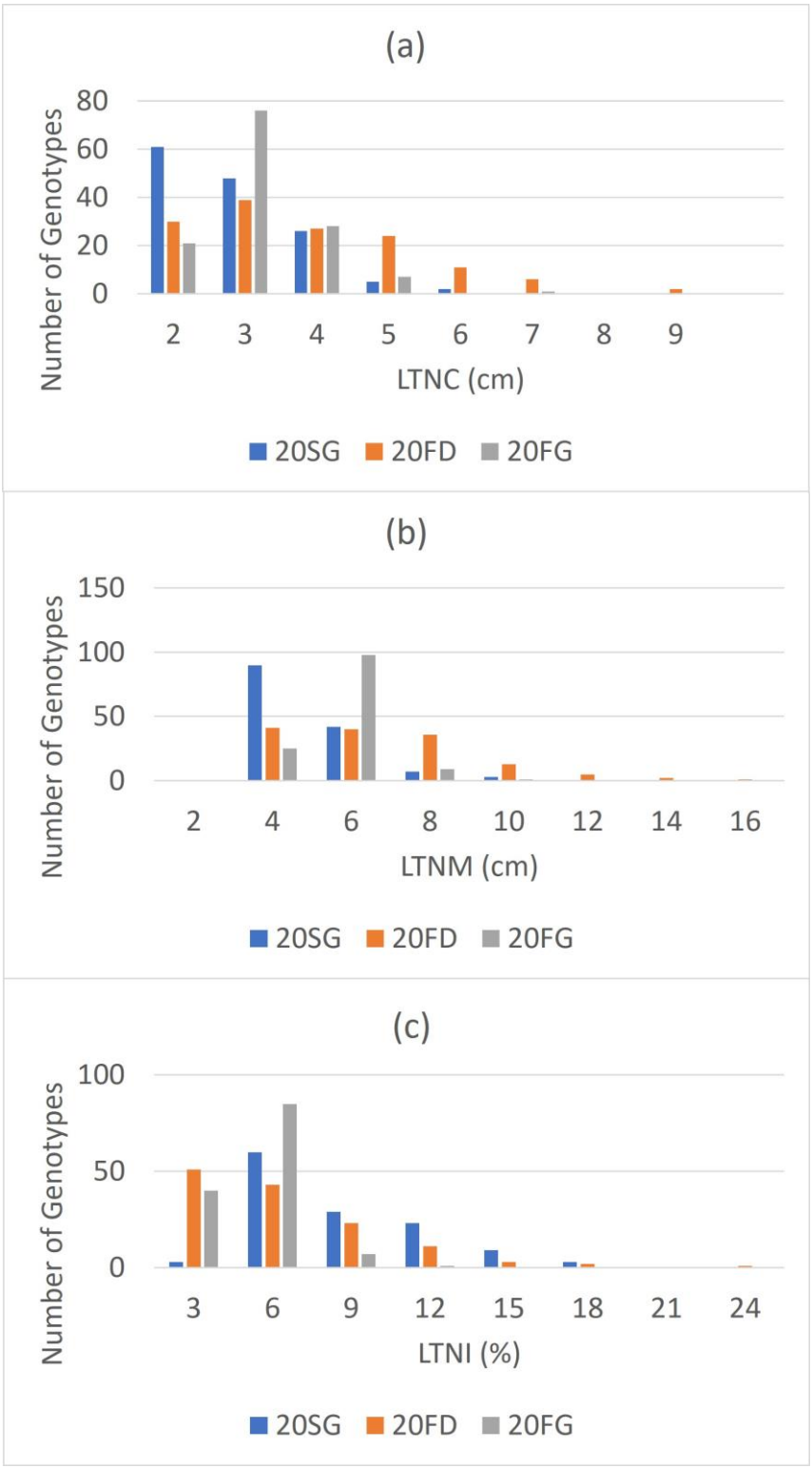

Figure 3-1. Histograms showing phenotypic distributions of the DH population for means of the traits (a) LTNC, (b), LTNM, and (c) LTNI collected within experimental greenhouse cycles 2020 Spring Greenhouse G (20SG), 2020 Fall Greenhouse D (20FD), and 2020 Fall Greenhouse G (20FG).

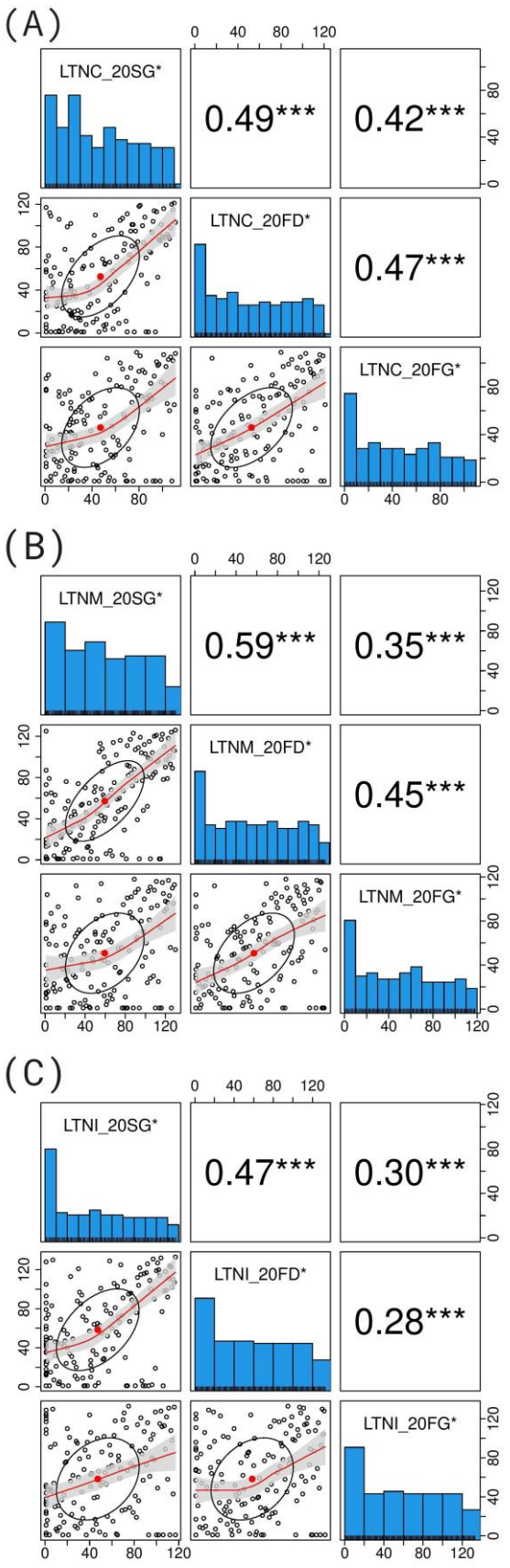
(A)
LTNC_20SG*
0.49***
0.42***
LTNC_20FD*
0.47***
LTNC_20FG*
(B)
LTNM_20SG*
0.59***
0.35***
LTNM_20FD*
0.45***
LTNM_20FG*
(C)
LTNI_20SG*
0.47***
0.30***
LTNI_20FD*
0.28***
LTNI_20FG*

2518

Figure 3-2. Scatterplot matrices showing comparisons of raw phenotypic values for each LTN trait between cycles (A-C). The diagonal shows the distribution of each variable as well as displaying the abbreviation for each LTN trait and the corresponding cycle (20SG, 20FD, and 20FG). The boxes in the top of the diagonal contain Pearson's correlation coefficients with asterisks displaying the significance of correlation, * ($P < 0.05$), ** ($P < 0.01$), *** ($P < 0.001$). The number in the lower right of the boxes corresponds to the number of data points used in each comparison. The boxes below the diagonal display the bivariate scatter plots fitted with a LOESS curve.

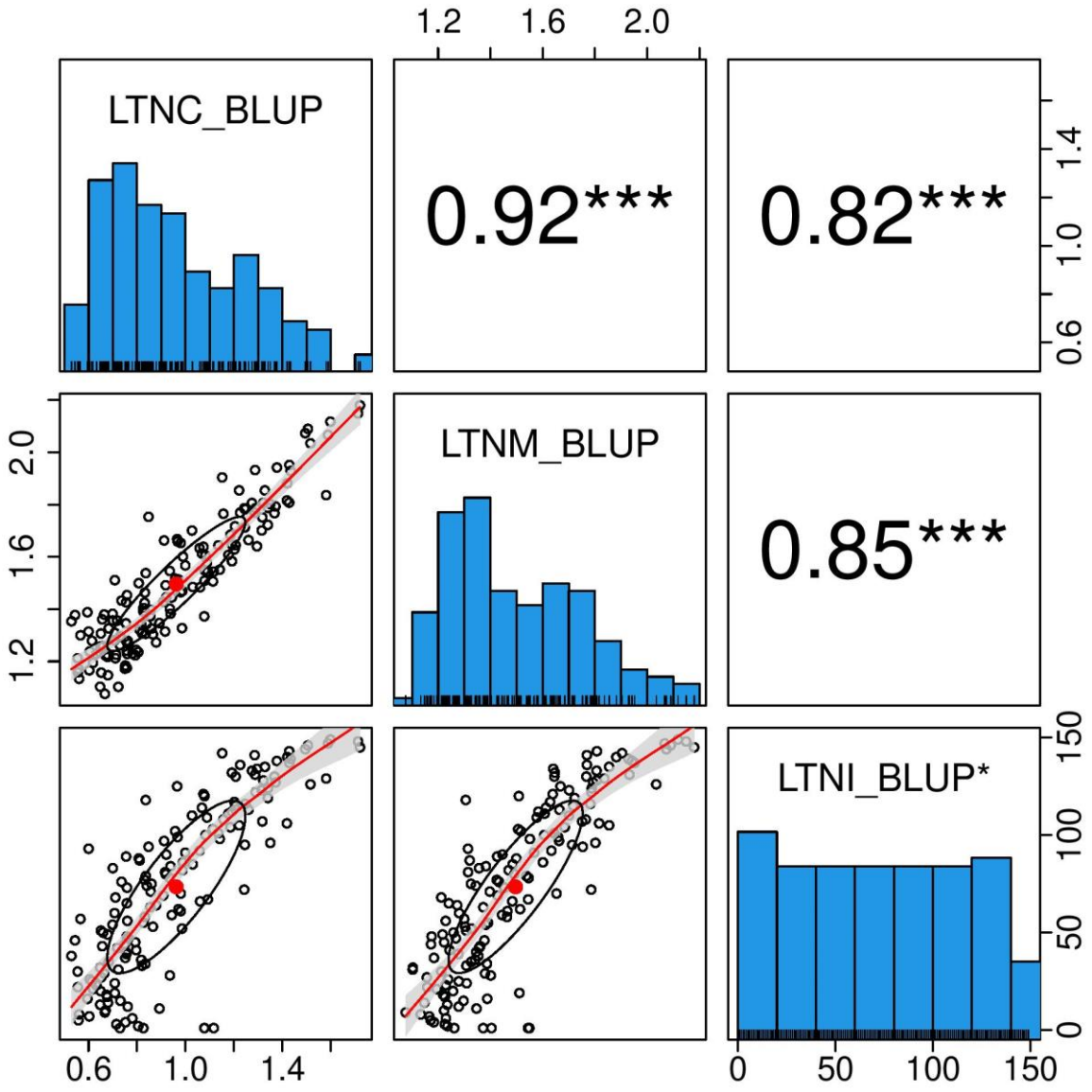

Figure 3-3. Scatterplot matrices showing comparisons of BLUPs between each LTN trait. The diagonal shows the distribution of each variable as well as displaying the abbreviation for each LTN trait. The boxes in the top of the diagonal contain Pearson's correlation coefficients with asterisks displaying the significance of correlation, * ($P < 0.05$), ** ($P < 0.01$), *** ($P < 0.001$). The number in the lower right of the boxes corresponds to the number of data points used in each comparison. The boxes below the diagonal display the bivariate scatter plots fitted with a LOESS curve.

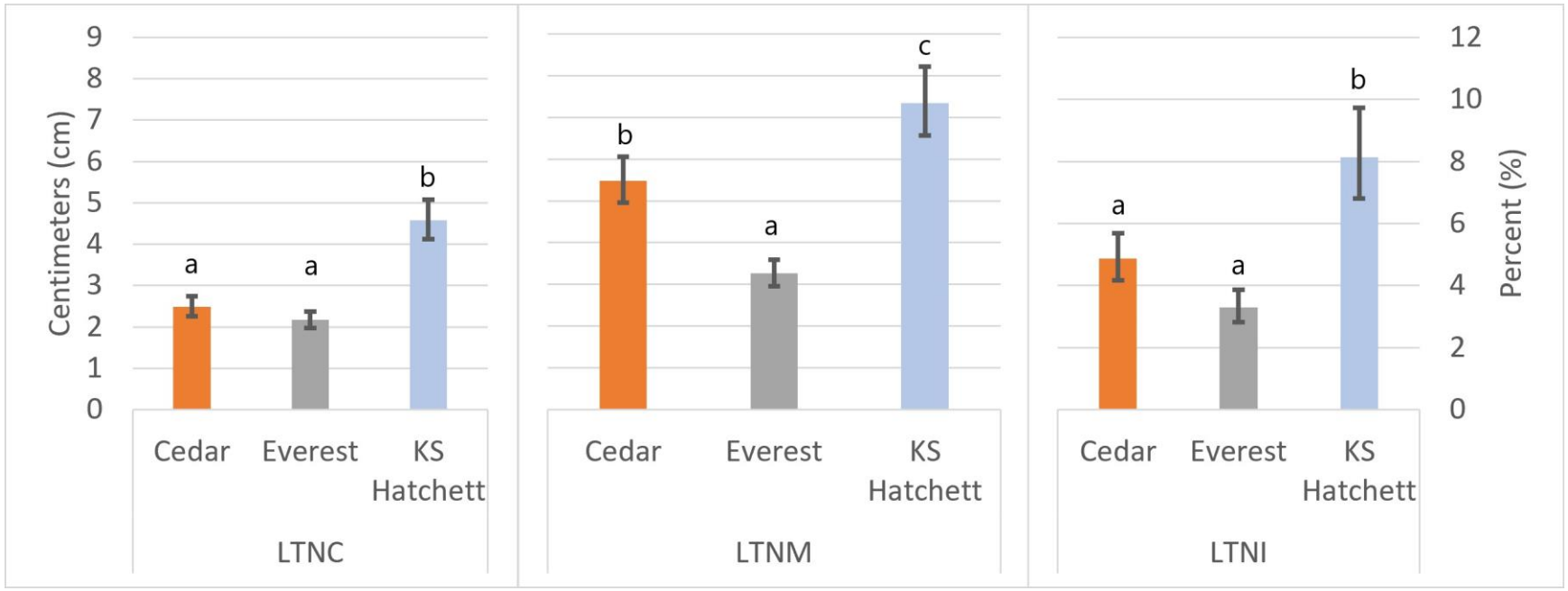

Figure 3-4. Bar charts displaying BLUPS for (a) LTNC, (b) LTNM, and (c) LTNI for the cultivars Everest, WB-Cedar, and 'KS Hatchett'. Error bars represent upper and lower 95% confidence intervals. Letters above each bar denote significance of mean differences based on pairwise comparisons using a Bonferroni correction at $P<0.05$.

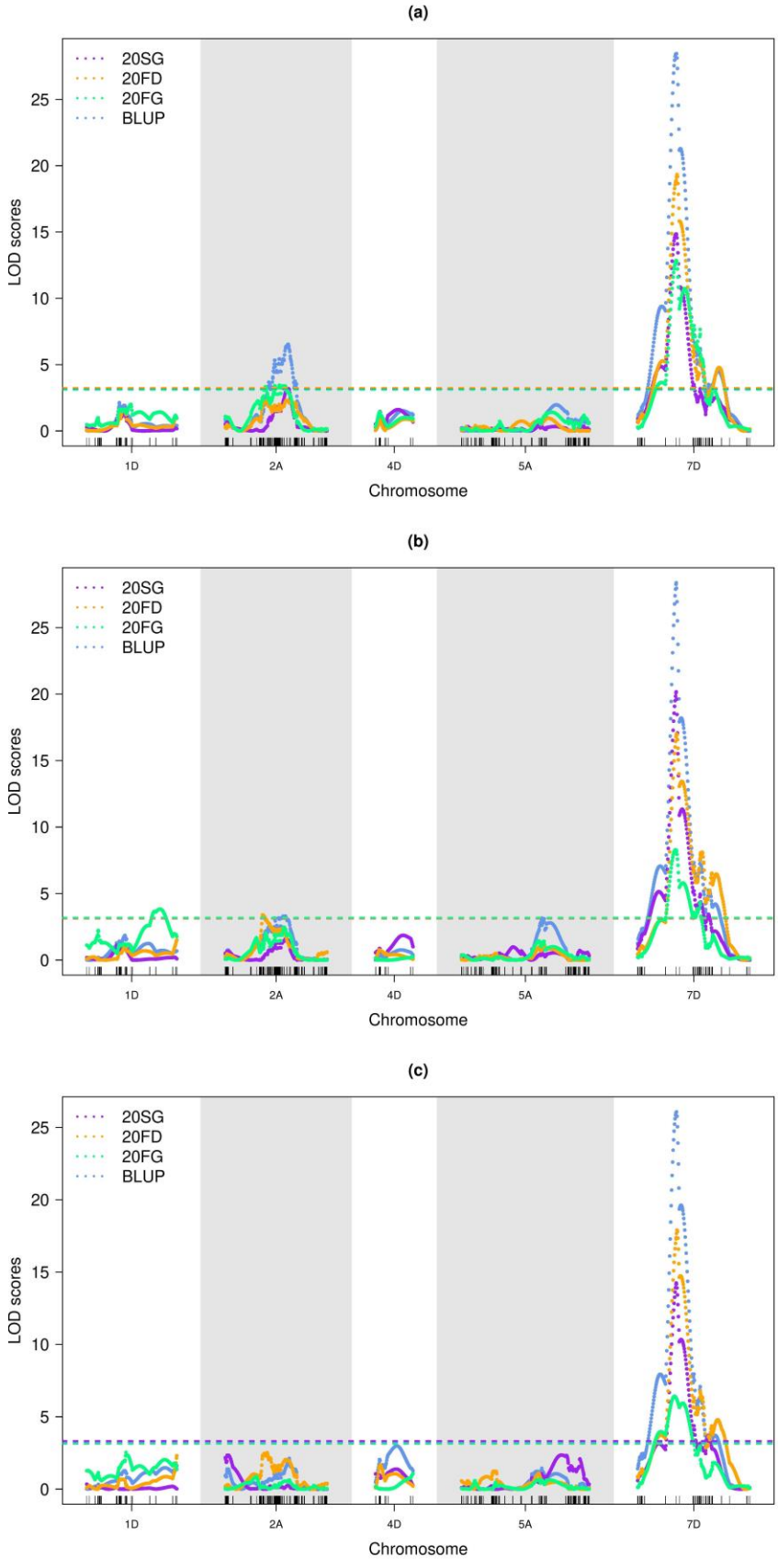
(a)
20SG
20FD
20FG
BLUP
LOD scores
0
5
10
15
20
25
1D
2A
4D
5A
7D
Chromosome
(b)
20SG
20FD
20FG
BLUP
LOD scores
0
5
10
15
20
25
1D
2A
4D
5A
7D
Chromosome
(c)
20SG
20FD
20FG
BLUP
LOD scores
0
5
10
15
20
25
1D
2A
4D
5A
7D
Chromosome

2539

Figure 3-5. Genome-wide logarithm of the odds (LOD) values obtained from composite interval mapping of the DH population for (a) LTNC, (b) LTNM, and (c) LTNI. Color of dotted lines corresponds to greenhouse cycles 2020 Spring Greenhouse G, 2020 Fall Greenhouse D, 2020 Fall Greenhouse G, and BLUPs calculated across cycles. Individual points on the LOD curve represent SNPs. Horizontal dashed lines represent the genome-wide LOD thresholds ($P<0.05$).

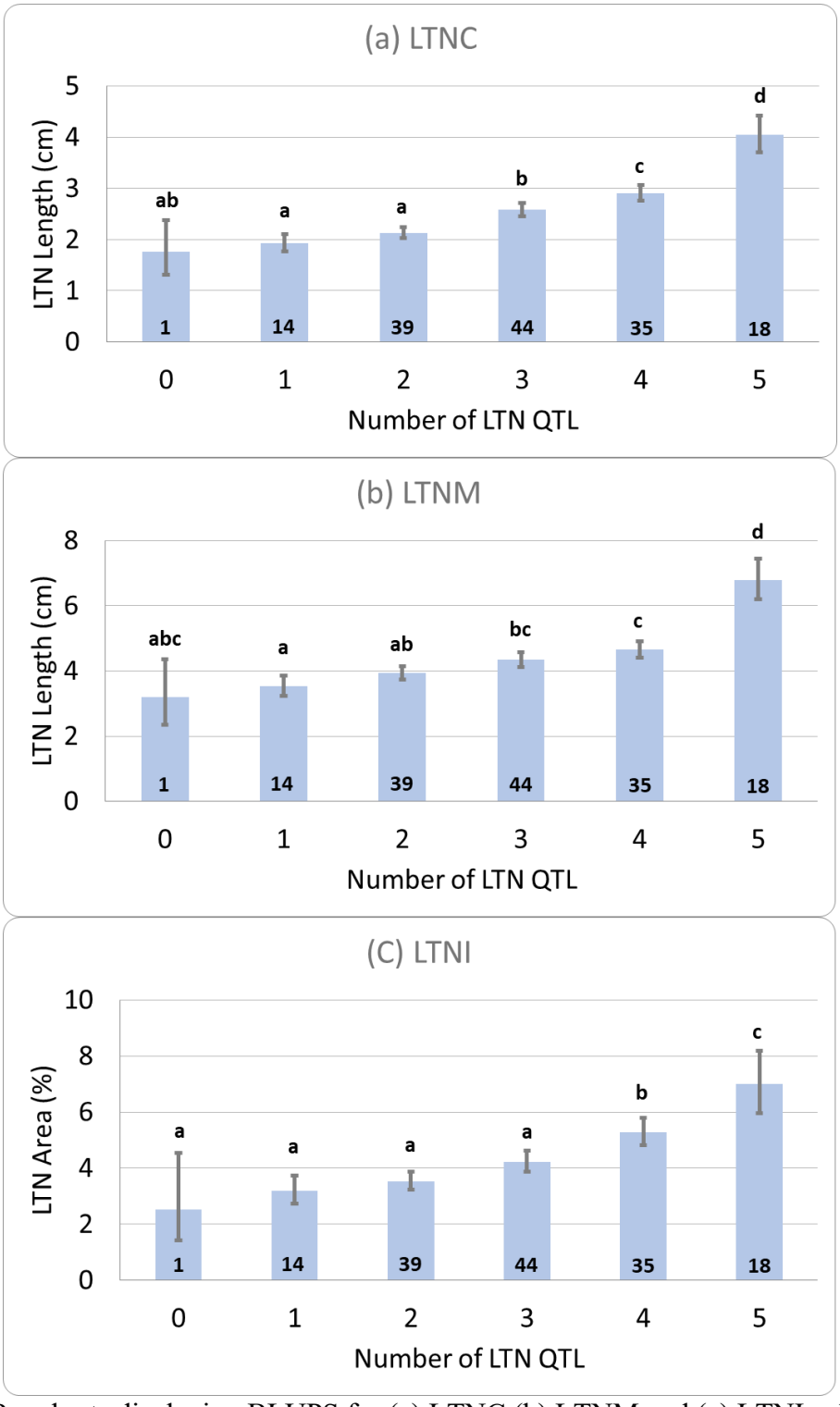

Figure 3-6. Bar charts displaying BLUPS for (a) LTNC (b) LTNM and (c) LTNI calculated between groups of DH lines based on the number of LTN alleles present for each QTL. Numbers on the X-axis correspond to the number of LTN alleles carried by lines within each group. Numbers at the base of each bar represent the number of DH lines within each group. Error bars represent upper and lower 95% confidence intervals. Letters above each bar denote significance of mean differences based on pairwise comparisons using a Bonferroni correction at $P<0.05$.

Table 3-1. Descriptive statistics of individual cycle trait means for Everest, Cedar, KS Hatchett and the DH population for LTNC, LTNM, and LTNI. Broad sense heritability was calculated for each trait across greenhouse cycles.

Trait	ENV	Parents		Check	DH Lines			H^2
		Everest (mean±SEM)	Cedar (mean±SEM)	KS Hatchett (mean±SEM)	Mean (±SEM)	MIN	MAX	
LTNC	20SG	1.8±0.07	1.8±0.07	4.6±0.10	2.4±0.09	1.4	6.0	
	20FD	2.3±0.10	4.8±0.10	5.4±0.10	3.4±0.11	1.6	8.4	
	20FG	2.5±0.08	1.9±0.10	3.8±0.09	2.7±0.10	1.6	6.2	
	BLUP	2.2±0.13	2.5±0.13	4.6±0.11	2.7±0.05	1.7	5.6	0.77
LTNM	20SG	2.5±0.07	3.6±0.07	7.0±0.10	4.1±0.19	2.1	9.6	
	20FD	3.8±0.11	9.1±0.10	8.5±0.11	5.7±0.22	2.0	15.1	
	20FG	3.9±0.09	4.8±0.10	6.6±0.09	4.7±0.21	3.0	8.6	
	BLUP	3.3±0.11	5.5±0.09	7.3±0.10	4.6±0.09	2.9	8.8	0.73
LTNI	20SG	4.3±0.16	4.5±0.19	12.6±0.23	7.1±0.29	2.8	17.5	
	20FD	2.9±0.17	9.8±0.15	8.2±0.13	5.1±0.24	1.6	22.4	
	20FG	3.3±0.14	3.3±0.14	5.2±0.16	3.8±0.25	2.1	9.7	
	BLUP	3.3±0.15	4.9±0.16	8.1±0.18	4.5±0.18	2.4	13.5	0.72

Table 3-2. Summary of quantitative trait loci associated with leaf tip necrosis traits. Logorithm of the odds (LOD) values obtained from composite interval mapping (CIM) and multiple QTL mapping (MQM) are presented for each significant association. The percent variance (R^2) explained by each QTL is provided.

QTL	Trait	Peak Marker*	Alleles	Genetic Position (cM)	1.5 LOD Interval (cM)	LOD Threshold$^{\varphi}$	LOD CIM	LOD MQM	Variance Explained	Source‡
Qltn.ksu-1DL	LTNM	snp-1D-364069796	C/T	78.8	61.40-91.26	3.11	2.94	3.12	3.64	WB-Cedar
Qltn.ksu-2A	LTNC	snp-2A-678001212	A/G	130.0	117.25-146.45	3.26	4.87	4.94	6.19	Everest
Qltn.ksu-2A	LTNM	snp-2A-580855803	A/C	121.0	109.96-134.43	3.11	3.31	4.51	5,37	Everest
Qltn.ksu-4DL	LTNC	snp-4D-504199409	C/T	56.0	25.86-77.22	3.26	3.06	3.75	4.62	Everest
Qltn.ksu-5AL	LTNM	snp-5A-617359065	T/C	188.0	172.02-214.34	3.11	3.15	3.53	4.13	Everest
Qltn.ksu-7DS	LTNC	*Lr34*	A/T	78.0	57.31-85.82	3.26	27.23	29.25	54.17	WB-Cedar
Qltn.ksu-7DS	LTNM	*Lr34*	A/T	79.4	57.31-114.13	3.11	28.37	27.42	47.07	WB-Cedar
Qltn.ksu-7DS	LTNI	*Lr34*	A/T	79.4	57.31-85.82	3.23	16.65	22.51	49.89	WB-Cedar

* Labels for markers contain the chromosome and the physical position in bp anchored to the Chinese Spring reference genome. φ LOD thresholds for each trait-environment combination derived from 1,000 permutations at P≤0.05. ‡ The source of the QTL associated with LTNC, LTNM, and LTNI corresponds with alleles for higher expression of LTN.

References

Browder, L. E. (1971). Pathogenic specialization in cereal rust fungi, especially Puccinia recondita f. sp. tritici : Concepts, methods of study, and application. *Naldc.nal.usda.gov*. https://naldc.nal.usda.gov/catalog/CAT71328703

Drijepondt, S. C., & Pretorius, Z. A. (1989). Greenhouse Evaluation of Adult-Plant Resistance Conferred by the Gene Lr34 to Leaf Rust of Wheat. *Plant Disease*, *73*(8), 669. https://doi.org/10.1094/pd-73-0669

Dyck, P. L. (1987). The association of a gene for leaf rust resistance with the chromosome 7D suppressor of stem rust resistance in common wheat. *Genome*, *29*(3), 467–469. https://doi.org/10.1139/g87-081

Dyck, P. L. (1991). Genetics of Adult-Plant Leaf Rust Resistance in “Chinese Spring” and “Sturdy” Wheats. *Crop Science*, *31*(2), 309–311. https://doi.org/10.2135/cropsci1991.0011183x003100020016x

Dyck, P. L., & Samborski, D. J. (1979). Adult-plant leaf rust resistance in PI 250413, an introduction of common wheat. *Canadian Journal of Plant Science*, *59*(2), 329–332. https://doi.org/10.4141/cjps79-053

Dyck, P. L., Samborski, D. J., & Anderson, R. G. (1966). INHERITANCE OF ADULT-PLANT LEAF RUST RESISTANCE DERIVED FROM THE COMMON WHEAT VARIETIES EXCHANGE AND FRONTANA. *Canadian Journal of Genetics and Cytology*, *8*(4), 665–671. https://doi.org/10.1139/g66-082

Ellis, J. G., Lagudah, E. S., Spielmeyer, W., & Dodds, P. N. (2014). The past, present and future of breeding rust resistant wheat. *Frontiers in Plant Science*, *5*. https://doi.org/10.3389/fpls.2014.00641

German, S. E., & Kolmer, J. A. (1992). Effect of gene Lr34 in the enhancement of resistance to leaf rust of wheat. *Theoretical and Applied Genetics*, *84*(1-2), 97–105. https://doi.org/10.1007/bf00223987

Herrera-Foessel, S. A., Singh, R. P., Huerta-Espino, J., Rosewarne, G. M., Periyannan, S. K., Viccars, L., Calvo-Salazar, V., Lan, C., & Lagudah, E. S. (2012). Lr68: a new gene conferring slow rusting resistance to leaf rust in wheat. *Theoretical and Applied Genetics*, *124*(8), 1475–1486. https://doi.org/10.1007/s00122-012-1802-1

Herrera-Foessel, S. A., Singh, R. P., Lillemo, M., Huerta-Espino, J., Bhavani, S., Singh, S., Lan, C., Calvo-Salazar, V., & Lagudah, E. S. (2014). Lr67/Yr46 confers adult plant resistance to stem rust and powdery mildew in wheat. *Theoretical and Applied Genetics*, *127*(4), 781–789. https://doi.org/10.1007/s00122-013-2256-9

Hiebert, C. W., Thomas, J. B., McCallum, B. D., Humphreys, D. G., DePauw, R. M., Hayden, M. J., Mago, R., Schnippenkoetter, W., & Spielmeyer, W. (2010). An introgression on wheat chromosome 4DL in RL6077 (Thatcher*6/PI 250413) confers adult plant resistance to stripe rust and leaf rust (Lr67). *Theoretical and Applied Genetics*, *121*(6), 1083–1091. https://doi.org/10.1007/s00122-010-1373-y

Huerta-Espino, J., Singh, R. P., Germán, S., McCallum, B. D., Park, R. F., Chen, W. Q., Bhardwaj, S. C., & Goyeau, H. (2011). Global status of wheat leaf rust caused by Puccinia triticina. *Euphytica*, *179*(1), 143–160. https://doi.org/10.1007/s10681-011-0361-x

Huerta-Espino, J., Singh, R., Crespo-Herrera, L. A., Villaseñor-Mir, H. E., Rodriguez-Garcia, M. F., Dreisigacker, S., Barcenas-Santana, D., & Lagudah, E. (2020). Adult Plant Slow Rusting Genes Confer High Levels of Resistance to Rusts in Bread Wheat Cultivars

From Mexico. *Frontiers in Plant Science*, *11*. https://doi.org/10.3389/fpls.2020.00824

Johnson, R. (1984). A Critical Analysis of Durable Resistance. *Annual Review of Phytopathology*, *22*(1), 309–330. https://doi.org/10.1146/annurev.py.22.090184.001521

Juliana, P., Rutkoski, J. E., Poland, J. A., Singh, R. P., Murugasamy, S., Natesan, S., Barbier, H., & Sorrells, M. E. (2015). Genome-Wide Association Mapping for Leaf Tip Necrosis and Pseudo-black Chaff in Relation to Durable Rust Resistance in Wheat. *The Plant Genome*, *8*(2). https://doi.org/10.3835/plantgenome2015.01.0002

Kolmer, J. A. (2005). Tracking wheat rust on a continental scale. *Current Opinion in Plant Biology*, *8*(4), 441–449. https://doi.org/10.1016/j.pbi.2005.05.001

Kolmer, J. A. (2019). Virulence of Puccinia triticina, the Wheat Leaf Rust Fungus, in the United States in 2017. *Plant Disease*, *103*(8), 2113–2120. https://doi.org/10.1094/pdis-09-18-1638-sr

Kolmer, J. A., Su, Z., Bernardo, A., Bai, G., & Chao, S. (2019). A Backcross Line of Thatcher Wheat with Adult Plant Leaf Rust Resistance Derived from Duster Wheat has Lr46 and Lr77. *Phytopathology®*, *109*(1), 127–132. https://doi.org/10.1094/phyto-06-18-0184-r

Krattinger, S. G., Lagudah, E. S., Spielmeyer, W., Singh, R. P., Huerta-Espino, J., McFadden, H., Bossolini, E., Selter, L. L., & Keller, B. (2009). A Putative ABC Transporter Confers Durable Resistance to Multiple Fungal Pathogens in Wheat. *Science*, *323*(5919), 1360–1363. https://doi.org/10.1126/science.1166453

Liu, J. Q., & Kolmer, J. A. (1998). Genetics of Stem Rust Resistance in Wheat Cvs. Pasqua and AC Taber. *Phytopathology®*, *88*(2), 171–176. https://doi.org/10.1094/phyto.1998.88.2.171

Lowe, I., Cantu, D., & Dubcovsky, J. (2010). Durable resistance to the wheat rusts: integrating

systems biology and traditional phenotype-based research methods to guide the deployment of resistance genes. *Euphytica*, *179*(1), 69–79. https://doi.org/10.1007/s10681-010-0311-z

Maccaferri, M., Mantovani, P., Tuberosa, R., DeAmbrogio, E., Giuliani, S., Demontis, A., Massi, A., & Sanguineti, M. C. (2008). A major QTL for durable leaf rust resistance widely exploited in durum wheat breeding programs maps on the distal region of chromosome arm 7BL. *Theoretical and Applied Genetics*, *117*(8), 1225–1240. https://doi.org/10.1007/s00122-008-0857-5

McCallum, B. D., Cloutier, S., Hiebert, C., & Jordan, M. (2021). Leaf tip necrosis and seedling leaf rust resistance conditioned by Lr34 in wheat grown at low temperatures. *Canadian Journal of Plant Pathology*, *43*(sup2), S211–S217. https://doi.org/10.1080/07060661.2021.1960611

McIntosh, R. A. (2007). Close genetic linkage of genes conferring adult-plant resistance to leaf rust and stripe rust in wheat. *Plant Pathology*, *41*(5), 523–527. https://doi.org/10.1111/j.1365-3059.1992.tb02450.x

McIntosh, R. A., Wellings, C. R., & Park, R. F. (1995). Wheat Rusts: An Atlas of Resistance Genes. In *www.springer.com*. Springer Netherlands. https://www.springer.com/gp/book/9789401040419

Messmer, M. M., Seyfarth, R., Keller, M., Schachermayr, G., Winzeler, M., Zanetti, S., Feuillet, C., & Keller, B. (2000). Genetic analysis of durable leaf rust resistance in winter wheat. *Theoretical and Applied Genetics*, *100*(3-4), 419–431. https://doi.org/10.1007/s001220050055

Nyori, P. (2010). *Genetics of Resistance to Leaf and Stripe Rust Diseases in the Spring Wheat*

"Amadina" [Dissertation]. https://krex.k-state.edu/dspace/handle/2097/4611

Pethybridge, S. J., & Nelson, S. C. (2015). Leaf Doctor: A New Portable Application for Quantifying Plant Disease Severity. *Plant Disease*, *99*(10), 1310–1316. https://doi.org/10.1094/pdis-03-15-0319-re

Rinaldo, A., Gilbert, B., Boni, R., Krattinger, S. G., Singh, D., Park, R. F., Lagudah, E., & Ayliffe, M. (2017). The Lr34 adult plant rust resistance gene provides seedling resistance in durum wheat without senescence. *Plant Biotechnology Journal*, *15*(7), 894–905. https://doi.org/10.1111/pbi.12684

Rosewarne, G. M., Singh, R. P., Huerta-Espino, J., William, H. M., Bouchet, S., Cloutier, S., McFadden, H., & Lagudah, E. S. (2005). Leaf tip necrosis, molecular markers and β1-proteasome subunits associated with the slow rusting resistance genes Lr46/Yr29. *Theoretical and Applied Genetics*, *112*(3), 500–508. https://doi.org/10.1007/s00122-005-0153-6

Singh, A., Knox, R. E., DePauw, R. M., Singh, A. K., Cuthbert, R. D., Campbell, H. L., Shorter, S., & Bhavani, S. (2014). Stripe rust and leaf rust resistance QTL mapping, epistatic interactions, and co-localization with stem rust resistance loci in spring wheat evaluated over three continents. *Theoretical and Applied Genetics*, *127*(11), 2465–2477. https://doi.org/10.1007/s00122-014-2390-z

Singh, R. P. (1992). Association between Gene Lr34 for Leaf Rust Resistance and Leaf Tip Necrosis in Wheat. *Crop Science*, *32*(4), 874. https://doi.org/10.2135/cropsci1992.0011183x003200040008x

Singh, R. P. (1993). Genetic Association of GeneBdv1for Tolerance to Barley Yellow Dwarf Virus with GenesLr34andYr18for Adult Plant Resistance to Rusts in Bread Wheat. *Plant*

Disease, *77*(11), 1103. https://doi.org/10.1094/pd-77-1103

Singh, R. P., Huerta-Espino, J., Bhavani, S., Herrera-Foessel, S. A., Singh, D., Singh, P. K., Velu, G., Mason, R. E., Jin, Y., Njau, P., & Crossa, J. (2010). Race non-specific resistance to rust diseases in CIMMYT spring wheats. *Euphytica*, *179*(1), 175–186. https://doi.org/10.1007/s10681-010-0322-9

Singh, R. P., Mujeeb-Kazi, A., & Huerta-Espino, J. (1998). Lr46: A Gene Conferring Slow-Rusting Resistance to Leaf Rust in Wheat. *Phytopathology*®, *88*(9), 890–894. https://doi.org/10.1094/phyto.1998.88.9.890

Spielmeyer, W., McIntosh, R. A., Kolmer, J., & Lagudah, E. S. (2005). Powdery mildew resistance and Lr34/Yr18 genes for durable resistance to leaf and stripe rust cosegregate at a locus on the short arm of chromosome 7D of wheat. *Theoretical and Applied Genetics*, *111*(4), 731–735. https://doi.org/10.1007/s00122-005-2058-9

William, M., Singh, R. P., Huerta-Espino, J., Islas, S. O., & Hoisington, D. (2003). Molecular Marker Mapping of Leaf Rust Resistance Gene Lr46 and Its Association with Stripe Rust Resistance Gene Yr29 in Wheat. *Phytopathology*®, *93*(2), 153–159. https://doi.org/10.1094/phyto.2003.93.2.153

Appendix A - Chapter 1 Supplemental Figures and Tables

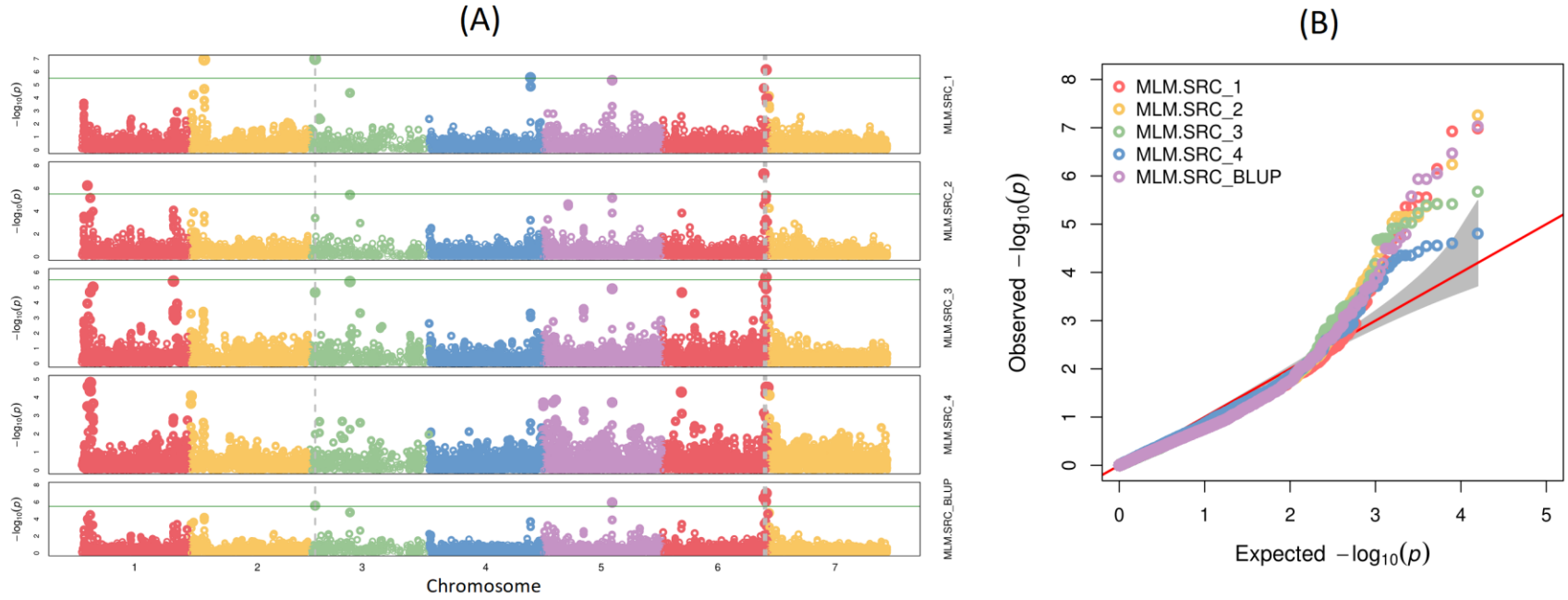

Appendix Figure A.1. (A) Manhattan plots for haplotype-based genome-wide association mapping of solvent retention capacity within each environment and the BLUP. The y-axis displays the -log10(p) for association between haplotype and solvent retention capacity. The chromosomes are on the x-axis. (B) Quantile-Quantile plot showing observed -log10(p) on the y-axis versus expected -log10(p) on the x-axis. Colors represent different environments.

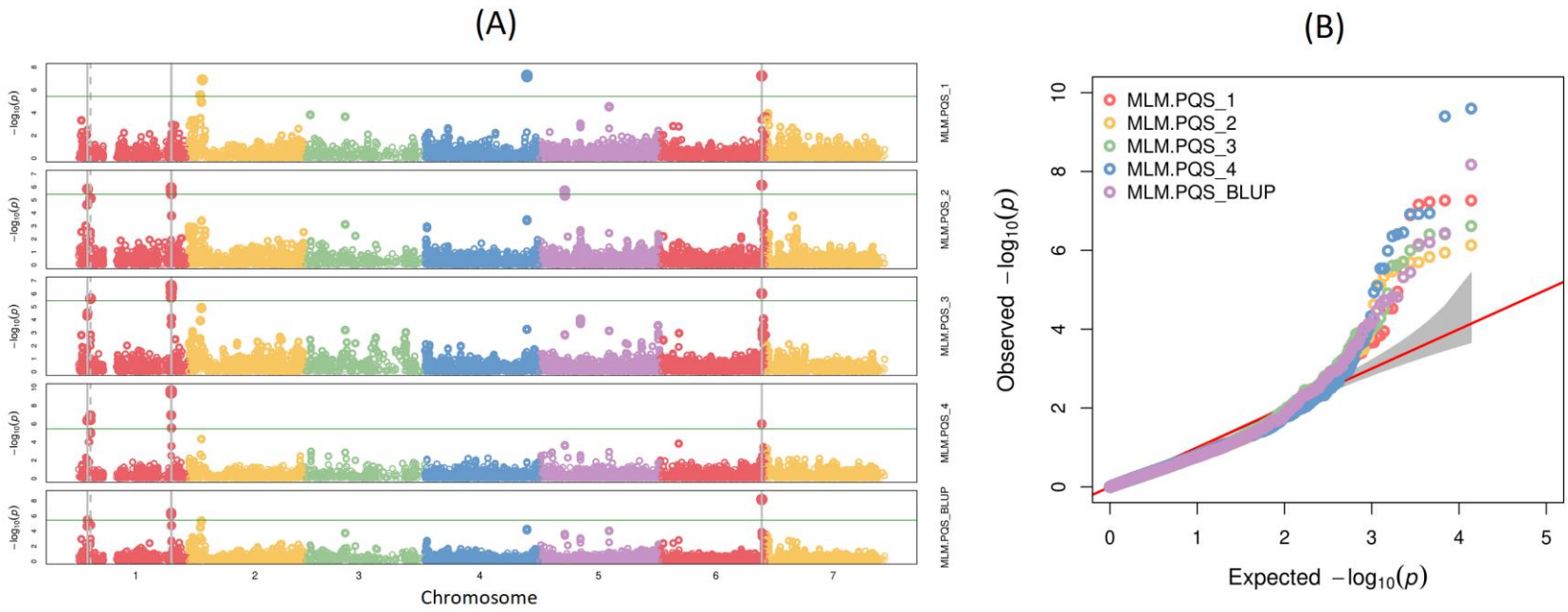

Appendix Figure A.2. (A) Manhattan plots for haplotype-based genome-wide association mapping of protein quality score within each environment and the BLUP. The y-axis displays the -$\log_{10}(p)$ for association between haplotype and protein quality score. The chromosomes are on the x-axis. (B) Quantile-Quantile plot showing observed -$\log_{10}(p)$ on the y-axis versus expected -$\log_{10}(p)$ on the x-axis. Colors represent the different environments. haplotype and protein quality score. The chromosomes are on the x-axis. (B) Quantile-Quantile plot showing observed -$\log_{10}(p)$ on the y-axis versus expected -$\log_{10}(p)$ on the x-axis. Colors represent the different environments.

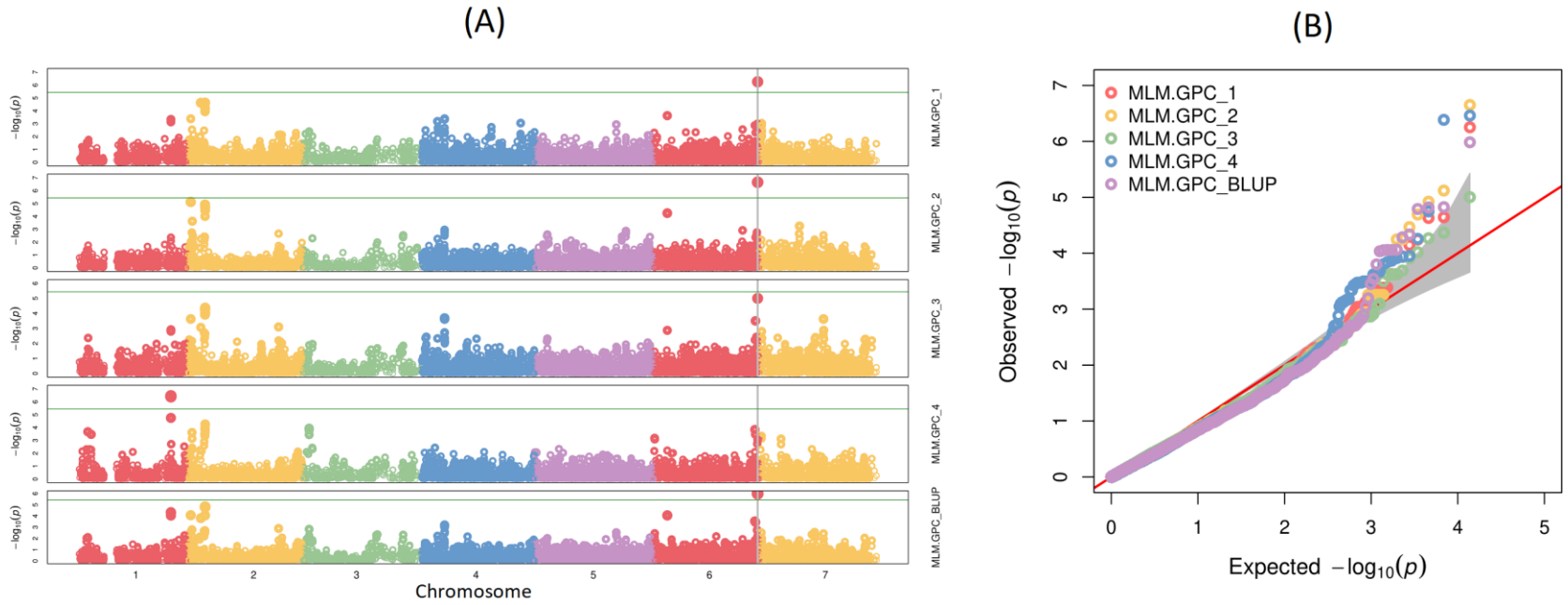

Appendix Figure A.3. (A) Manhattan plots for haplotype-based genome-wide association mapping of grain protein content within each environment and the BLUP. The y-axis displays the -log$_{10}$*(p)* for association between haplotype and grain protein content. The chromosomes are on the x-axis. (B) Quantile-Quantile plot showing observed -log$_{10}$*(p)* on the y-axis versus expected -log$_{10}$*(p)* on the x-axis. Colors represent different environments. *(p)* for association between haplotype and grain protein content. The chromosomes are on the x-axis. (B) Quantile-Quantile plot showing observed -log$_{10}$*(p)* on the y-axis versus expected -log$_{10}$*(p)* on the x-axis. Colors represent different environments.

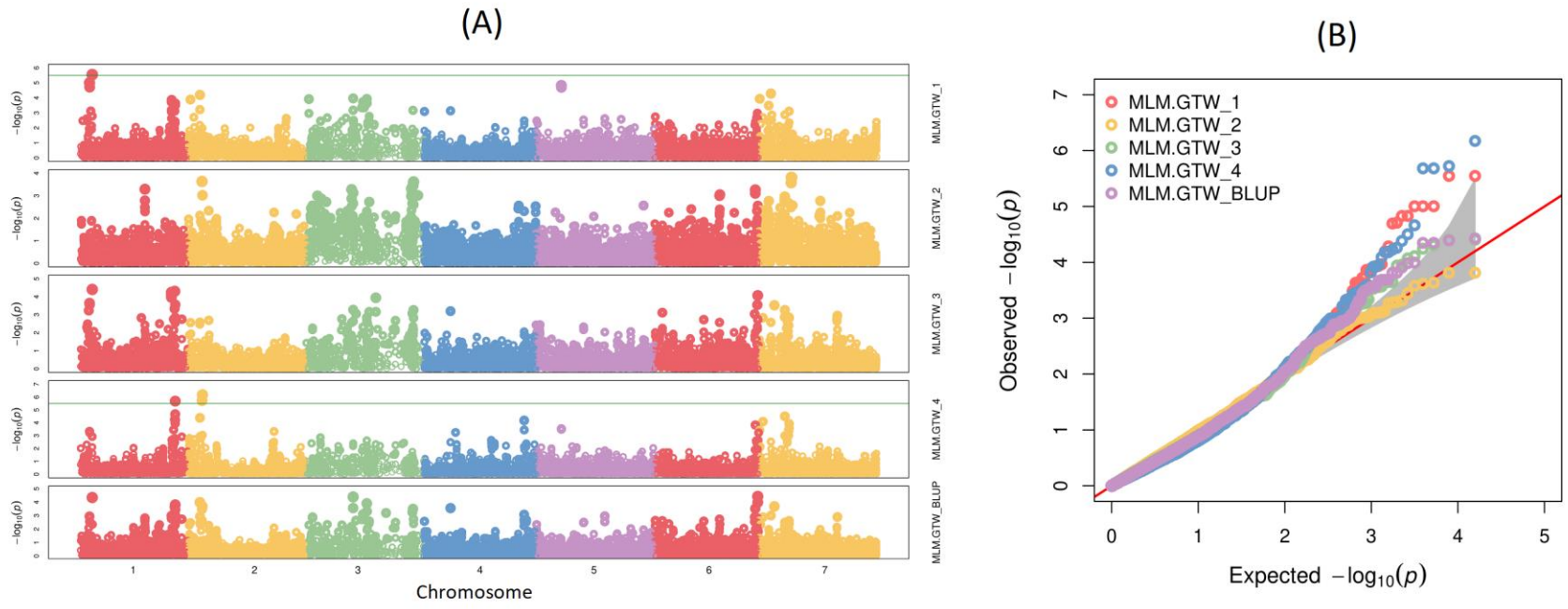

Appendix Figure A.4. (A) Manhattan plots for haplotype-based genome-wide association mapping of grain test weight within each environment and the BLUP. The y-axis displays the -$\log_{10}(p)$ for association between haplotype and grain test weight. The chromosomes are on the x-axis. (B) Quantile-Quantile plot showing observed -$\log_{10}(p)$ on the y-axis versus expected -$\log_{10}(p)$ on the x-axis. Colors represent different environments. and the BLUP. The y-axis displays the -$\log_{10}(p)$ for association between haplotype and grain test weight. The chromosomes are on the x-axis. (B) Quantile-Quantile plot showing observed -$\log_{10}(p)$ on the y-axis versus expected -$\log_{10}(p)$ on the x-axis. Colors represent different environments.

Appendix Table A.1. List of six *T. aestivum* wheat lines used as recurrent parents and 21 *Ae. tauschii* accessions.

Genotype	Species
KanMark	*T. aestivum*
Danby	*T. aestivum*
Larry	*T. aestivum*
KS061278M-4	*T. aestivum*
KS061406LN~26	*T. aestivum*
KS061862M-17	*T. aestivum*
TA10077	*Ae. tauschii*
TA10106	*Ae. tauschii*
TA10155	*Ae. tauschii*
TA10166	*Ae. tauschii*
TA10189	*Ae. tauschii*
TA10193	*Ae. tauschii*
TA1634	*Ae. tauschii*
TA2374	*Ae. tauschii*
TA2378	*Ae. tauschii*
TA2388	*Ae. tauschii*
TA2389	*Ae. tauschii*
TA2395	*Ae. tauschii*
TA2398	*Ae. tauschii*
TA2489	*Ae. tauschii*
TA2521	*Ae. tauschii*
TA2536	*Ae. tauschii*
TA2538	*Ae. tauschii*
TA2543	*Ae. tauschii*
TA2567	*Ae. tauschii*
TA10142	*Ae. tauschii*
TA1642	*Ae. tauschii*

Appendix Table A.2. GPS coordinates of field trials for the four environments, E1, E2, E3, and E4.

Growing Season	Environment	Location	Latitude	Longitude
2018	E1	Colby, Kansas	39°23'16.0"N	101°04'16.0"W
2019	E2	Colby, Kansas	39°23'14.8"N	101°04'04.7"W
2019	E3	Colby, Kansas	39°23'14.6"N	101°04'17.2"W
2020	E4	Ashland, Kansas	39°07'37.0"N	96°36'40.2"W

Appendix Table A.3. Monthly precipitation and temperatures collected by weather stations at Colby, KS and Manhattan, KS.

Station	Month-Year	Precipitation (cm)	Min Temp (°C)	Max Temp (°C)
Colby, KS	Oct-17	1.83	2.78	20.56
Colby, KS	Nov-17	0.44	-2.78	13.89
Colby, KS	Dec-17	0.21	-9.45	6.67
Colby, KS	Jan-18	3.59	-11.12	6.67
Colby, KS	Feb-18	0.94	-11.12	5
Colby, KS	Mar-18	1.53	-4.45	15.56
Colby, KS	Apr-18	2.57	-1.67	16.12
Colby, KS	May-18	11.28	10.56	26.67
Colby, KS	Jun-18	8.36	15.56	32.23
Colby, KS	Jul-18	6.63	17.23	32.23
Colby, KS	Aug-18	7.14	14.45	30
Colby, KS	Sep-18	1.5	12.23	27.23
Colby, KS	Oct-18	8.82	1.67	16.67
Colby, KS	Nov-18	1.07	-5.56	10.56
Colby, KS	Dec-18	2.47	-7.78	7.23
Colby, KS	Jan-19	1.1	-7.78	5
Colby, KS	Feb-19	2.21	-11.67	1.67
Colby, KS	Mar-19	5.95	-5.56	7.23
Colby, KS	Apr-19	0.77	2.23	20.56
Colby, KS	May-19	17.51	6.12	19.45
Colby, KS	Jun-19	7.29	12.78	28.89
Colby, KS	Jul-19	2.49	17.23	33.34
Manhattan, KS	Aug-19	21.85	19.45	29.45
Manhattan, KS	Sep-19	5.97	18.89	30
Manhattan, KS	Oct-19	6.94	3.89	17.23
Manhattan, KS	Nov-19	1.55	-1.67	11.67
Manhattan, KS	Dec-19	2.7	-3.89	8.89
Manhattan, KS	Jan-20	4.63	-5	5.56
Manhattan, KS	Feb-20	1.99	-4.45	7.78
Manhattan, KS	Mar-20	5.9	3.34	14.45
Manhattan, KS	Apr-20	6.1	5	18.89
Manhattan, KS	May-20	18.93	11.12	22.23
Manhattan, KS	Jun-20	12.81	19.45	32.23
Manhattan, KS	Jul-20	25.74	21.12	31.67

Appendix Table A.4. Details of 13 haplotype blocks associated with end-use quality traits in individual environments.

Trait	HB[a]	Chr.	Start (bp)[b]	End (bp)[c]	E1[d]	E2	E3	E4	R^2 (%)[e]	Positive Source[f]
SRC	HAP_3D_B47	3D	2.6E+07	2.7E+07	***	ns	ns	**	5.09 – 6.62	*Ae. Tauschii*
SRC	HAP_6D_B2354	6D	4.5E+08	4.5E+08	ns	***	ns	**	6.03 – 7.18	*T. aestivum*
SRC	HAP_6D_B2384	6D	4.6E+08	4.6E+08	ns	ns	*	**	5.58 – 5.75	*Ae. Tauschii*
SRC	HAP_6D_B2393	6D	4.7E+08	4.7E+08	**	ns	ns	**	5.72 – 6.64	Both
PQS	HAP_1D_B120	1D	4.2E+07	4.2E+07	ns	**	ns	***	6.29 – 7.72	Both
PQS	HAP_1D_B188	1D	5.5E+07	5.6E+07	ns	ns	**	***	6.17 – 8.37	Both
PQS	HAP_1D_B189	1D	5.6E+07	5.6E+07	ns	ns	**	***	6.17 – 8.37	Both
PQS	HAP_1D_B2116	1D	4.1E+08	4.1E+08	ns	**	**	***	6.05 – 12.18	Both
PQS	HAP_1D_B2117	1D	4.1E+08	4.1E+08	ns	**	**	***	6.43 – 11.89	Both
PQS	HAP_1D_B2118	1D	4.1E+08	4.1E+08	ns	**	**	***	6.12 – 8.4	Both
PQS	HAP_1D_B2121	1D	4.2E+08	4.2E+08	ns	ns	**	**	6.47 – 7.18	Both
PQS	HAP_1D_B2122	1D	4.2E+08	4.2E+08	ns	ns	**	**	6.47 – 7.18	Both
PQS	HAP_6D_B2354	6D	4.5E+08	4.5E+08	***	**	**	**	6.66 – 8.62	*T. aestivum*
GPC	HAP_1D_B2116	1D	4.1E+08	4.1E+08	ns	ns	ns	**	7.63	Both
GPC	HAP_1D_B2117	1D	4.1E+08	4.1E+08	ns	ns	ns	**	7.53	Both
GPC	HAP_6D_B2399	6D	4.7E+08	4.7E+08	**	**	ns	ns	5.62 – 6.74	Both
GTW	HAP_1D_B188	1D	5.5E+07	5.6E+07	*	ns	ns	ns	6.66	Both
GTW	HAP_1D_B189	1D	5.6E+07	5.6E+07	*	ns	ns	ns	6.66	Both

[a]Stable haplotype blocks associated with end-use quality traits in more than one environment for atleast one trait. [bc]Physical genetic interval of each HB in base pairs. [d]Significance of GWAS result for each individual environment using MLM following an FDR controlling procedure where * = ($P < 0.05$), ** = ($P < 0.01$), and *** = ($P < 0.001$). [e]Percent of phenotypic variance explained by each HB. [f]Parental species containing the beneficial haplotype associated with each trait.

Appendix Table A.5. Candidate gene information including Ae. Tauschii orthologs and gene ontology for stable haplotype-trait associations.

Trait	HB[a]	Start (bp)[b]	End (bp)[c]	Positive Source[d]	Candidate Gene[e]	CG Location[f]	*Ae. Tauschii* Ortholog	Gene Ontology
SRC	HAP_3D_B47	26382902	26738476	Tauschii	TraesCS3D02G060800	within HB	AET3Gv20140100	myosin binding
SRC	HAP_3D_B47	26382902	26738476	Tauschii	TraesCS3D02G060900	within HB	AET3Gv20140200	
SRC	HAP_3D_B47	26382902	26738476	Tauschii	TraesCS3D02G061000	within HB	AET3Gv20140300	response to abscisic acid
SRC	HAP_3D_B47	26382902	26738476	Tauschii	TraesCS3D02G061200	within HB	AET3Gv20141200	protein phosphorylation
SRC	HAP_3D_B47	26382902	26738476	Tauschii	TraesCS3D02G061400	within HB	AET3Gv20141400	enzyme inhibitor activity
SRC	HAP_3D_B47	26382902	26738476	Tauschii	TraesCS3D02G061500	within HB	AET3Gv20141500	oxidation-reduction process
SRC	HAP_3D_B47	26382902	26738476	Tauschii	TraesCS3D02G061600	within HB	AET3Gv20141600	
SRC	HAP_6D_B2354	454636091	454639980	Aestivum	TraesCS6D02G365200	545 bp proximal	AET6Gv20933800	protein binding
SRC	HAP_6D_B2354	454636091	454639980	Aestivum	TraesCS6D02G365300	2356 bp distal		
SRC	HAP_6D_B2354	454636091	454639980	Aestivum	TraesCS6D02G365400	7580 bp distal		oxidation-reduction process
SRC	HAP_6D_B2354	454636091	454639980	Aestivum	TraesCS6D02G365600	13900 bp distal	AET6Gv20934200	oxidation-reduction process
SRC	HAP_6D_B2384	463775852	463809722	Tauschii	TraesCS6D02G386300	within HB	AET6Gv20974400	oxidation-reduction process
SRC	HAP_6D_B2393	465141041	465177049	Both	TraesCS6D02G390100	24720 bp distal	AET6Gv20981600	ATP binding, phosphatidylinositol phosphate kinase activity, 1-phosphatidylinositol-4-phosphate 5-kinase activity
PQS	HAP_1D_B120	42036362	42298955	Both	TraesCS1D02G062400	within HB	AET1Gv20151300	
PQS	HAP_1D_B120	42036362	42298955	Both	TraesCS1D02G062300	29623 bp distal	AET1Gv20150800	protein phosphorylation
PQS	HAP_1D_B188	55409819	55828553	Both	TraesCS1D02G073900	within HB	AET1Gv20182000	mitochondrial pyruvate transmembrane transport
PQS	HAP_1D_B188	55409819	55828553	Both	TraesCS1D02G074300	within HB	AET1Gv20182800	oxidation-reduction process
PQS	HAP_1D_B188	55409819	55828553	Both	TraesCS1D02G074400	within HB	AET1Gv20182900	transmembrane transport
PQS	HAP_1D_B189	55840612	55876147	Both	TraesCS1D02G074500	15625 bp proximal	AET1Gv20183200	glutathione biosynthetic process, cellular modified amino acid biosynthetic process

PQS	HAP_1D_B2116	414902844	414917687	Both	TraesCS1D02G317211	2739533 bp proximal		GLU-D1: High molecular weight glutenin subunit
PQS	HAP_1D_B2116	414902844	414917687	Both	TraesCS1D02G321500	22961 bp distal	AET1Gv20765500	DNA-binding transcription factor activity
PQS	HAP_1D_B2117	414917730	414929805	Both	TraesCS1D02G317211	2754419 bp proximal		GLU-D1: High molecular weight glutenin subunit
PQS	HAP_1D_B2117	414917730	414929805	Both	TraesCS1D02G321500	10843 bp distal	AET1Gv20765500	DNA-binding transcription factor activity
PQS	HAP_1D_B2118	414929899	414939966	Both	TraesCS1D02G317211	2766588 bp proximal		GLU-D1: High molecular weight glutenin subunit
PQS	HAP_1D_B2121	415981474	416162575	Both	TraesCS1D02G317211	3818163 bp proximal		GLU-D1: High molecular weight glutenin subunit
PQS	HAP_1D_B2121	415981474	416162575	Both	TraesCS1D02G323100	within HB	AET1Gv20772800	box H/ACA snoRNP assembly, pseudouridine synthesis, ribosome biogenesis
PQS	HAP_1D_B2121	415981474	416162575	Both	TraesCS1D02G323200	within HB	AET1Gv20772900	
PQS	HAP_1D_B2121	415981474	416162575	Both	TraesCS1D02G323500	within HB	AET1Gv20773700	
PQS	HAP_1D_B2121	415981474	416162575	Both	TraesCS1D02G323600	within HB		anaphase-promoting complex-dependent catabolic process
PQS	HAP_1D_B2122	416162607	416219156	Both	TraesCS1D02G317211	3999296 bp proximal		GLU-D1: High molecular weight glutenin subunit
PQS	HAP_6D_B2354	454636091	454639980	Aestivum	TraesCS6D02G365200	545 bp proximal	AET6Gv20933800	protein binding
PQS	HAP_6D_B2354	454636091	454639980	Aestivum	TraesCS6D02G365300	2356 bp distal		
PQS	HAP_6D_B2354	454636091	454639980	Aestivum	TraesCS6D02G365400	7580 bp distal		oxidation-reduction process
PQS	HAP_6D_B2354	454636091	454639980	Aestivum	TraesCS6D02G365600	13900 bp distal	AET6Gv20934200	oxidation-reduction process
GPC	HAP_1D_B2116	414902844	414917687	Both	TraesCS1D02G317211	2739533 bp proximal		GLU-D1: High molecular weight glutenin subunit
GPC	HAP_1D_B2116	414902844	414917687	Both	TraesCS1D02G321500	22961 bp distal	AET1Gv20765500	DNA-binding transcription factor activity
GPC	HAP_1D_B2117	414917730	414929805	Both	TraesCS1D02G321500	10843 bp distal	AET1Gv20765500	DNA-binding transcription factor activity
GPC	HAP_1D_B2117	414917730	414929805	Both	TraesCS1D02G321500	10843 bp distal	AET1Gv20765500	DNA-binding transcription factor activity

GPC	HAP_6D_B2399	467210863	467211385	Both	TraesCS6D02G393400	10180 bp proximal	AET6Gv20989500	integral component of membrane
GPC	HAP_6D_B2399	467210863	467211385	Both	TraesCS6D02G393300	22947 bp proximal	AET6Gv20989400	protein binding
GTW	HAP_1D_B188	55409819	55828553	Both	TraesCS1D02G073900	within HB	AET1Gv20182000	mitochondrial pyruvate transmembrane transport
GTW	HAP_1D_B188	55409819	55828553	Both	TraesCS1D02G074300	within HB	AET1Gv20182800	carotenoid biosynthetic process, oxidation-reduction process
GTW	HAP_1D_B188	55409819	55828553	Both	TraesCS1D02G074400	within HB	AET1Gv20182900	cation transport, transmembrane transport
GTW	HAP_1D_B189	55840612	55876147	Both	TraesCS1D02G074500	15625 bp proximal	AET1Gv20183200	glutathione biosynthetic process, cellular modified amino acid biosynthetic process

[a]Stable haplotype blocks associated with end-use quality traits in more than one environment. [bc]Physical genetic interval of each HB in base pairs. [d]Parental species containing the beneficial haplotype associated with each trait.[e]*T. aestivum* candidate gene designations from Plants Ensemble database. [f]Location of the candidate gene in relation to the associated haplotype block with physical distance in base pairs. [g]*Ae. tauschii* orthologue corresponding to the *T. aestivum* candidate gene. [h]Gene ontology of corresponding candidate gene.

Appendix B - Chapter 2 Supplemental Figures and Tables

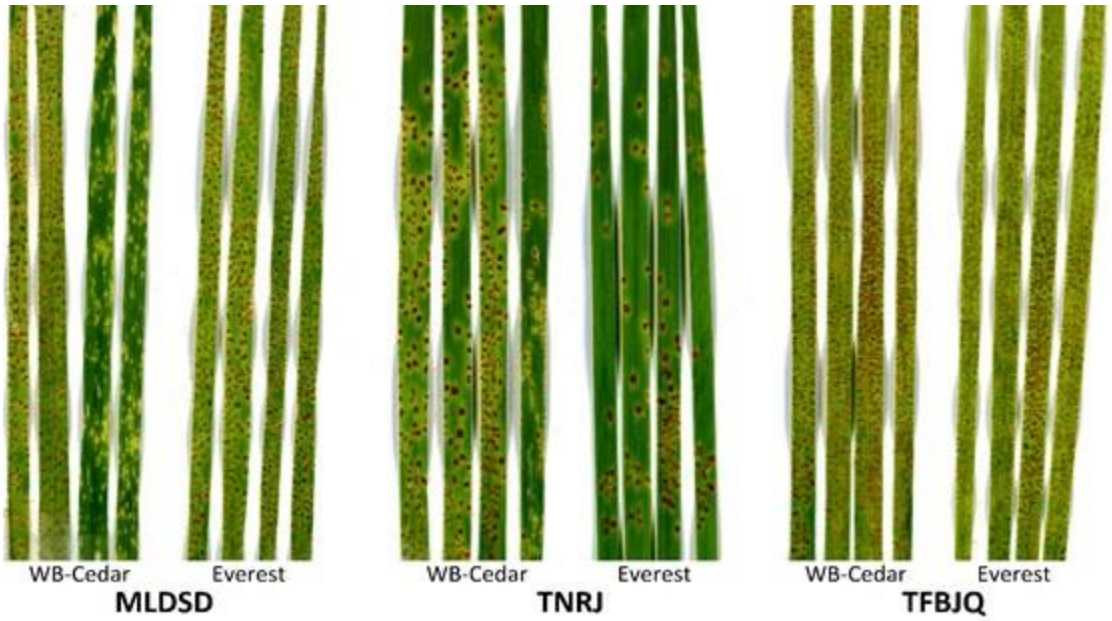

Appendix Figure B.1. Visual response of parental lines Everest and WB-Cedar to leaf rust infection at the seedling stage using races MLDSD, TNRJ, and TFBJQ.

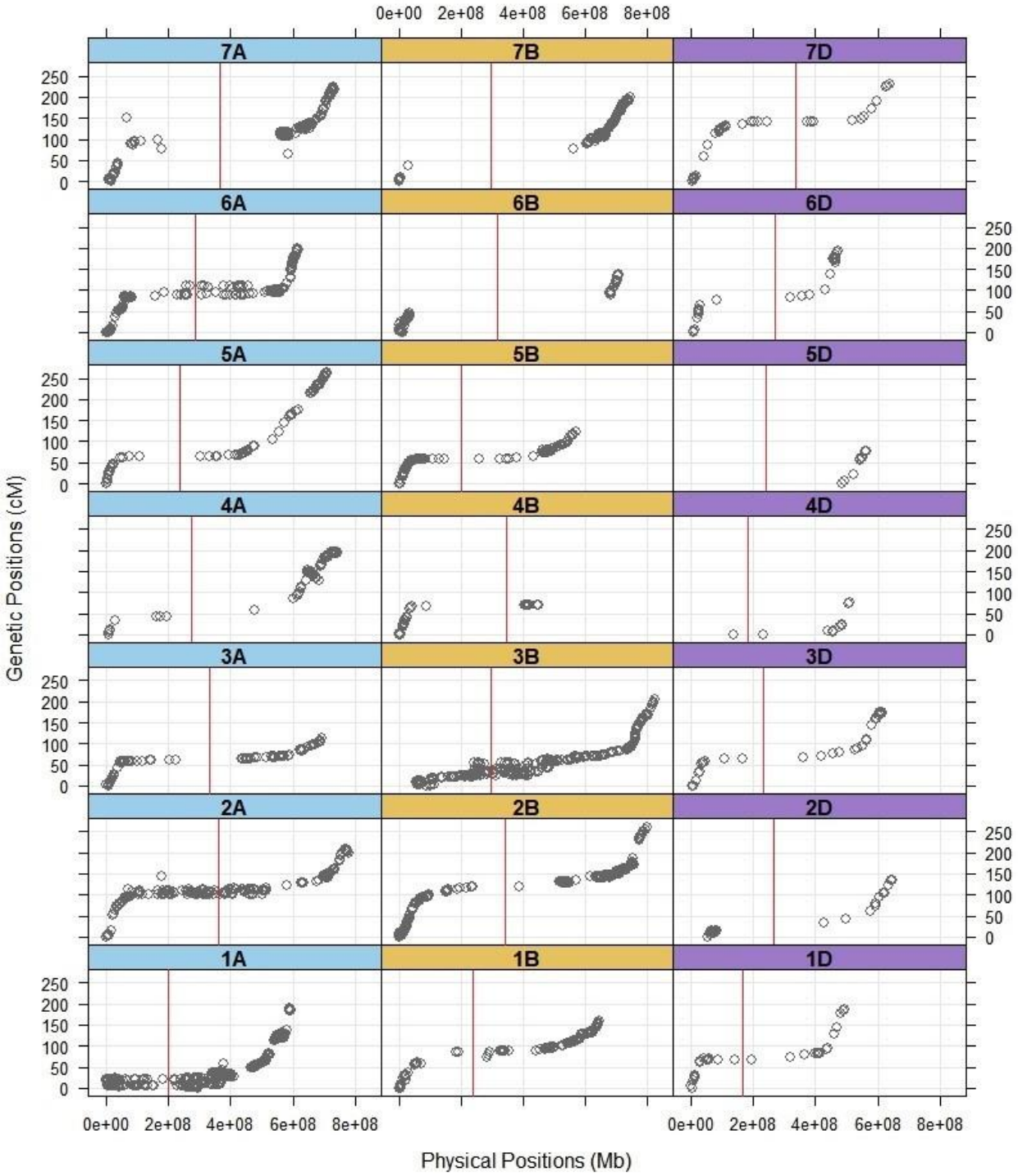

Appendix Figure B.2. Scatterplot showing collinearity between genetic positions in centimorgans (vertical axis) and physical position in megabases (horizontal axis) for the SNPs positioned on each of the twenty-one wheat chromosomes. Vertical red bars represent the approximate position of the centromere for each chromosome according to the Chinese Spring reference.

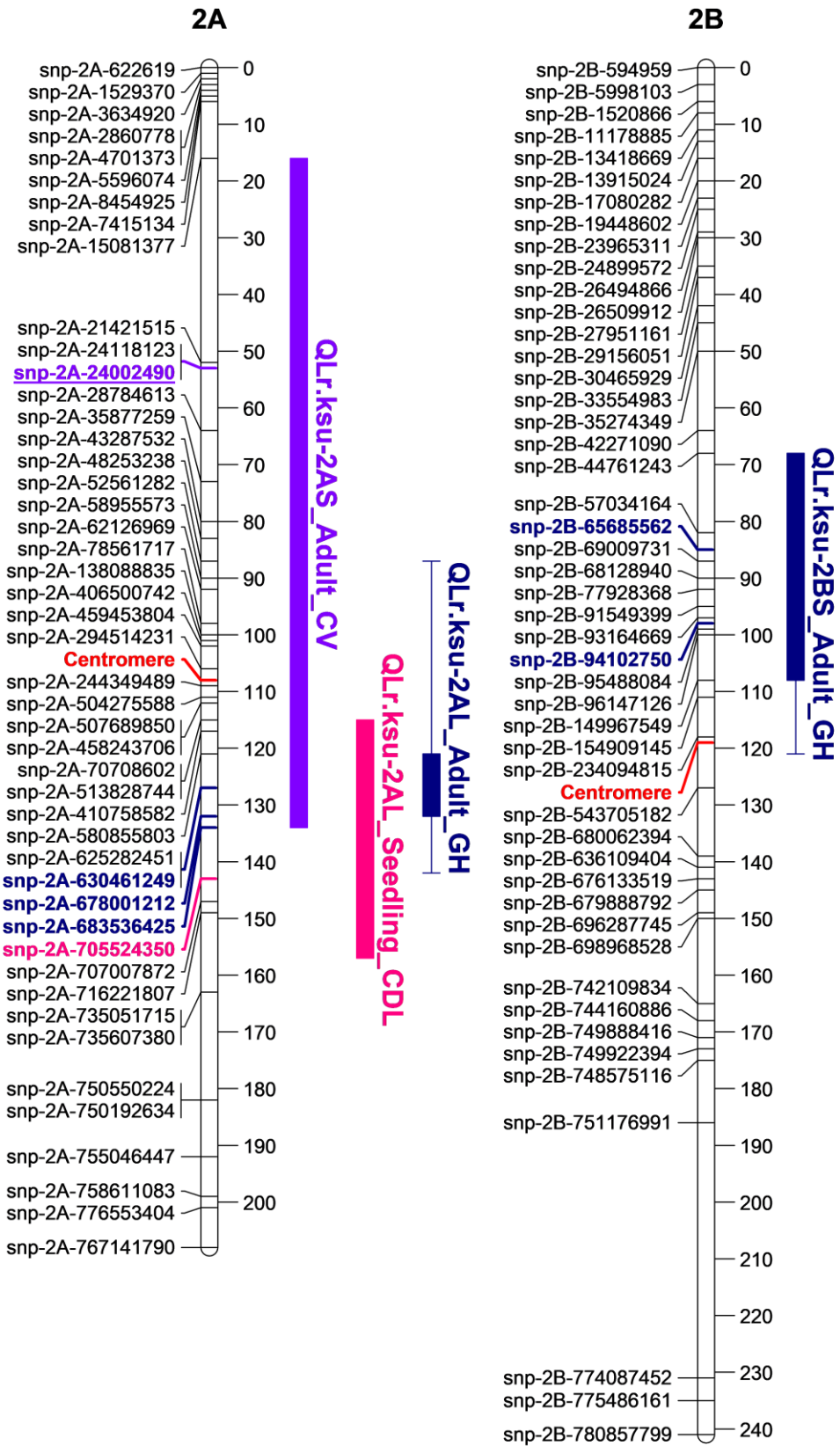
2A
snp-2A-622619
snp-2A-1529370
snp-2A-3634920
snp-2A-2860778
snp-2A-4701373
snp-2A-5596074
snp-2A-8454925
snp-2A-7415134
snp-2A-15081377
snp-2A-21421515
snp-2A-24118123
snp-2A-24002490
snp-2A-28784613
snp-2A-35877259
snp-2A-43287532
snp-2A-48253238
snp-2A-52561282
snp-2A-58955573
snp-2A-62126969
snp-2A-78561717
snp-2A-138088835
snp-2A-406500742
snp-2A-459453804
snp-2A-294514231
Centromere
snp-2A-244349489
snp-2A-504275588
snp-2A-507689850
snp-2A-458243706
snp-2A-70708602
snp-2A-513828744
snp-2A-410758582
snp-2A-580855803
snp-2A-625282451
snp-2A-630461249
snp-2A-678001212
snp-2A-683536425
snp-2A-705524350
snp-2A-707007872
snp-2A-716221807
snp-2A-735051715
snp-2A-735607380
snp-2A-750550224
snp-2A-750192634
snp-2A-755046447
snp-2A-758611083
snp-2A-776553404
snp-2A-767141790
0
10
20
30
40
50
60
70
80
90
100
110
120
130
140
150
160
170
180
190
200
QLr.ksu-2AS_Adult_CV
QLr.ksu-2AL_Adult_GH
QLr.ksu-2AL_Seedling_CDL
2B
snp-2B-594959
snp-2B-5998103
snp-2B-1520866
snp-2B-11178885
snp-2B-13418669
snp-2B-13915024
snp-2B-17080282
snp-2B-19448602
snp-2B-23965311
snp-2B-24899572
snp-2B-26494866
snp-2B-26509912
snp-2B-27951161
snp-2B-29156051
snp-2B-30465929
snp-2B-33554983
snp-2B-35274349
snp-2B-42271090
snp-2B-44761243
snp-2B-57034164
snp-2B-65685562
snp-2B-69009731
snp-2B-68128940
snp-2B-77928368
snp-2B-91549399
snp-2B-93164669
snp-2B-94102750
snp-2B-95488084
snp-2B-96147126
snp-2B-149967549
snp-2B-154909145
snp-2B-234094815
Centromere
snp-2B-543705182
snp-2B-680062394
snp-2B-636109404
snp-2B-676133519
snp-2B-679888792
snp-2B-696287745
snp-2B-698968528
snp-2B-742109834
snp-2B-744160886
snp-2B-749888416
snp-2B-749922394
snp-2B-748575116
snp-2B-751176991
snp-2B-774087452
snp-2B-775486161
snp-2B-780857799
0
10
20
30
40
50
60
70
80
90
100
110
120
130
140
150
160
170
180
190
200
210
220
230
240
QLr.ksu-2BS_Adult_GH

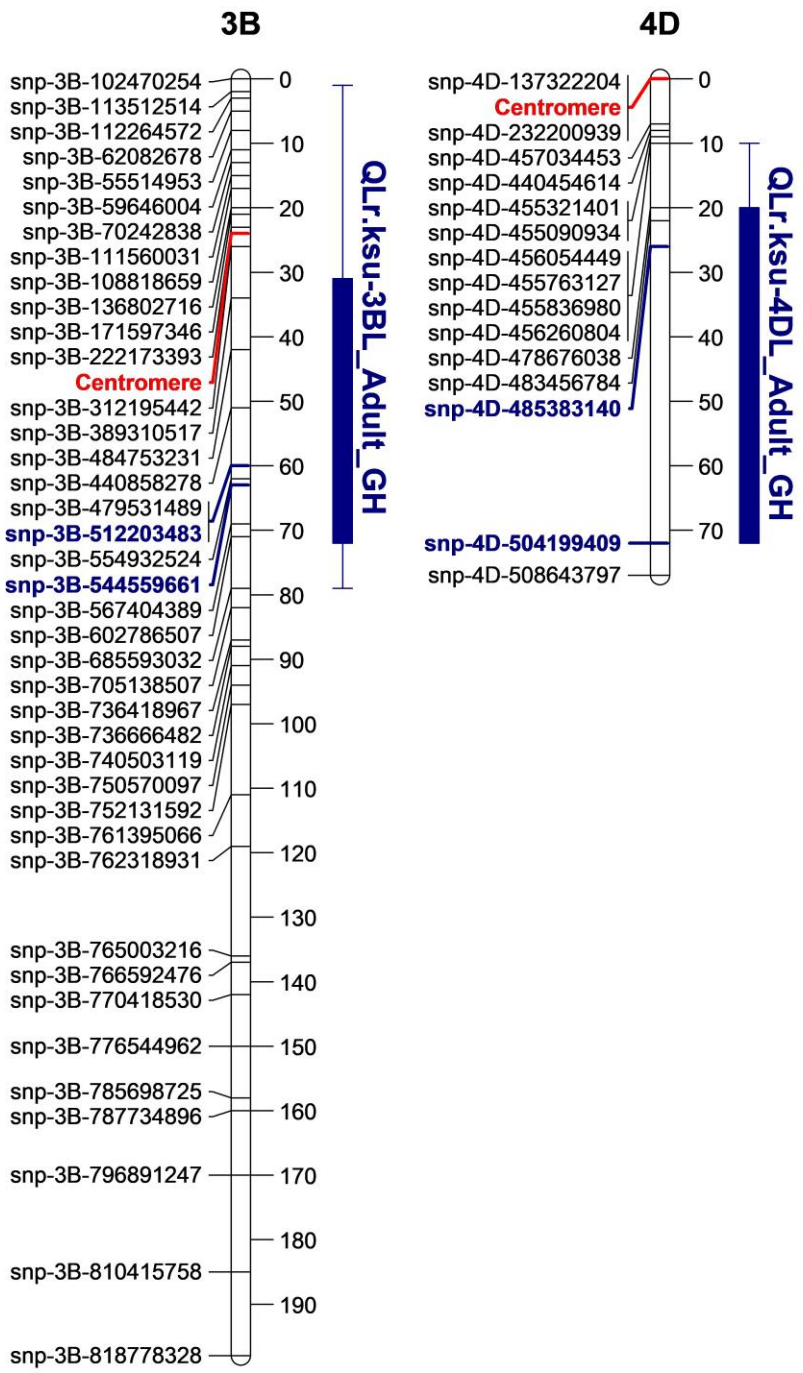
3B
4D
snp-3B-102470254
snp-3B-113512514
snp-3B-112264572
snp-3B-62082678
snp-3B-55514953
snp-3B-59646004
snp-3B-70242838
snp-3B-111560031
snp-3B-108818659
snp-3B-136802716
snp-3B-171597346
snp-3B-222173393
Centromere
snp-3B-312195442
snp-3B-389310517
snp-3B-484753231
snp-3B-440858278
snp-3B-479531489
snp-3B-512203483
snp-3B-554932524
snp-3B-544559661
snp-3B-567404389
snp-3B-602786507
snp-3B-685593032
snp-3B-705138507
snp-3B-736418967
snp-3B-736666482
snp-3B-740503119
snp-3B-750570097
snp-3B-752131592
snp-3B-761395066
snp-3B-762318931
snp-3B-765003216
snp-3B-766592476
snp-3B-770418530
snp-3B-776544962
snp-3B-785698725
snp-3B-787734896
snp-3B-796891247
snp-3B-810415758
snp-3B-818778328
0
10
20
30
40
50
60
70
80
90
100
110
120
130
140
150
160
170
180
190
QLr.ksu-3BL_Adult_GH
snp-4D-137322204
Centromere
snp-4D-232200939
snp-4D-457034453
snp-4D-440454614
snp-4D-455321401
snp-4D-455090934
snp-4D-456054449
snp-4D-455763127
snp-4D-455836980
snp-4D-456260804
snp-4D-478676038
snp-4D-483456784
snp-4D-485383140
snp-4D-504199409
snp-4D-508643797
0
10
20
30
40
50
60
70
QLr.ksu-4DL_Adult_GH

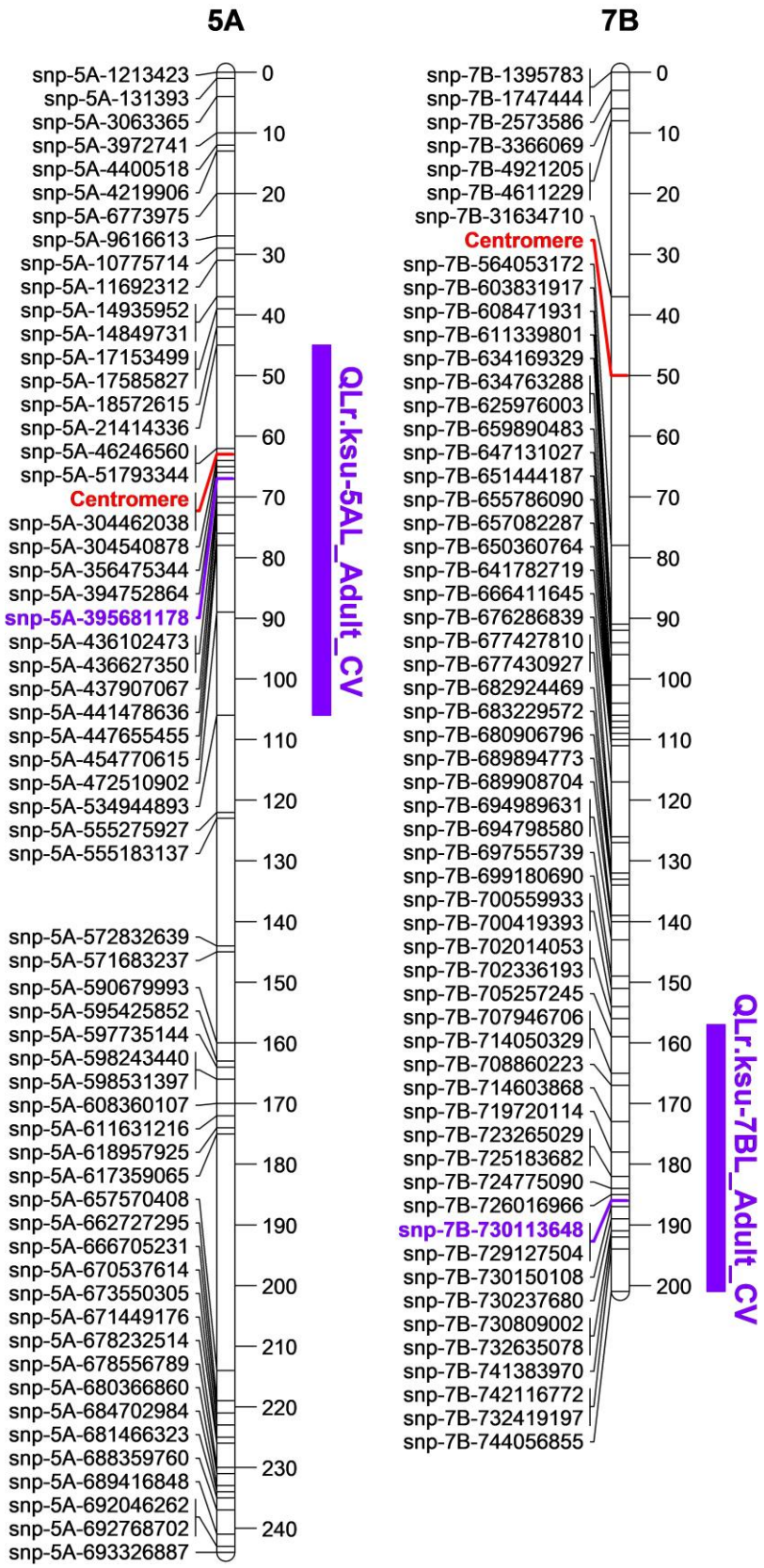
5A
snp-5A-1213423
snp-5A-131393
snp-5A-3063365
snp-5A-3972741
snp-5A-4400518
snp-5A-4219906
snp-5A-6773975
snp-5A-9616613
snp-5A-10775714
snp-5A-11692312
snp-5A-14935952
snp-5A-14849731
snp-5A-17153499
snp-5A-17585827
snp-5A-18572615
snp-5A-21414336
snp-5A-46246560
snp-5A-51793344
Centromere
snp-5A-304462038
snp-5A-304540878
snp-5A-356475344
snp-5A-394752864
snp-5A-395681178
snp-5A-436102473
snp-5A-436627350
snp-5A-437907067
snp-5A-441478636
snp-5A-447655455
snp-5A-454770615
snp-5A-472510902
snp-5A-534944893
snp-5A-555275927
snp-5A-555183137
snp-5A-572832639
snp-5A-571683237
snp-5A-590679993
snp-5A-595425852
snp-5A-597735144
snp-5A-598243440
snp-5A-598531397
snp-5A-608360107
snp-5A-611631216
snp-5A-618957925
snp-5A-617359065
snp-5A-657570408
snp-5A-662727295
snp-5A-666705231
snp-5A-670537614
snp-5A-673550305
snp-5A-671449176
snp-5A-678232514
snp-5A-678556789
snp-5A-680366860
snp-5A-684702984
snp-5A-681466323
snp-5A-688359760
snp-5A-689416848
snp-5A-692046262
snp-5A-692768702
snp-5A-693326887
0
10
20
30
40
50
60
70
80
90
100
110
120
130
140
150
160
170
180
190
200
210
220
230
240
QLr.ksu-5AL_Adult_CV
7B
snp-7B-1395783
snp-7B-1747444
snp-7B-2573586
snp-7B-3366069
snp-7B-4921205
snp-7B-4611229
snp-7B-31634710
Centromere
snp-7B-564053172
snp-7B-603831917
snp-7B-608471931
snp-7B-611339801
snp-7B-634169329
snp-7B-634763288
snp-7B-625976003
snp-7B-659890483
snp-7B-647131027
snp-7B-651444187
snp-7B-655786090
snp-7B-657082287
snp-7B-650360764
snp-7B-641782719
snp-7B-666411645
snp-7B-676286839
snp-7B-677427810
snp-7B-677430927
snp-7B-682924469
snp-7B-683229572
snp-7B-680906796
snp-7B-689894773
snp-7B-689908704
snp-7B-694989631
snp-7B-694798580
snp-7B-697555739
snp-7B-699180690
snp-7B-700559933
snp-7B-700419393
snp-7B-702014053
snp-7B-702336193
snp-7B-705257245
snp-7B-707946706
snp-7B-714050329
snp-7B-708860223
snp-7B-714603868
snp-7B-719720114
snp-7B-723265029
snp-7B-725183682
snp-7B-724775090
snp-7B-726016966
snp-7B-730113648
snp-7B-729127504
snp-7B-730150108
snp-7B-730237680
snp-7B-730809002
snp-7B-732635078
snp-7B-741383970
snp-7B-742116772
snp-7B-732419197
snp-7B-744056855
0
10
20
30
40
50
60
70
80
90
100
110
120
130
140
150
160
170
180
190
200
QLr.ksu-7BL_Adult_CV

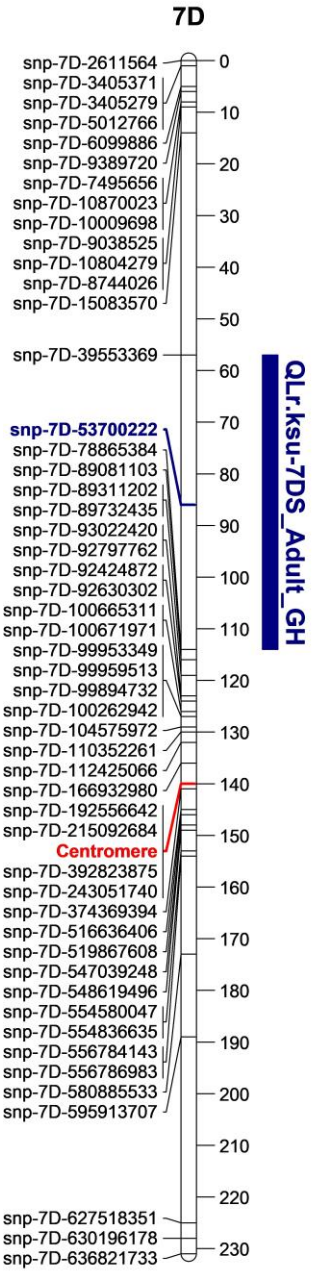

Appendix Figure B.3. Chromosomal positions of quantitative trait loci (QTL) associated with leaf rust traits in the DH population. Marker names for each SNP are located to the left of each chromosome and genetic positions in cM are located to the right of each chromosome. The approximate position of the centromere according to the Chinese Spring reference is highlighted in red. Bars to the right of each chromosome represent QTL positions and are color coded according to seedling, adult greenhouse, and adult field experiments. Solid bars represent the interval between peak markers detected across different traits or experiments and error bars represent the genetic distance between 1.5 LOD intervals. The most stable peak markers for each QTL are colored coded to match the QTL bar.

Appendix Table B.1. KASP assay primer sequences for *Lr34* and *Lr68*.

Primer	Forward 5'-3'		Reverse 5'-3'
*Lr34*Exon11-KASP	GGGAGCATTATTTTTTTCCATCA	GGGAGCATTATTTTTTTCCATCT	AGCGAATCCAGTATGGAAAT
*Lr34*JagExon22-KASP	AATGTATCGTGAGAGATTTGCAG	AATGTATCGTGAGAGATTTGCAT	AGGTGAATAAATATGAGCATCAGT
Lr68-2-KASP	CGTGTCTTGGACCTGAGCAAT	CGTGTCTTGGACCTGAGCAAC	TGACCTGAGTCCCGTCAAGA

Appendix Table B.2. Summary of quantitative trait loci associated with means for leaf rust resistance traits collected in individual datasets.

QTL	Trait	Plant Stage	Data Set	Peak Marker*	Alleles	Genetic Position (cM)	1.5 LOD Interval (cM)	LOD Threshold (P<0.05)φ	LOD-CIM	LOD-MQM	Variance Explained	Source‡
QLr.ksu-1BL	ISEV	Adult	GH19F	snp-1B-499556038	T/G	97.40	59.41-105.96	3.15	3.48	4.71	8.40	Everest
QLr.ksu-2AL	IT	Seedling	CDL18F	snp-2A-705760167	T/C	142.89	114.99-157.19	3.14	3.79	2.91	7.48	Everest
QLr.ksu-2AL	IT	Adult	GH19F	snp-2A-678001212	A/G	132.00	120.89-142.07	3.19	6.41	6.77	13.55	Everest
QLr.ksu-2AL	VSEV	Adult	GH19F	snp-2A-630461249	C/T	127.20	120.89-131.96	3.03	8.24	7.80	13.51	Everest
QLr.ksu-2AL	ISEV	Adult	GH19F	snp-2A-625282451	A/G	127.20	86.94-142.07	3.15	5.46	5.40	9.73	Everest
QLr.ksu-2AL	ISEV	Adult	GH19S	snp-2A-513828744	C/T	114.99	86.94-131.96	3.02	3.32	3.14	7.36	Everest
QLr.ksu-2AL	IT	Adult	GH20S	snp-2A-625282451	A/G	127.20	120.89-131.96	3.27	4.63	4.61	10.11	Everest
QLr.ksu-2AL	VSEV	Adult	GH20S	snp-2A-635347504	C/G	128.00	64.19-148.58	3.21	3.70	3.70	8.00	Everest
QLr.ksu-2BS	IT	Adult	GH19S	snp-2B-94102750	C/T	97.67	67.78-120.74	3.23	4.05	3.74	9.06	Everest
QLr.ksu-4DL	VSEV	Adult	GH19F	snp-4D-485383140	T/C	46.23	10.48-72.47	3.03	4.04	4.14	6.78	Everest
QLr.ksu-7DS	IT	Adult	GH19F	*Lr34*	A/T	80.00	57.31-114.13	3.19	13.00	12.58	27.55	WB-Cedar
QLr.ksu-7DS	VSEV	Adult	GH19F	*Lr34*	A/T	80.00	57.31-114.13	3.03	15.24	15.81	31.05	WB-Cedar
QLr.ksu-7DS	ISEV	Adult	GH19F	*Lr34*	A/T	79.40	57.31-114.13	3.15	13.75	13.99	29.05	WB-Cedar
QLr.ksu-7DS	IT	Adult	GH19S	*Lr34*	A/T	81.00	57.31-114.13	3.23	5.93	4.78	11.77	WB-Cedar
QLr.ksu-7DS	VSEV	Adult	GH19S	snp-7D-53700222	C/T	84.00	57.31-114.13	3.12	4.49	4.46	12.33	WB-Cedar
QLr.ksu-7DS	ISEV	Adult	GH19S	snp-7D-53700222	C/T	85.82	57.31-114.13	3.02	8.86	7.83	19.67	WB-Cedar
QLr.ksu-7DS	IT	Adult	GH20S	snp-7D-53700222	C/T	85.80	57.31-114.13	3.27	10.85	10.65	25.70	WB-Cedar
QLr.ksu-7DS	VSEV	Adult	GH20S	snp-7D-53700222	C/T	84.00	57.31-114.13	3.21	11.80	11.43	27.82	WB-Cedar
QLr.ksu-7DS	ISEV	Adult	GH20S	snp-7D-53700222	C/T	83.00	57.31-114.13	3.26	6.14	4.85	14.64	WB-Cedar

* Labels for markers contain the chromosome and the physical position in bp anchored to the Chinese Spring reference genome. φ LOD thresholds for each trait-environment combination derived from 1,000 permutations at P≤0.05. ‡ The source of the QTL associated with IT, SEV, and SEVLD corresponds with the resistance alleles.

Appendix Table B.3. Potential candidate genes associated with each QTL detected in the study.

QTL	Peak Marker*	QTL Physical Position (Mb)	Candidate Genes (CG)	CG Source/Location[#]	Reference
QLr.ksu-1BL	snp-1B-499556038	499.6	*Lr26*	*Secale cereale* L.	Singh et al., 1990
			Lr33	133.1 Mb - 163.1 Mb	Dyck, 1977; Che et al., 2019
			Lr44	*Triticum aestivum* spp. *spelta* L.	Dyck & Sykes, 1994; Zhou et al., 2013
			Lr46	672.6 Mb - 673.8 Mb	Singh et al., 1998; Yuan et al., 2020
			Lr51	*Aegilops speltoides*	Dvořák, 1977
QLr.ksu-2AS	snp-2A-24002490	24.0	*Lr17*	3.6 Mb - 6.1 Mb	Xue et al., 2018
			Lr37	*Aegilops ventricosa*	Helguera et al., 2003
			Lr45	*Secale cereale* L.	McIntosh, Friebe, et al., 1995
			QLr.ags-2AS	62 cM	Sapkota et al., 2020
QLr.ksu-2AL	snp-2A-630461249	513.8 - 678.0	*Lr38*	*Agropyron intermedium*	Wienhues, 1966
			LrTt1	*Triticum timopheevii*	Leonova et al., 2010
			QLr.sfr-2AL	Centromeric - 63 cM	Schnurbusch et al., 2004
			QLr.ubo-2AL	Telomeric - 143 cM	Maccaferri et al., 2008
			QLr.cimmyt-2AL	Centromeric - 63 cM	Rosewarne et al., 2012
			QLr.hebau-2AL	Centromeric - 103 cM	Zhang et al., 2017
QLr.ksu-2BS	snp-2B-65685562 snp-2B-94102750	65.7 - 94.1	*Lr13*	157.7 Mb - 158 Mb	Qiu et al., 2020.
			Lr16	5 Mb - 6 Mb*	Kassa et al., 2017
			Lr23	93 Mb*	Chhetri et al., 2017
			Lr35	*Aegilops speltoides*	Seyfarth et al., 1999
			Lr48	91 Mb - 94 Mb*	Saini et al., 2002
			Lr73	Telomeric	Park et al., 2014
QLr.ksu-3BL	snp-3B-512203483	512.2 - 544.6	*Lr77*	743.2 Mb	Kolmer et al., 2018; Qureshi et al., 2018
			Lr79	752.4 Mb	Qureshi et al., 2018
			QLr.sfrs-3B	Centromeric	Messmer et al., 2000; Li et al., 2014
			QLr.fcu-3BL	586.5 Mb	Chu et al., 2009
			QLr.hebau-3BL	761.3 Mb - 761.6 Mb	Zhang et al., 2019
		485.4 - 504.2	*Lr67*	405 Mb	Herrera-Foessel et al., 2010; Hiebert et al., 2010

QLr.ksu-4DL	snp-4D-485383140 snp-4D-504199409		*QTL QLr.fcu-4DL*	412.7 Mb	Chu et al., 2009
			QLr.hebau-4D	428.6 Mb	Zhang et al., 2019
			QLr.jki-4D.1	465 Mb	Rollar et al., 2020
QLr.ksu-5AL	snp-5A-395681178	395.7	*QLr.hebau-5AL*	589.3 Mb - 591.5 Mb	Zhang et al., 2019
			QLr.hebau-5AL	436.1 Mb - 441.1 Mb	Gebrewahid et al., 2020
			QLr.cimmyt-5AL	587.0 Mb	Rosewarne et al., 2012
QLr.ksu-7BL	snp-7B-730113648	730.1	*Lr14*	739.9 Mb	Mcintosh et al., 1967; Terracciano et al., 2013
			Lr19	*Agropyron elongatum*	Browder, 1972
			Lr68	734.2 Mb	Herrera-Foessel et al., 2012
QLr.ksu-7DS	*Lr34*	53.7	*Lr34*	47.4 Mb	Dyck, 1987

* Labels for markers contain the chromosome and the physical position in bp anchored to the Chinese Spring reference genome. # Physical and genetic positions of candidate genes provided from the literature or determined through alignment of marker sequence to the Chinese Spring reference. Unknown positions are broadly labeled to regions of the chromosome arm or to segments introgressed from other species.

Appendix C - Chapter 3 Supplemental Figures and Tables

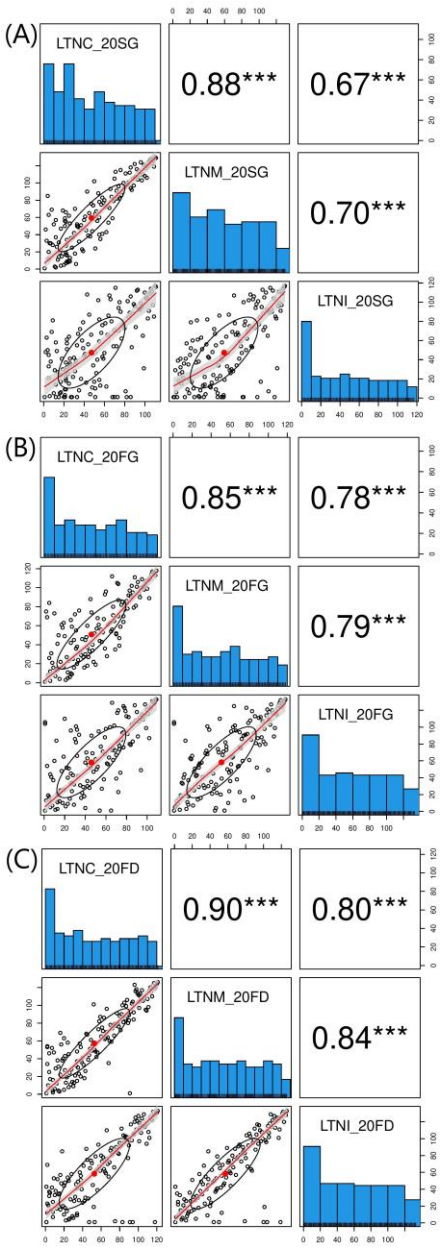

Appendix Figure C.1. Scatterplot matrices showing comparisons of raw phenotypic values between each LTN trait within individual cycles. The diagonal shows the distribution of each variable as well as displaying the abbreviation for each LTN trait and the corresponding cycle (A) 2020 Spring Greenhouse G (20SG), (B) 2020 Fall Greenhouse D (20FD), and (C) 2020 Fall Greenhouse G (20FG). The boxes in the top of the diagonal contain Pearson's correlation coefficients with asterisks displaying the significance of correlation, * ($P < 0.05$), ** ($P < 0.01$), *** ($P < 0.001$). The number in the lower right of the boxes corresponds to the number of data points used in each comparison. The boxes below the diagonal display the bivariate scatter plots fitted with a LOESS curve.

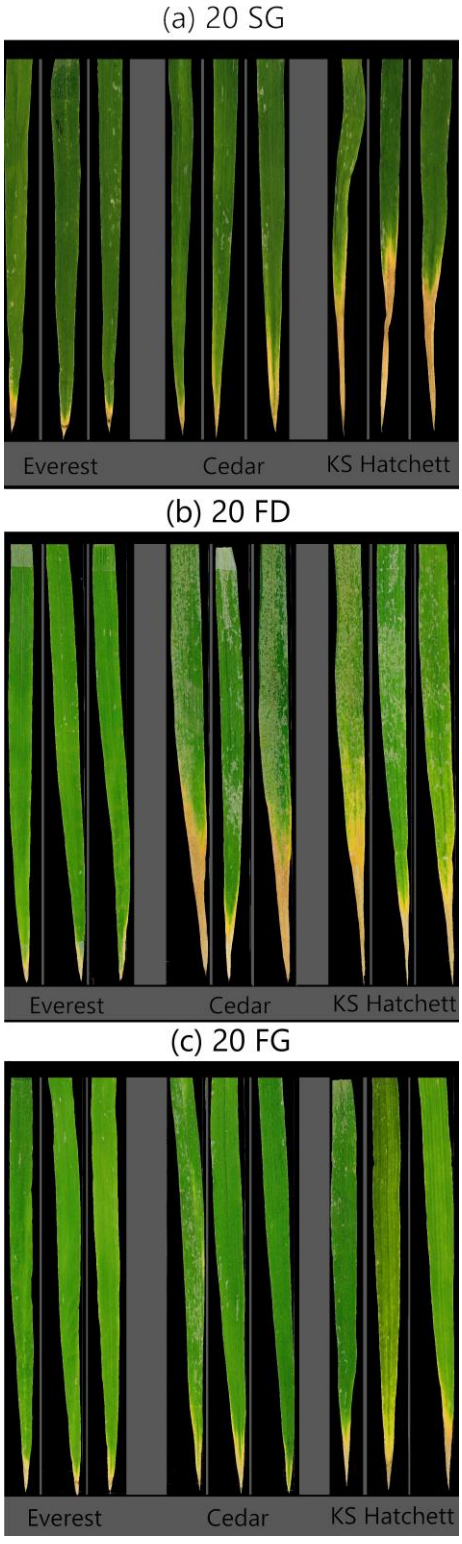

Appendix Figure C.2. Leaf images showing extent of leaf tip necrosis for the cultivars Everest, WB-Cedar, and 'KS Hatchett' collected from three individual plants during the three greenhouse cycles (a) 2020 Spring Greenhouse G (20SG), (b) 2020 Fall Greenhouse D (20FD), and (c) 2020 Fall Greenhouse G (20FG).

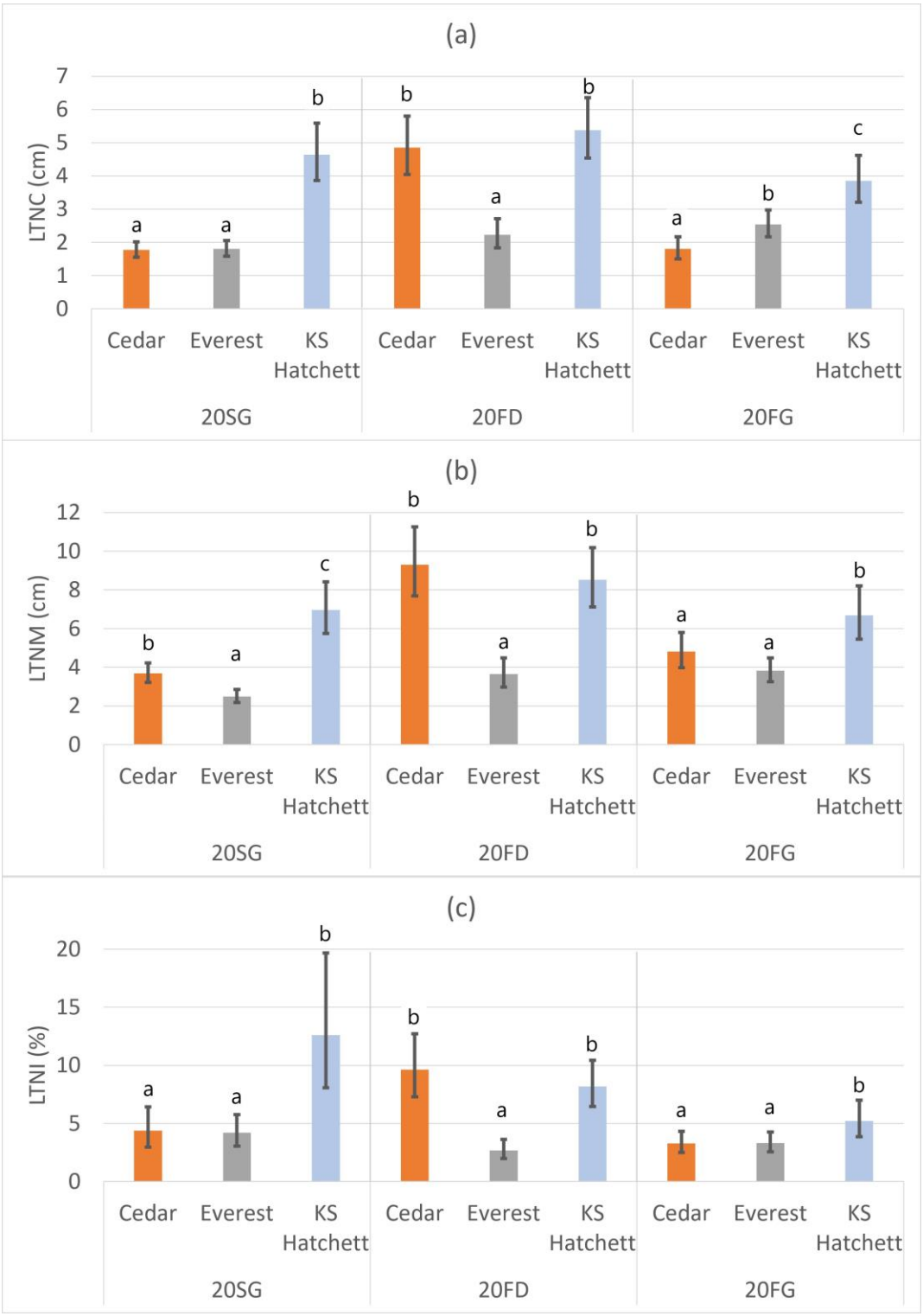

Appendix Figure C.3. Bar charts displaying individual greenhouse cycle means for the traits (a) LTNC, (b) LTNM, and (c) LTNI for the cultivars Everest, WB-Cedar, and 'KS Hatchett'. Error bars represent upper and lower 95% confidence intervals. Letters above each bar denote significance of mean differences based on pairwise comparisons using a Bonferroni correction at $P<0.05$.

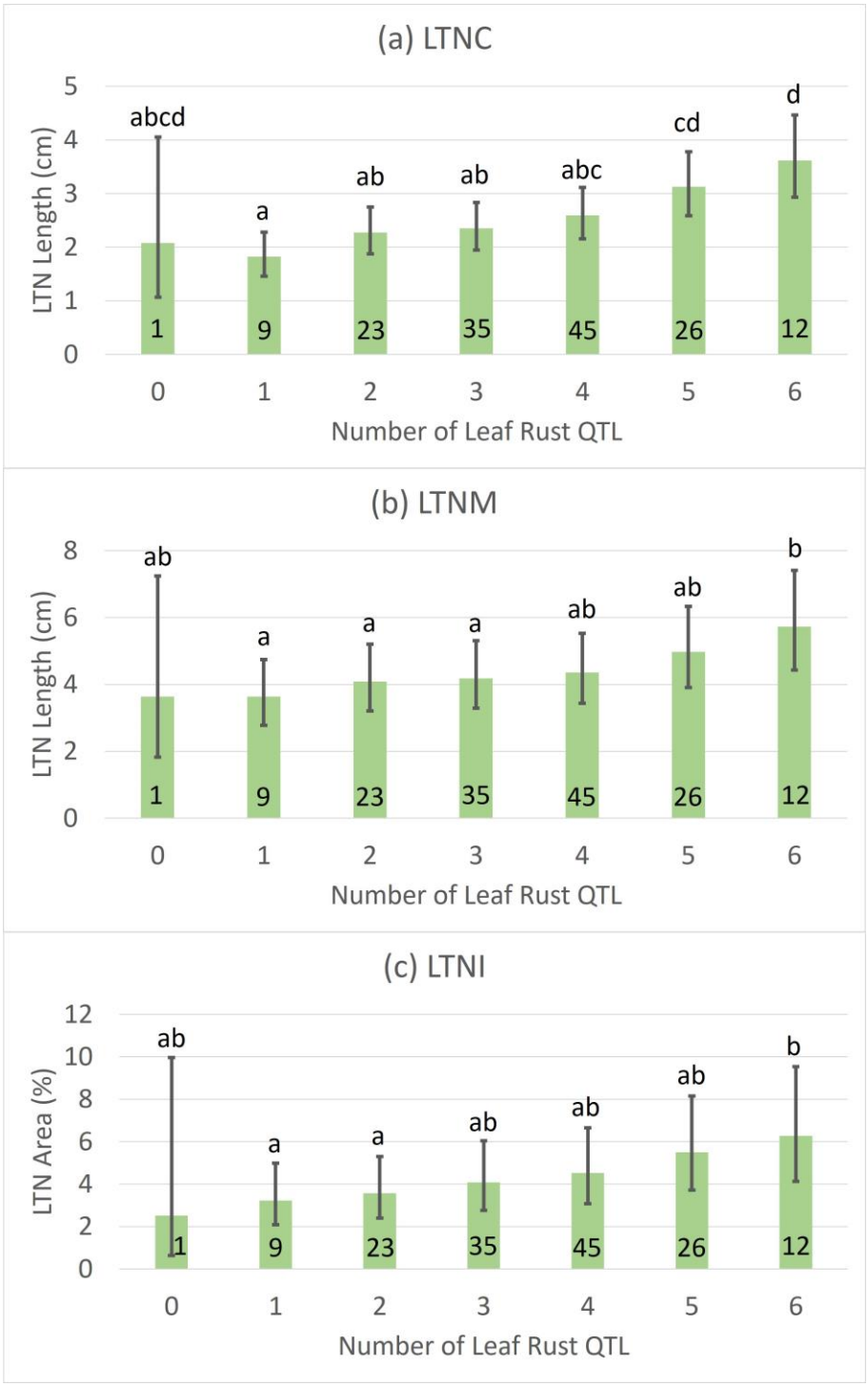

Appendix Figure C.4. Bar charts displaying BLUPS for (a) LTNC (b) LTNM and (c) LTNI calculated between groups of DH lines based on the number of resistance alleles present for leaf rust QTL. Numbers on the X-axis correspond to the number of resistance alleles carried by lines within each group. Numbers at the base of each bar represent the number of DH lines within each group. Error bars represent upper and lower 95% confidence intervals. Letters above each bar denote significance of mean differences based on pairwise comparisons using a Bonferroni correction at $P<0.05$

Appendix Table C.1. Summary of quantitative trait loci associated with individual cycle means estimated for leaf tip necrosis traits. Logarithm of the odds (LOD) values obtained from composite interval mapping (CIM) and multiple QTL mapping (MQM) are presented for each significant association. The percent variance (R2) explained by each QTL is provided.

QTL	Data Set	Trait	Peak Marker*	Alleles	Genetic Position (cM)	1.5 LOD Interval (cM)	LOD Threshold (P<0.05)ϕ	LOD-CIM	LOD-MQM	Variance Explained	Source‡
Qltn.ksu-2A	20FD	LTNM	snp-2A-42194536	C/G	77.0	72.29-127.19	3.16	3.85	3.19	6.00	Everest
Qltn.ksu-7DS	20FD	LTNC	*Lr34*	A/T	81.0	57.31-85.81	3.16	19.1	17.41	45.03	WB-Cedar
Qltn.ksu-7DS	20FD	LTNI	*Lr34*	A/T	81.0	57.31-85.81	3.12	13.80	15.84	43.21	WB-Cedar
Qltn.ksu-7DS	20FD	LTNM	*Lr34*	A/T	80.0	57.31-85.81	3.16	17.00	16.79	40.49	WB-Cedar
Qltn.ksu-1DL	20FG	LTNM	snp-1D-468798653	C/T	153.0	94.23-176.91	3.20	3.77	3.08	8.27	WB-Cedar
Qltn.ksu-2A	20FG	LTNC	snp-2A-580855803	A/C	123.0	78.62-142.07	3.26	3.44	3.44	8.05	Everest
Qltn.ksu-7DS	20FG	LTNC	*Lr34*	A/T	79.4	57.31-85.81	3.26	12.30	11.89	32.60	WB-Cedar
Qltn.ksu-7DS	20FG	LTNI	*Lr34*	A/T	79.4	57.31-85.81	3.13	8.05	7.56	23.66	WB-Cedar
Qltn.ksu-7DS	20FG	LTNM	*Lr34*	A/T	79.4	57.31-85.81	3.20	8.29	7.18	20.83	WB-Cedar
Qltn.ksu-2A	20SG	LTNC	snp-2A-678001212	A/G	131.0	97.82-146.86	3.17	3.18	2.44	4.82	Everest
Qltn.ksu-7DS	20SG	LTNC	*Lr34*	A/T	79.4	57.31-85.81	3.17	14.85	15.08	36.61	WB-Cedar
Qltn.ksu-7DS	20SG	LTNI	*Lr34*	A/T	79.4	57.31-85.81	3.33	14.30	12.47	36.14	WB-Cedar
Qltn.ksu-7DS	20SG	LTNM	*Lr34*	A/T	79.4	57.31-85.81	3.15	20.20	20.20	47.86	WB-Cedar

* Labels for markers contain the chromosome and the physical position in bp anchored to the Chinese Spring reference genome. ϕ LOD thresholds for each trait-environment combination derived from 1,000 permutations at P≤0.05. ‡ The source of the QTL associated with IT, SEV, and SEVLD corresponds with the resistance alleles.